Important Notice

THE UNIVERSITY OF CALGARY

Elastic Wavefield Modeling by Phase Shift Cascade

By

Chanpen Silawongsawat

A THESIS
SUBMITTED TO THE FACULTY OF GRADUATE STUDIES
IN PARTIAL FULFILLMENT OF THE REQUIREMENTS FOR THE
DEGREE OF MASTER OF SCIENCE

DEPARTMENT OF GEOLOGY AND GEOPHYSICS

CALGARY, ALBERTA

JUNE, 1998

ABSTRACT

A numerical technique for 2-D elastic wavefield modeling in a stratified medium is presented. A cylindrical source waveform is decomposed into Fourier plane waves. Plane wave potentials, P and S, are advanced in depth by phase shift across each layer of the stratified system. Every Fourier plane wave is propagated through a computation grid and all multiples and mode conversions can be computed in a phase shift cascade.

At an interface, the four incoming potentials are related to the four scattered potentials by the 4x4 scattering matrix, in which scattering coefficients are computed using the Zoeppritz equations. The explicit use of the scattering matrix allows a partitioned modeling which can also be depth dependent.

After cascading, options for free-surface effects and displacement conversions are made. The seismograms are obtained by inverse Fourier transformation. A connection between phase shift cascade to the propagator method is explored.

ACKNOWLEDGEMENTS

DEDICATION

To Mama and Papa for the time I've been away.

TABLE OF CONTENTS

LIST OF FIGURES

CHAPTER **1**

Introduction

1.1. Thesis organization

This thesis is organized as follows. In chapter 1, some background of seismic forward modeling and brief discussions of other modeling methods are given. Due to its close relation to phase shift cascade, mathematical expressions of the propagator matrix method are clearly described. Chapter 2 contains a complete derivation of phase shift cascade from the elastic equations of motion. The point source of compressional waves is described as a superposition of Fourier plane waves. From the explicit formulation in section 2.3, it is clear that by modifying the scattering matrix, many physical phenomena can be separately analyzed from any depth. The implementation of the numerical modeling is entirely outlined. Feature comparison to the propagator matrix method is discussed at the end of this chapter.

In chapter 3, phase shift cascade is examined and the results are discussed. Section 3.1 considers the case of a horizontally layered earth model and its response to a vertically traveling plane wave, the simple one-dimensional problem. The results are also compared with the conventional method normally used in industry. In the remaining two parts, synthetic seismograms are presented for the 2D elastic case in a layered earth model. The results achieved from the simplest models, a single interface, are displayed in

the second part, 3.2. This resolved a lot of programming problems and gives an important verification of this work. A technique to deal with one of the most serious problems, spatial wraparound, was developed and implemented at this phase. In part 3.3 a realistic model, from real (Blackfoot 08-08) well log data, was used and some applications of wavefield separations are presented. The run time and memory requirement are analyzed and improved upon working with this data set. Some other technical and programming problems also showed up at this stage. Some of them are solved, some suppressed. A few techniques and extensions are discussed in chapter 4, along with the conclusions. The package of elastic modeling in the Matlab environment, to synthesize 2-D seismic data in horizontally layered media by the phase shift cascade method, was written and is referred to as *Elmo* (*El*astic *mo*deling) throughout the thesis.

1.2. Introduction

1.2.1. Background

The goal of geophysics is to use all available data to derive an indirect description of the earth's subsurface as completely as possible. In the seismic method, forward modeling plays a significant role in data interpretation to estimate the earth's parameters in both exploration and global geophysics. Basically, seismic modeling generates artificial signals of reflections from impedance contrasts within the earth. In this way, a seismologist can produce a subsurface model that matches the actual data in some acceptable sense.

Synthetic seismograms are commonly used for many applications including refining the subsurface model by relating the computed traveltimes and amplitudes with those of recorded seismic data (inversion), testing new processing techniques, and investigating seismic wave propagation theory. Before they were employed to achieve the offset dependent responses of increasingly complex geological models, they were commonly used as a means to simulate the normal incidence reflection response.

The numerical computation of synthetic seismograms is mostly based on the solution of the equations of motion of an elastic medium. Exact analytical solutions of these equations for seismic wave propagation in complex, variable velocity structures are unknown (Dohr, 1985). However, in a few simple cases there are some variable analytic solutions. The construction of 2-D seismograms is possible with several existing numerical methods. They all have varying degrees of computing time and memory requirements, accuracy and implementional ease, and have different assumptions and constraints. Therefore a suitable method has to be chosen for a particular result in order to optimize the time and memory needed to the desired details of the synthetics. There is yet no algorithm which is applicable in all situations (Dohr, 1985), however these procedures can complement each other. In general there are two main approaches to create elastic seismograms: ray theory based and wave equation based methods. Under ray theory, a high frequency approximation is required if the ray series is to converge rapidly. Based on the wave equation, there are numerous methodologies. However a few main algorithms are briefly discussed in the next section. Wave equation modeling gives very realistic results which are difficult to analyze whereas the raytracing is very versatile but unlikely to produce all real effects.

This thesis will present a new method of elastic modeling, *phase shift cascade*, which combines many of the best features of ray trace and wave equation schemes. The phase shift cascade is closely related to the propagation matrix method which has been widely used and is summarized in section 1.4. Both methods can be used to compute seismograms for a layered earth with no lateral variation in properties. A line or point source can be constructed by the superposition of a sufficiently large number of plane waves in the Fourier domain. Short descriptions of other matrix methods are also given in section 1.3.

1.2.2. Ray tracing

Typically this technique computes amplitude and traveltime for a particular event by tracing its trajectory from a source to a receiver. For instance, SYNTH (Lawton and

Howell, 1992, Margrave and Foltinek, 1995), an elastic modeling package developed at the University of Calgary, uses Snell's law for ray paths and the Zoeppritz equations for amplitudes. As such it is very flexible in allowing effects to be turned on and off. Compared to the other existing methods, ray tracing has found the more popular applications in seismic prospecting due mainly to its' fast computation and its' intuitiveness and flexibility. It can also synthesize the propagation of high-frequency seismic waves in rather complicated laterally varying structures. Considerable utility has come from the ability to investigate wave modes separately, including multiply reflected waves with any number of reflections, transmissions and conversions. However the numerical procedure is usually based on one-by-one events. A model with very thin layering and high velocity contrasts, which will produce many internal multiples and mode conversions, is difficult to treat with simple ray methods.

There are many techniques with varying levels of approximation in the ray tracing approach. More details of those classifications are found in Dohr (1985, chapter 1 by Cerveny) and Cerveny et al. (1977). Because of the high-frequency requirement, most of the ray techniques are best suited for models with smooth features compared to the prevailing wavelength. In situations which do not meet this condition, though simple ray tracing is commonly used, it is necessary to remember that it may yield inaccurate results.

The ray method has been used to study head waves extensively by Cerveny and Ravindra (1971). Krebes and Le (1994) presented an application for inhomogeneous plane waves and cylindrical waves in anisotropic anelastic media. Wave propagation in anelastic media has been investigated using complex rays by Hearn and Krebes (1990), and Krebes and Slawinski (1991).

1.2.3. Finite difference methods

Among the techniques available for the purpose of forward modeling, the finite difference (and finite element) method is a direct numerical solution of the equations of motion. The output is not biased by any physical approximation. Highly accurate numerical solutions to the elastic wave equation can be generated for most subsurface

configurations of exploration interest. However, since this method is based directly on the equations of motion without physical approximations, finite differencing generates every event possible, e.g. multiples, converted waves, head waves, diffracted waves, etc. Hence the results can be difficult to interpret because the technique provides very little physical insight and flexibility.

The basic idea is to approximate the derivatives in the equations of motion as differences between values of the motion fields at points on a space-time grid. A good introduction to the theory and application of this method is given by Kelly et al. (1976), and Bording and Lines (1997). An alternative technique to finite differencing, pseudospectral methods can be found in Fornberg (1987). The technique uses Fourier methods to build higher order approximations to the derivatives in the equations of motion.

One of the main problems, which naturally occurs in this kind of numerical method, is cumulative error. From initial values, the recursive computation of the algorithm can amplify small roundoff errors in certain circumstances. Accuracy requires that the ratio of temporal to spatial grid sizes, $\Delta t/\Delta x$, be small enough to over sample all wavelengths of the wavefield. Another problem involves nonphysical reflections arising from artificial boundaries in the spatial grid. In order to avoid this problem, the numerical edges should be sufficiently expanded so that the spurious reflections do not arrive at the receivers during the time interval of interest, or absorbing boundary conditions (Clayton and Enquist 1977) can be implemented.

1.3. Variety of matrix algorithms

1.3.1. Matrix method

The matrix method is based on a reformulation of the elastic wave equation for displacement into an equation which is first order in depth derivatives with displacement and stress as unknowns. The unknowns are grouped into a vector called the *displacement-stress vector* or *motion vector*. In this method, the complexity of the wave propagation

problem is reduced by assuming that the elastic properties depend only on depth. For this vertically heterogeneous earth model, coupled ordinary differential equations involving displacement and traction elements are derived from the equation of motion. The solutions to such a system of equations can be expressed by the product integral, or propagator, of the matrix of coefficients (Gilbert and Backus, 1966).

1.3.2. Thomson-Haskell method

A very first application of the matrix method was given by Thomson (1950) and corrected by Haskell (1953) for the layered earth model. However, a practical problem arises specifying the radiation condition by which certain waves are suppressed at infinity, rather than by a constraint on the motion-vector directly. This is because the presence of upgoing and downgoing wave types in the lower half-space needs to be related to the motion-stress vector (Aki and Richards, 1980, p.277). Thus, at large horizontal wave numbers, these wave types have grown or decayed exponentially with depth. This problem is a concern of the other following matrix applications.

1.3.3. Propagator matrix method

The propagator matrix method (Fuchs and Muller, 1971, Kennett and Kerry, 1979 and 1980) considers a stratified medium equivalent to a single composite layer (or layer-stack) between two half-spaces. The total response, including all multiple reflections, mode-converted waves and refracted waves, is computed in terms of normalized total upgoing and downgoing waves or, so-called overall reflection and transmission coefficients. Such coefficients are defined for the whole region embedded between uniform half spaces and then produced by relating the wave systems in the upper and lower half spaces. Thus, for example, an initial condition of only a unit incident P-wave from the topmost of the layer-stacks may be applied. The efficient calculation procedure progresses from the base of the layering towards the surface, to avoid numerical problems associated with growing solutions of the differential equations at depth (Kennett and Kerry, 1979).

The numerical integration of plane wave reflection coefficients, to synthesize a point source, is carried out in the frequency-slowness domain. The seismograms of displacement responses are obtained after multiplication with the source spectrum and inverse Fourier transformation.

The advantage of the propagator matrix method lies in the inclusion of all multiples and converted waves from the reflecting zone. Therefore the synthetic seismograms have high accuracy. Its disadvantages are long computing times (if the reflection response has a long duration) and algorithmic inflexibility which requires all modes to be computed. A package for AVO modeling (CRUST) has been developed by Frasier (1980) based on a propagator matrix scheme to enable some offset effects to be turned on and off for pre-critical amplitude analysis.

1.3.4. Reflectivity method

This method has been developed by Fuchs (1968, 1970) and Fuchs and Muller (1971) based on the matrix method of Thomson-Haskell originally to generate synthetic amplitude information for crustal studies. It is thus an application of the propagator technique, to compute the overall responses from a particular portion of the composite homogeneous stacked layers in terms of a total reflection coefficient. In the practical application of the method, only the reflection responses from deeper zones of the entire layered earth model are calculated. Sometimes the region of interest lies deep in a layered medium whereas the reflections from the upper portion can be neglected or calculated separately. These deep reflections endure transmission losses and time shifts from a stack of layers above the reflecting medium which must be taken into account (Fuchs and Muller, 1971). Originally by Fuchs and Muller (1971), composite reflection coefficients for the layered region are constructed by the propagator matrix for potentials, which can include all multiples and mode conversions.

1.4. Mathematical outline of propagator matrix theory

1.4.1. Matrix formulation of the equations of motion

The methodology involves spherical wave decomposition and the calculations are carried out in the frequency-ray parameter (horizontal-slowness) domain. The displacement and stress are directly used as the motion-stress vector of the wave system. The evolution of the stress-displacement field with depth is developed by the *propagator matrix*. This method is most closely related to phase shift cascade. So we explore it here in some detail. The ultimate goal is to show explicitly how the propagator matrix is related to the scattering matrix used in phase shift cascade.

The matrix approach has been extensively developed for the three-dimensional seismic problem that includes all *P*, *SV* and *SH* components for body and surface waves. Nonetheless the discussion here is limited to the two-dimensional *P-SV* problem for simplicity. It should be mentioned that the derivation in this section is adapted from Kennett (1983).

For plane waves in a vertically inhomogeneous medium, the equation of motion and constitutive relation can be combined in such a way that only first-order depth derivatives of stress and displacement are needed (Aki and Richards, 1980).

$$\frac{\partial \mathbf{f}}{\partial z} = \mathbf{A}\mathbf{f} \qquad\qquad (1\text{-}1)$$

where, for a P-SV system, $\mathbf{f} = \mathbf{f}(z)$ is a column vector giving the depth dependence of particle displacement and stress and $\mathbf{A}$ is a 4x4 matrix, with entries depending on elastic properties of the medium, horizontal slowness p, and frequency ω. An explicit formula for $\mathbf{A}$ is given by Aki and Richards (1980, p.164) for a uniform layer. For this system of plane waves, the motion wavefields at an offset x and time t, can be considered such that the (x,t) dependence is only via a factor $e^{i\omega(px-t)}$:

$$\mathbf{f}(z)e^{i\omega(px-t)} = \begin{pmatrix} u_x \\ u_z \\ \tau_{zx} \\ \tau_{zz} \end{pmatrix}. \tag{1-2}$$

This column vector, which is made up from vertical and horizontal components of displacements and stresses, u_x, u_z, τ_{xz}, τ_{zz}, is called a motion vector or a displacement-stress vector. For a homogeneous layer there are four possible eigen-solutions for equation (1-1) (Aki and Richards, 1980, p.166) in the P-SV motion system: downgoing P, downgoing S, upgoing P and upgoing S (with various vertical phase factors referred to a common reference level $z=0$). Their denotations are given as motion vectors $\mathbf{D}_p e^{ik_{zp}z}$, $\mathbf{D}_s e^{ik_{zs}z}$, $\mathbf{U}_p e^{-ik_{zp}z}$ and $\mathbf{U}_s e^{-ik_{zs}z}$, respectively. Let a matrix $\mathbf{F}$ have columns consisting of those different solutions,

$$F = \left(\begin{pmatrix} u_x \\ u_z \\ \tau_{zx} \\ \tau_{zz} \end{pmatrix}_{dp} e^{ik_{zp}z} \quad \begin{pmatrix} u_x \\ u_z \\ \tau_{zx} \\ \tau_{zz} \end{pmatrix}_{ds} e^{ik_{zs}z} \quad \begin{pmatrix} u_x \\ u_z \\ \tau_{zx} \\ \tau_{zz} \end{pmatrix}_{up} e^{-ik_{zp}z} \quad \begin{pmatrix} u_x \\ u_z \\ \tau_{zx} \\ \tau_{zz} \end{pmatrix}_{us} e^{-ik_{zs}z} \right), \tag{1-3}$$

where the vertical wave number for P waves k_{zp} is defined by

$$k_{zp}^2 = \frac{\omega^2}{\alpha^2} - k_x^2 \tag{1-4}$$

and k_{zs} is similarly obtained by replacing the P wave velocity α in equation (1-4) with the S wave velocity β. Then the matrix $\mathbf{F}$ also satisfies equation (1-1) on column-wise basis and is called an *integral matrix* of (1-1) by Gilbert and Backus (1966) or a *fundamental matrix* by Kennett (1983). It can be explicitly factored into a matrix $\mathbf{E}$, made up from four eigen vectors, times a diagonal matrix $\mathbf{\Lambda}$ containing the vertical propagation phase factors.

$$\mathbf{F} = \mathbf{E}\mathbf{\Lambda} = \begin{pmatrix} \mathbf{D}_p & \mathbf{D}_s & \mathbf{U}_p & \mathbf{U}_s \end{pmatrix} \begin{pmatrix} e^{ik_{zp}z} & 0 & 0 & 0 \\ 0 & e^{ik_{zs}z} & 0 & 0 \\ 0 & 0 & e^{-ik_{zp}z} & 0 \\ 0 & 0 & 0 & e^{-ik_{zs}z} \end{pmatrix} \qquad (1\text{-}5)$$

Therefore, the complete solution $\mathbf{f}$ to the Equation (1-1), at any depth can be stated as a linear combination of all four different solutions,

$$\mathbf{f} = \mathbf{F}\mathbf{w} = \mathbf{E}\mathbf{\Lambda}\mathbf{w}. \qquad (1\text{-}6)$$

where

$$\mathbf{E} = \begin{pmatrix} \mathbf{D}_p & \mathbf{D}_s & \mathbf{U}_p & \mathbf{U}_s \end{pmatrix}, \qquad (1\text{-}7)$$

$$\mathbf{\Lambda} = \begin{pmatrix} e^{ik_{zp}z} & 0 & 0 & 0 \\ 0 & e^{ik_{zs}z} & 0 & 0 \\ 0 & 0 & e^{-ik_{zp}z} & 0 \\ 0 & 0 & 0 & e^{-ik_{zs}z} \end{pmatrix}, \qquad (1\text{-}8)$$

and

$$\mathbf{w} = \begin{pmatrix} W_{dp} \\ W_{ds} \\ W_{up} \\ W_{us} \end{pmatrix}. \qquad (1\text{-}9)$$

The complex scalar amplitude and propagation phase factors of each solution are given in a weighting matrix $\mathbf{w}$ and a diagonal matrix $\mathbf{\Lambda}$, respectively. The weight matrix components come from matching boundary conditions.

1.4.2. Propagator-matrix method

A special case of the propagator matrix approach according to Gilbert and Backus (1966) was introduced as the Thomson-Haskell method. In their method, the vertically heterogeneous medium is replaced by a stack of homogeneous layers overlaying a homogeneous half-space, Figure (1-1). An alternative derivation, other than that used here which is based mostly on Kennett (1983), is to derive a propagator matrix as a function of the elastic property matrix $\mathbf{A}$ of each layer as given in Aki and Richards (1980). The approximation of taking $\mathbf{A}(z)$ constant within a given depth interval, i.e. a

homogeneous layer, simplifies the propagator matrix expression into an exponential of the constant matrix **A**, which can either be expanded as a Taylor series or evaluated by Sylvester's formula (Aki and Richards, 1980).

In the vertically heterogeneous medium, a propagator matrix, $\mathbf{P}(z_m, z_n)$, is a 4x4 matrix which extrapolates a stress-displacement wave system at a depth z_n to another wave system at another depth z_m as

$$\mathbf{f}(z_m) = \mathbf{P}(z_m, z_n)\mathbf{f}(z_n).\qquad(1\text{-}10)$$

The inversion of $\mathbf{P}(z_m, z_n)$, on the other hand, also relates those two wave fields, however in the opposite direction:

$$\mathbf{f}(z_n) = \mathbf{P}^{-1}(z_m, z_n)\mathbf{f}(z_m) = \mathbf{P}(z_n, z_m)\mathbf{f}(z_m).\qquad(1\text{-}11)$$

Therefore propagator equations can be used in either up or down directions, to relate the complete wave systems from above to below or vice versa. Their propagator matrices are an inverse to each other. The propagator solution thus does allow a complete specification of the seismic wavefield. An important property of the propagator matrix for such heterogeneous media, is that an overall propagator can be split at any intermediate level (Aki and Richards, 1980, p.276) as

$$\mathbf{f}(z_m) = \mathbf{P}(z_m, z_{m+1})\mathbf{P}(z_{m+1}, z_{m+2})...\mathbf{P}(z_{n-1}, z_n)\mathbf{f}(z_n),$$

$$= \prod_{k=m}^{n-1} \mathbf{P}(z_k, z_{k+1})\mathbf{f}(z_n),\qquad(1\text{-}12)$$

This chain rule relation also holds in media with elastic discontinuities. Since the seismic boundary conditions that **f** is continuous across an interface ensure the continuity of $\mathbf{P}(z_m, z_n)$. Hence the overall propagator is just a matrix product of the propagator matrix of each layer between the levels z_m and z_n. Due to this property, the approximation of a stack of many homogeneous layers, usually called the layered earth model, for the vertical heterogeneous medium can be derived. Later in this chapter, the wave potentials will be introduced into the derivation to simplify the mathematics. The propagator matrix

method is also applicable in the case where the elastic properties of any layer vary smoothly with depth, when the WKBJ approximation is used (Kennett, 1983).
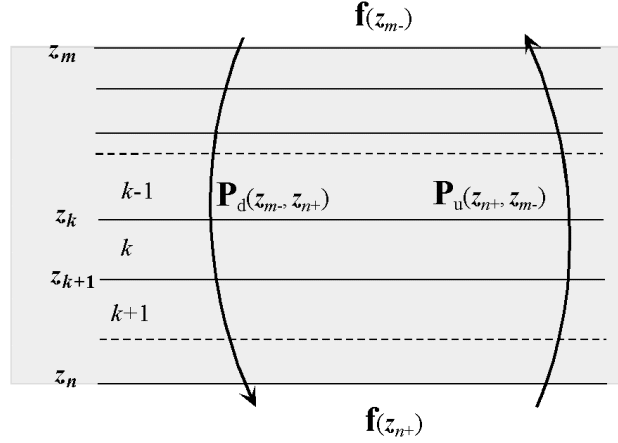
Figure 1-1. Horizontal layered earth model between two uniform half spaces with numbering system for layers and interfaces. Upward and downward propagator matrices are also shown.

1.4.3. Homogeneous layer propagator matrix

Let both z_k^+ and z_{k+1}^- be located within the same homogeneous layer immediately below z_k and above z_{k+1}, respectively, in which their $\mathbf{E}$ matrices and weighting matrices $\mathbf{w}$ are the same. Then, substituting equation (1-6) into (1-10) leads to

$$\left(\mathbf{F}(z_{k+1}^-) - \mathbf{P}(z_{k+1}^-, z_k^+)\mathbf{F}(z_k^+)\right)\mathbf{w} = 0. \tag{1-13}$$

If this is to be true for arbitrary $\mathbf{w}$ then the term in brackets must vanish. Thus $\mathbf{F}$ satisfies an equation like (1-10) on a column wise basis and $\mathbf{P}$ can be solved using equation (1-5) for

$$
\begin{aligned}
\mathbf{P}(z_{k+1}^-, z_k^+) &= \mathbf{F}(z_{k+1}^-)\mathbf{F}^{-1}(z_k^+) = \mathbf{E}_k \mathbf{\Lambda}_{z_{k+1}} \mathbf{\Lambda}_{z_k}^{-1} \mathbf{E}_k^{-1} \\
&\equiv \mathbf{E}_k \mathbf{\Lambda}_k \mathbf{E}_k^{-1}
\end{aligned} \tag{1-14}
$$

where

$$\mathbf{\Lambda}_k \equiv \mathbf{\Lambda}_{\Delta z_k} = \mathbf{\Lambda}_{z_{k+1}}\mathbf{\Lambda}_{z_k}^{-1}. \qquad (1\text{-}15)$$

Using equation (1-8), this phase shift expression becomes

$$\mathbf{\Lambda}_k = \begin{pmatrix} e^{ik_{zp}\Delta z_k} & 0 & 0 & 0 \\ 0 & e^{ik_{zs}\Delta z_k} & 0 & 0 \\ 0 & 0 & e^{-ik_{zp}\Delta z_k} & 0 \\ 0 & 0 & 0 & e^{-ik_{zs}\Delta z_k} \end{pmatrix}, \qquad (1\text{-}16)$$

where $\Delta z_k = z_{k+1} - z_k$. For a homogeneous layer k, $\mathbf{E}$ and $\mathbf{E}^{-1}$ matrices are given by Aki and Richards as

$$\mathbf{E} = \begin{pmatrix} \alpha p & \beta\eta & \alpha p & \beta\eta \\ \alpha\xi & -\beta p & -\alpha\xi & \beta p \\ 2i\omega\rho\alpha\beta^2 p\xi & i\omega\rho\beta(1-2\beta^2 p^2) & -2i\omega\rho\alpha\beta^2 p\xi & -i\omega\rho\beta(1-2\beta^2 p^2) \\ i\omega\rho\alpha(1-2\beta^2 p^2) & -2i\omega\rho\beta^3 p\eta & i\omega\rho\alpha(1-2\beta^2 p^2) & -2i\omega\rho\beta^3 p\eta \end{pmatrix} \quad (1\text{-}17)$$

and

$$\mathbf{E}^{-1} = \begin{pmatrix} \dfrac{\beta^2 p}{\alpha} & \dfrac{1-2\beta^2 p^2}{2\alpha\xi} & \dfrac{-ip}{2\omega\rho\alpha\xi} & \dfrac{-i}{2\omega\rho\alpha} \\[2mm] \dfrac{1-2\beta^2 p^2}{2\beta\eta} & -\beta p & \dfrac{-i}{2\omega\rho\beta} & \dfrac{ip}{2\omega\rho\beta\eta} \\[2mm] \dfrac{\beta^2 p}{\alpha} & -\dfrac{(1-2\beta^2 p^2)}{2\alpha\xi} & \dfrac{ip}{2\omega\rho\alpha\xi} & \dfrac{-i}{2\omega\rho\alpha} \\[2mm] \dfrac{1-2\beta^2 p^2}{2\beta\eta} & \beta p & \dfrac{i}{2\omega\rho\beta} & \dfrac{ip}{2\omega\rho\beta\eta} \end{pmatrix}, \qquad (1\text{-}18)$$

where all of the elastic parameters, including density ρ, in these expressions are to be evaluated in a particular layer k. The other plane wave parameters can be found as

the horizontal slowness or ray parameter: $p = \dfrac{k_x}{\omega}$ $\qquad\qquad\qquad (1\text{-}19)$

the vertical slowness for P waves: $\quad \xi = \dfrac{k_{zp}}{\omega}$ $\qquad\qquad\qquad (1\text{-}20)$

the vertical slowness for S waves: $\quad \eta = \dfrac{k_{zs}}{\omega}$ $\qquad\qquad\qquad (1\text{-}21)$

Thus the propagator equation in (1-10) for a homogeneous medium becomes

$$\mathbf{f}(z_{k+1}^{-}) = \mathbf{E}_k \mathbf{\Lambda}_k \mathbf{E}_k^{-1} \mathbf{f}(z_k^{+}). \tag{1-22}$$

The operation of this propagator matrix can be considered such that the $\mathbf{E}^{-1}$ matrix decomposes the motion vector $\mathbf{f}$ into up and down going of P and S waves for the phase-shift matrix $\mathbf{\Lambda}_k$ and then the $\mathbf{E}$ matrix recomposes those waves into a vector of total displacements and stresses at a new level z_{k+1}^{-}. Therefore the propagator matrix in a uniform medium can be recognized as a phase-shift extrapolator for a motion vector. It can be considered as a generalization of an approach for 1-D media using Z transforms outlined by Robinson (1967).

1.4.4. Interface propagator matrix

The particle motion and stress at any depth should be continuous, to maintain non-cavitation and stabilization throughout the medium. Therefore the motion propagator matrix at a depth z_k has to be a unit matrix, even though the elastic properties of medium may change discontinuously. This is an important constraint for the propagator matrix that

$$\mathbf{P}(z_k, z_k) = \mathbf{I}. \tag{1-23}$$

At a layer interface, the propagator matrix between the wave systems immediately above and below the interface holds the continuity of particle displacement and stress in both horizontal and vertical directions. Propagation equation (1-10) to downward continue the total wavefields across an interface at z_k, becomes

$$\mathbf{f}(z_k^{+}) = \mathbf{P}(z_k^{+}, z_k^{-}) \mathbf{f}(z_k^{-}) = \mathbf{P}_\mathrm{d}(z_k) \mathbf{f}(z_k^{-}). \tag{1-24}$$

Since the boundary conditions require continuity of $\mathbf{f}$ across the interface, we must have

$$\mathbf{P}(z_k^{+}, z_k^{-}) = \mathbf{P}_\mathrm{d}(z_k) = \mathbf{I}. \tag{1-25}$$

Similarly, the inverse propagator in the upward direction is:

$$\mathbf{P}(z_k^{-}, z_k^{+}) = \mathbf{P}_\mathrm{u}(z_k) = \mathbf{I}. \tag{1-26}$$

Though the motion-stress interface propagator must be the identity matrix at an interface, the elastic wavefields immediately above and below the interface have different eigen-vector weights. That is, their decomposition in terms of up and down going P and S wavefields generally changes. The analysis of this effect is possible through the use of a "wavefield" propagator, **Q**, to be introduced in equation (1-29) from (1-28).

The interface propagator describes the continuity of the total seismic wavefield between two levels through the discontinuities in the elastic parameters. These propagators satisfy the boundary conditions, at an interface *k*, for the total wavefields. In phase-shift cascade, a similar description for interface conditions between incident and scattered wave potentials is given as a scattering matrix which is stated later on in equation (1-39). Nonetheless this interface propagator is more powerful because it is developed from the total wavefields, at a fixed depth. That means it includes all the possible incident waves and the resultant waves. Therefore a propagator matrix across a homogenous layer from above the top to below the bottom will produce every possible multiple and converted mode.

In order to visualize this effect, we have to consider closely the formula of the interface propagator matrix. For simplification, the expression will now be derived in terms of the scalar plane-wave displacement-potentials Φ_d, Ψ_d, Φ_u and Ψ_u for the downgoing P, downgoing S, upgoing P and upgoing S, respectively. This reduces the number of wavefield elements and also allows comparison to the phase shift cascade. The conversion of a wave potential to the motion vector is merely a multiplication by a constant 4x4 matrix **D** whose elements are plane wave spatial derivatives and elastic parameters. Thus the vector **f** can be written as

$$\mathbf{f} = \mathbf{E\Lambda w} = \mathbf{Dv} = \mathbf{D} \begin{pmatrix} \Phi_d \\ \Psi_d \\ \Phi_u \\ \Psi_u \end{pmatrix} \tag{1-27}$$

and the propagator equation for wave potentials is expressed from substitution of (1-27) into (1-10) to get

$$\mathbf{v}(z_m) = \mathbf{D}^{-1}(z_m)\mathbf{P}(z_m, z_n)\mathbf{D}(z_n)\mathbf{v}(z_n) \tag{1-28}$$

or
$$\mathbf{v}(z_m) = \mathbf{Q}(z_m, z_n)\mathbf{v}(z_n). \tag{1-29}$$

The potential propagator matrix $\mathbf{Q}$, also called the wavefield propagator, is defined in terms of the motion propagator matrix as

$$\mathbf{Q}(z_m, z_n) = \mathbf{D}^{-1}(z_m)\mathbf{P}(z_m, z_n)\mathbf{D}(z_n), \tag{1-30}$$

or the $\mathbf{P}$ matrix can be expressed in term of the $\mathbf{Q}$ matrix as

$$\mathbf{P}(z_m, z_n) = \mathbf{D}(z_m)\mathbf{Q}(z_m, z_n)\mathbf{D}^{-1}(z_n). \tag{1-31}$$

Therefore, in a uniform medium, the layer propagator for potentials can be given by substituting (1-14) into (1-30) as

$$\begin{aligned} \mathbf{Q}(z_{k+1}^-, z_k^+) &= \mathbf{D}_k^{-1}\mathbf{P}(z_{k+1}^-, z_k^+)\mathbf{D}_k \\ &= \mathbf{D}_k^{-1}\mathbf{E}_k\mathbf{\Lambda}_k\mathbf{E}_k^{-1}\mathbf{D}_k \end{aligned}. \tag{1-32}$$

Note that the terms $\mathbf{D}_k^{-1}\mathbf{E}_k$ and $\mathbf{E}_k^{-1}\mathbf{D}_k$ are diagonal matrices and are the inverses of one another. This can be understood by considering $\mathbf{D}_k^{-1}\mathbf{E}_k$. Each column of the matrix $\mathbf{E}$ is an eigen vector of up or downgoing of P or S waves (equation 1-7). The inverse matrix $\mathbf{D}^{-1}$ decompose a motion vector into its equivalent potentials (see equations 1-27 and 1-2)

$$\begin{pmatrix} \Phi_d \\ \Psi_d \\ \Phi_u \\ \Psi_u \end{pmatrix} = \mathbf{D}^{-1} \begin{pmatrix} u_x \\ u_z \\ \tau_{zx} \\ \tau_{zz} \end{pmatrix}. \tag{1-33}$$

Since each eigen vector of E is a pure wave, it must come from a single potential for up or downgoing P or S. Thus the application of $\mathbf{D}_k^{-1}$ to $\mathbf{E}_k$ produces a diagonal matrix whose diagonal elements are the potentials for each eigen vector (eigen potentials). The same consideration is applicable to the term $\mathbf{E}_k^{-1}\mathbf{D}_k$. Then the three terms of $\mathbf{D}_k^{-1}\mathbf{E}_k$, $\mathbf{\Lambda}_k$ and $\mathbf{E}_k^{-1}\mathbf{D}_k$ in equation (1-32) are freely commutable and consequently the expression for $\mathbf{Q}$ in a homogeneous layer becomes simply a phase shift matrix

$$\mathbf{Q}(z_{k+1}^{-}, z_k^{+}) = \mathbf{D}_k^{-1}\mathbf{E}_k\mathbf{E}_k^{-1}\mathbf{D}_k\mathbf{\Lambda}_k = \mathbf{\Lambda}_k , \tag{1-34}$$

which is given in equation (1-16).

It will be shown later in chapter 2 that, in phase shift cascade method, this homogeneous-layer propagator equation is comparable to phase-shift extrapolation equations combined in a matrix form. For the rest of this chapter, this homogeneous layer propagator is broken-down into four 2x2 matrices. Then, with phase delay and phase advance matrices identified as

$$\mathbf{\Lambda}_k^{+} = \begin{pmatrix} e^{ik_{zp}\Delta z_k} & 0 \\ 0 & e^{ik_{zs}\Delta z_k} \end{pmatrix} \text{and } \mathbf{\Lambda}_k^{-} = \begin{pmatrix} e^{-ik_{zp}\Delta z_k} & 0 \\ 0 & e^{-ik_{zs}\Delta z_k} \end{pmatrix} \tag{1-35}$$

respectively, the phase shift propagator can be now expressed as

$$\mathbf{\Lambda}_k = \begin{pmatrix} \mathbf{\Lambda}_k^{+} & \underline{0} \\ \underline{0} & \mathbf{\Lambda}_k^{-} \end{pmatrix}, \tag{1-36}$$

where $\underline{0}$ is a 2x2 zero matrix. While at an interface z_k, the downward wave propagator becomes (from 1-30 and 1-25)

$$\mathbf{Q}_{\mathrm{d}}(z_k^{-}, z_k^{+}) = \mathbf{D}^{-1}(z_k^{+})\mathbf{P}_{\mathrm{d}}(z_k)\mathbf{D}(z_k^{-}) \equiv \mathbf{D}_k^{-1}\,\mathbf{D}_{k-1} \tag{1-37}$$

or the upward wave propagator

$$\mathbf{Q}_{\mathrm{u}}(z_k) = \mathbf{D}^{-1}(z_k^{-})\mathbf{P}_{\mathrm{u}}(z_k)\mathbf{D}(z_k^{+}) \equiv \mathbf{D}_{k-1}^{-1}\,\mathbf{D}_k . \tag{1-38}$$

Compared to the motion propagator matrices $\mathbf{P}$ for a homogeneous layer in equation (1-14), $\mathbf{Q}$ in (1-34) is as well a phase shift propagator, because both potential and motion-stress vectors are constant plane waves in such medium. However the formula of homogeneous layer propagator $\mathbf{P}$ must contain a decomposition and recomposition factors for the phase shift application. The interface propagators $\mathbf{P}_{\mathrm{I}}$, in (1-25) and (1-26), and $\mathbf{Q}_{\mathrm{I}}$, in (1-37) and (1-38), are also different due to the potential-to-displacement conversion matrix $\mathbf{D}$ which changes with the elastic properties of the medium. To write a more explicit formula for the interface wavefield propagator matrix,

$\mathbf{Q}_I(z_k)$, first consider the scattering equation given by Aki and Richards (1980, p.144-151) at interface z_k between two homogeneous layers:

$$\begin{pmatrix} \Phi_{d(k+)} \\ \Psi_{d(k+)} \\ \Phi_{u(k-)} \\ \Psi_{u(k-)} \end{pmatrix}_{sc} = \begin{pmatrix} T_{pp} & T_{sp} & \overline{R}_{pp} & \overline{R}_{sp} \\ T_{ps} & T_{ss} & \overline{R}_{ps} & \overline{R}_{ss} \\ R_{pp} & R_{sp} & \overline{T}_{pp} & \overline{T}_{sp} \\ R_{ps} & R_{ss} & \overline{T}_{ps} & \overline{T}_{ss} \end{pmatrix} \begin{pmatrix} \Phi_{d(k-)} \\ \Psi_{d(k-)} \\ \Phi_{u(k+)} \\ \Psi_{u(k+)} \end{pmatrix}_{inc} . \qquad (1\text{-}39)$$

Here T/R are potential transmission/reflection coefficients for incident and resultant wave types as specified by their subscripts, P or S. The over-bar indicates coefficients of an incident wave from below the boundary. In the P-SV problem of a displacement plane wave incident on a plane surface, Aki and Richards (1980, p.150-151) have given the explicit formulae for every element of this scattering matrix. These formulae are known as the Zoeppritz equations and are easily modified for potentials. This scattering equation describes how each of the four scattered waves, going out from above and below the boundary, are related to each of the four incident waves, coming into the boundary also from both directions. The scattering matrix can be partitioned into four 2x2 submatrices, which are designated by a bold letter for a particular scattering coefficient. There are either reflection or transmission elements in a coefficient matrix. For example,

$$\mathbf{T} = \begin{pmatrix} T_{pp} & T_{sp} \\ T_{ps} & T_{ss} \end{pmatrix} \quad \text{or} \quad \overline{\mathbf{R}} = \begin{pmatrix} \overline{R}_{pp} & \overline{R}_{sp} \\ \overline{R}_{ps} & \overline{R}_{ss} \end{pmatrix}. \qquad (1\text{-}40)$$

Then, in a compact representation, the scattering equation becomes

$$\begin{pmatrix} \Phi_{d(k+)} \\ \Psi_{d(k+)} \\ \Phi_{u(k-)} \\ \Psi_{u(k-)} \end{pmatrix}_{sc} = \begin{pmatrix} \mathbf{T} & \overline{\mathbf{R}} \\ \mathbf{R} & \overline{\mathbf{T}} \end{pmatrix} \begin{pmatrix} \Phi_{d(k-)} \\ \Psi_{d(k-)} \\ \Phi_{u(k+)} \\ \Psi_{u(k+)} \end{pmatrix}_{inc} . \qquad (1\text{-}41)$$

Thus all the interrelations between incident waves and scattered waves are available. Considering each half of the scattering equation, the scattered downgoing waves below the interface k at z_{k+} are given as

$$\begin{pmatrix} \Phi_u \\ \Psi_u \end{pmatrix}_{k+} = \mathbf{T} \begin{pmatrix} \Phi_d \\ \Psi_d \end{pmatrix}_{k-} + \overline{\mathbf{R}} \begin{pmatrix} \Phi_u \\ \Psi_u \end{pmatrix}_{k+} \quad . \tag{1-42}$$

So, in the upper layer k, the downcoming waves are given by

$$\begin{pmatrix} \Phi_d \\ \Psi_d \end{pmatrix}_{k-} = \mathbf{T}^{-1} \begin{pmatrix} \Phi_d \\ \Psi_d \end{pmatrix}_{k+} - \mathbf{T}^{-1}\overline{\mathbf{R}} \begin{pmatrix} \Phi_u \\ \Psi_u \end{pmatrix}_{k+} \quad . \tag{1-43}$$

The other half of the scattering expression represents the upgoing waves at z_{k-} as

$$\begin{pmatrix} \Phi_u \\ \Psi_u \end{pmatrix}_{k-} = \mathbf{R} \begin{pmatrix} \Phi_d \\ \Psi_d \end{pmatrix}_{k-} + \overline{\mathbf{T}} \begin{pmatrix} \Phi_u \\ \Psi_u \end{pmatrix}_{k+} \quad . \tag{1-44}$$

Substitution into this representation with $\begin{pmatrix} \Phi_d \\ \Psi_d \end{pmatrix}_{k-}$ from equation (1-43) gives

$$\begin{pmatrix} \Phi_u \\ \Psi_u \end{pmatrix}_{k-} = \mathbf{R}\,\mathbf{T}^{-1} \begin{pmatrix} \Phi_d \\ \Psi_d \end{pmatrix}_{k+} + \left[\overline{\mathbf{T}} - \mathbf{R}\,\mathbf{T}^{-1}\overline{\mathbf{R}}\right] \begin{pmatrix} \Phi_u \\ \Psi_u \end{pmatrix}_{k+} \quad . \tag{1-45}$$

Then, at a depth z_k, the complete wave potentials in the upper layer k are described in terms of potential components in the lower layer $(k+1)$ by combining (1-43) and (1-45) as

$$\begin{pmatrix} \Phi_d \\ \Psi_d \\ \Phi_u \\ \Psi_u \end{pmatrix}_{k-} = \begin{pmatrix} \mathbf{T}^{-1} & -\mathbf{T}^{-1}\overline{\mathbf{R}} \\ \mathbf{R}\,\mathbf{T}^{-1} & \overline{\mathbf{T}} - \mathbf{R}\,\mathbf{T}^{-1}\overline{\mathbf{R}} \end{pmatrix} \begin{pmatrix} \Phi_d \\ \Psi_d \\ \Phi_u \\ \Psi_u \end{pmatrix}_{k+} \quad . \tag{1-46}$$

The sequence of physical effects for any individual term is to be read from right to left. Thus a matrix of a single interface wavefield propagator for potentials to propagate the total waves through a welded boundary in upward direction can be written as

$$\mathbf{Q}_u(z_k) = \mathbf{Q}(z_k^-, z_k^+) = \begin{pmatrix} \mathbf{T}^{-1} & -\mathbf{T}^{-1}\overline{\mathbf{R}} \\ \mathbf{R}\,\mathbf{T}^{-1} & \overline{\mathbf{T}} - \mathbf{R}\,\mathbf{T}^{-1}\overline{\mathbf{R}} \end{pmatrix}. \tag{1-47}$$

With a similar analysis, the downward interface propagator matrix is

$$\mathbf{Q}_d(z_k) = \mathbf{Q}(z_k^+, z_k^-) = \begin{pmatrix} \mathbf{T} - \overline{\mathbf{R}}\,\overline{\mathbf{T}}^{-1}\mathbf{R} & \overline{\mathbf{R}}\,\overline{\mathbf{T}}^{-1} \\ -\overline{\mathbf{T}}^{-1}\mathbf{R} & \overline{\mathbf{T}}^{-1} \end{pmatrix}. \tag{1-48}$$

If the elastic properties of the medium are continuous at z_k: $\mathbf{T} = \overline{\mathbf{T}} = \mathbf{I}$ and

$\mathbf{R} = \overline{\mathbf{R}} = \underline{\mathbf{0}}$, where $\mathbf{I}$ is the unit matrix of appropriate dimensionality. Then these two interface propagators satisfy

$$\mathbf{Q}_{\mathrm{I}}(z_k) = \mathbf{Q}(z_k^{\mp}, z_k^{\pm}) = \mathbf{I}. \qquad (1\text{-}49)$$

(a). Up and down interface propagators
between two uniform half spaces.

(b). Scattering matrix.
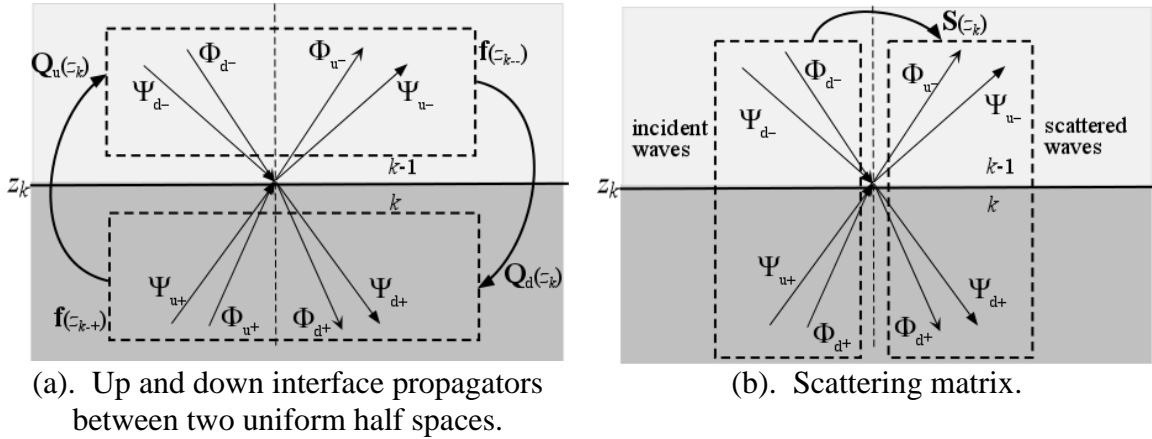
Figure 1-2. Pictorial comparison between the interface propagator
matrix and the scattering matrix.

Thus the interface propagator, $\mathbf{Q}_{\mathrm{I}}$, for a single interface embedded between two half spaces is merely a reformulation of the scattering matrix. The interface propagator relates wave systems above the interface to those below, while the scattering matrix relates the incident waves to scattered waves (Figure 1-2).

1.4.5. Composite scattering coefficients from propagator matrix

Nonetheless in a composite layer model, since all wavefields are taken into account, the propagator matrix includes all multiple scattering effects at any level. Let the scattering coefficients of stacked interfaces from the mth to the nth be designated by a square bracket around the coefficient letter with a subscript mn, e.g. a total reflection

matrix $[\mathbf{R}]_{mn} = \begin{pmatrix} [R_{\mathrm{pp}}] & [R_{\mathrm{sp}}] \\ [R_{\mathrm{ps}}] & [R_{\mathrm{ss}}] \end{pmatrix}_{mn}$.   In principle, if every incident plane wave at the

boundary is given, the complete scattered waves can be achieved merely using the scattering equation, 1-39.

The simplest case of stacked layers is a homogeneous layer inserted between the two half spaces, at z_k and z_{k+1}. So instead of a single interface as the previous example, here is a two-interface composite model that produces overall reflection and transmission coefficients. Note that unless the minus sign is indicated, the wave systems $\mathbf{f}(z_{k+1})$ are immediately below z_{k+1}, to omit the plus sign. Then similar to the single interface case, the wave potentials in the upper half space at z_k are represented as an upward propagation from the lower half space at z_{k+1}

$$
\begin{pmatrix} \Phi_d \\ \Psi_d \\ \Phi_u \\ \Psi_u \end{pmatrix}_{k-} = \begin{pmatrix} [\mathbf{T}]^{-1} & -[\mathbf{T}]^{-1}[\overline{\mathbf{R}}] \\ [\mathbf{R}][\mathbf{T}]^{-1} & [\overline{\mathbf{T}}]-[\mathbf{R}][\mathbf{T}]^{-1}[\overline{\mathbf{R}}] \end{pmatrix}_{k(k+1)} \begin{pmatrix} \Phi_d \\ \Psi_d \\ \Phi_u \\ \Psi_u \end{pmatrix}_{k+1}. \tag{1-50}
$$

In term of the wavefield propagator from equation 1-19:

$$
\mathbf{v}(z_k^-) = \mathbf{Q}(z_k^-, z_{k+1})\,\mathbf{v}(z_{k+1}) \tag{1-51}
$$

or

$$
\begin{pmatrix} \Phi_d \\ \Psi_d \\ \Phi_u \\ \Psi_u \end{pmatrix}_{k-} = \begin{pmatrix} \mathbf{Q}_{11}(z_k^-, z_{k+1}) & \mathbf{Q}_{12}(z_k^-, z_{k+1}) \\ \mathbf{Q}_{21}(z_k^-, z_{k+1}) & \mathbf{Q}_{22}(z_k^-, z_{k+1}) \end{pmatrix} \begin{pmatrix} \Phi_d \\ \Psi_d \\ \Phi_u \\ \Psi_u \end{pmatrix}_{k+1}, \tag{1-52}
$$

Due to the propagator chain rule from equation (1-12), this potential propagator can also be expanded into a product of interface propagators and a layer propagator:

$$
\mathbf{v}(z_k^-) = \mathbf{Q}_u(z_k)\mathbf{\Lambda}_k^{-1}\mathbf{Q}_u(z_{k+1})\,\mathbf{v}(z_{k+1}). \tag{1-53}
$$

When the homogeneous layer propagator from (1-36) and interface propagator from (1-47) are substituted, this becomes

$$
\begin{pmatrix} \Phi_d \\ \Psi_d \\ \Phi_u \\ \Psi_u \end{pmatrix}_{k-} = \begin{pmatrix} \mathbf{T}^{-1} & -\mathbf{T}^{-1}\overline{\mathbf{R}} \\ \mathbf{R}\,\mathbf{T}^{-1} & \overline{\mathbf{T}}-\mathbf{R}\,\mathbf{T}^{-1}\overline{\mathbf{R}} \end{pmatrix}_k \begin{pmatrix} \mathbf{\Lambda}_k^- & \underline{0} \\ \underline{0} & \mathbf{\Lambda}_k^+ \end{pmatrix} \begin{pmatrix} \mathbf{T}^{-1} & -\mathbf{T}^{-1}\overline{\mathbf{R}} \\ \mathbf{R}\,\mathbf{T}^{-1} & \overline{\mathbf{T}}-\mathbf{R}\,\mathbf{T}^{-1}\overline{\mathbf{R}} \end{pmatrix}_{k+1} \begin{pmatrix} \Phi_d \\ \Psi_d \\ \Phi_u \\ \Psi_u \end{pmatrix}_{k+1}
$$

$$
\tag{1-54}
$$

The result of matrix multiplication is elementally equated to the potential propagator in equation (1-50) and (1-52) in order to recover the expression of those overall scattering coefficients as follows:

$$
\mathbf{Q}_{11}(z_k^-, z_{k+1}): \quad [\mathbf{T}]_{k(k+1)}^{-1} \;=\; \mathbf{T}_k^{-1}\boldsymbol{\Lambda}_k^-\mathbf{T}_{k+1}^{-1} - \mathbf{T}_k^{-1}\overline{\mathbf{R}}_k\boldsymbol{\Lambda}_k^+\mathbf{R}_{k+1}\mathbf{T}_{k+1}^{-1}
$$
$$
=\; \mathbf{T}_k^{-1}\boldsymbol{\Lambda}_k^-\big[\mathbf{I} - \boldsymbol{\Lambda}_k^+\overline{\mathbf{R}}_k\boldsymbol{\Lambda}_k^+\mathbf{R}_{k+1}\big]\mathbf{T}_{k+1}^{-1} \quad . \tag{1-55}
$$

Therefore the composite transmission coefficient is

$$
[\mathbf{T}]_{k(k+1)} \;=\; \mathbf{T}_{k+1}\big[\mathbf{I} - \boldsymbol{\Lambda}_k^+\overline{\mathbf{R}}_k\boldsymbol{\Lambda}_k^+\mathbf{R}_{k+1}\big]^{-1}\boldsymbol{\Lambda}_k^+\mathbf{T}_k \quad . \tag{1-56}
$$

From the expression

$$
\mathbf{Q}_{21}(z_k^-, z_{k+1}): \quad [\mathbf{R}]_{k(k+1)}[\mathbf{T}]_{k(k+1)}^{-1} = \mathbf{R}_k\mathbf{T}_k^{-1}\boldsymbol{\Lambda}_k^-\mathbf{T}_{k+1}^{-1} + \big(\overline{\mathbf{T}} - \mathbf{R}\,\mathbf{T}^{-1}\overline{\mathbf{R}}\big)_k \boldsymbol{\Lambda}_k^+\mathbf{R}_{k+1}\mathbf{T}_{k+1}^{-1}
$$
$$
=\; \overline{\mathbf{T}}_k\boldsymbol{\Lambda}_k^+\mathbf{R}_{k+1}\mathbf{T}_{k+1}^{-1} + \mathbf{R}_k\mathbf{T}_k^{-1}\boldsymbol{\Lambda}_k^-\big[\mathbf{I} - \boldsymbol{\Lambda}_k^+\overline{\mathbf{R}}_k\boldsymbol{\Lambda}_k^+\mathbf{R}_{k+1}\big]\mathbf{T}_{k+1}^{-1}
$$
$$
\tag{1-57}
$$

the composite reflection coefficient is obtained:

$$
[\mathbf{R}]_{k(k+1)} \;=\; \overline{\mathbf{T}}_k\boldsymbol{\Lambda}_k^+\mathbf{R}_{k+1}\mathbf{T}_{k+1}^{-1}[\mathbf{T}]_{k(k+1)} + \mathbf{R}_k[\mathbf{T}]_{k(k+1)}^{-1}[\mathbf{T}]_{k(k+1)}
$$
$$
=\; \mathbf{R}_k + \overline{\mathbf{T}}_k\boldsymbol{\Lambda}_k^+\mathbf{R}_{k+1}\big[\mathbf{I} - \boldsymbol{\Lambda}_k^+\overline{\mathbf{R}}_k\boldsymbol{\Lambda}_k^+\mathbf{R}_{k+1}\big]^{-1}\mathbf{T}_k \tag{1-58}
$$

In a similar procedure, the wave potentials in the lower half space at z_{k+1} are related to those at z_k in the upper half space as

$$
\begin{pmatrix} \Phi_{\mathrm{d}} \\ \Psi_{\mathrm{d}} \\ \Phi_{\mathrm{u}} \\ \Psi_{\mathrm{u}} \end{pmatrix}_{k+1} = \begin{pmatrix} [\overline{\mathbf{T}}] - [\mathbf{R}][\mathbf{T}]^{-1}[\overline{\mathbf{R}}] & [\mathbf{R}][\mathbf{T}]^{-1} \\ -[\mathbf{T}]^{-1}[\overline{\mathbf{R}}] & [\mathbf{T}]^{-1} \end{pmatrix}_{(k+1)k} \begin{pmatrix} \Phi_{\mathrm{d}} \\ \Psi_{\mathrm{d}} \\ \Phi_{\mathrm{u}} \\ \Psi_{\mathrm{u}} \end{pmatrix}_{k-} . \tag{1-59}
$$

Then the downward propagator $\mathbf{Q}(z_{k+1}, z_k)$ is defined and applied with the chain rule expansion:

$$
\mathbf{v}(z_{k+1}) = \mathbf{Q}(z_{k+1}, z_k^-)\,\mathbf{v}(z_k^-) = \mathbf{Q}_{\mathrm{d}}(z_{k+1})\boldsymbol{\Lambda}_k\mathbf{Q}_{\mathrm{d}}(z_k)\,\mathbf{v}(z_k^-) \tag{1-60}
$$

while
$$
\begin{pmatrix} \Phi_{\mathrm{d}} \\ \Psi_{\mathrm{d}} \\ \Phi_{\mathrm{u}} \\ \Psi_{\mathrm{u}} \end{pmatrix}_{k+1} = \begin{pmatrix} \mathbf{Q}_{11}(z_{k+1},z_k^-) & \mathbf{Q}_{12}(z_{k+1},z_k^-) \\ \mathbf{Q}_{21}(z_{k+1},z_k^-) & \mathbf{Q}_{22}(z_{k+1},z_k^-) \end{pmatrix} \begin{pmatrix} \Phi_{\mathrm{d}} \\ \Psi_{\mathrm{d}} \\ \Phi_{\mathrm{u}} \\ \Psi_{\mathrm{u}} \end{pmatrix}_{k-} . \tag{1-61}
$$

Substitute the layer propagator and interface propagator into the expansion and equation (1-60) becomes

$$
\begin{pmatrix} \Phi_{\mathrm{d}} \\ \Psi_{\mathrm{d}} \\ \Phi_{\mathrm{u}} \\ \Psi_{\mathrm{u}} \end{pmatrix}_{k+1} = \begin{pmatrix} \mathbf{T}-\overline{\mathbf{R}}\,\overline{\mathbf{T}}^{-1}\mathbf{R} & \overline{\mathbf{R}}\,\overline{\mathbf{T}}^{-1} \\ -\overline{\mathbf{T}}^{-1}\mathbf{R} & \overline{\mathbf{T}}^{-1} \end{pmatrix}_{k+1} \begin{pmatrix} \mathbf{\Lambda}_k^+ & \underline{0} \\ \underline{0} & \mathbf{\Lambda}_k^- \end{pmatrix} \begin{pmatrix} \mathbf{T}-\overline{\mathbf{R}}\,\overline{\mathbf{T}}^{-1}\mathbf{R} & \overline{\mathbf{R}}\,\overline{\mathbf{T}}^{-1} \\ -\overline{\mathbf{T}}^{-1}\mathbf{R} & \overline{\mathbf{T}}^{-1} \end{pmatrix}_k \begin{pmatrix} \Phi_{\mathrm{d}} \\ \Psi_{\mathrm{d}} \\ \Phi_{\mathrm{u}} \\ \Psi_{\mathrm{u}} \end{pmatrix}_{k-} .
$$

$$\tag{1-62}$$

The overall transmission and reflection matrices of the incidence from below can be obtained again by matching the matrix elements between equation (1-59) and (1-62):

$$
\mathbf{Q}_{12}(z_{k+1},z_k^-): \qquad [\mathbf{T}]_{(k+1)k}^{-1} = \overline{\mathbf{T}}_{k+1}^{-1}\mathbf{\Lambda}_k^-\mathbf{T}_k^{-1} - \mathbf{T}_{k+1}^{-1}\overline{\mathbf{R}}_{k+1}\mathbf{\Lambda}_k^+\mathbf{R}_k\mathbf{T}_k^{-1}
$$
$$
= \mathbf{T}_{k+1}^{-1}\mathbf{\Lambda}_k^-\big[\mathbf{I}-\mathbf{\Lambda}_k^+\overline{\mathbf{R}}_{k+1}\mathbf{\Lambda}_k^+\mathbf{R}_k\big]\mathbf{T}_k^{-1} , \tag{1-63}
$$

$$
[\overline{\mathbf{T}}]_{(k+1)k} = \overline{\mathbf{T}}_k\big[\mathbf{I}-\mathbf{\Lambda}_k^+\mathbf{R}_{k+1}\mathbf{\Lambda}_k^+\overline{\mathbf{R}}_k\big]^{-1}\mathbf{\Lambda}_k^+\overline{\mathbf{T}}_{k+1} . \tag{1-64}
$$

$$
\mathbf{Q}_{22}(z_{k+1},z_k^-): \qquad [\overline{\mathbf{R}}]_{(k+1)k} = \overline{\mathbf{R}}_{k+1} + \mathbf{T}_{k+1}\mathbf{\Lambda}_k^+\overline{\mathbf{R}}_k\big[\mathbf{I}-\mathbf{\Lambda}_k^+\mathbf{R}_{k+1}\mathbf{\Lambda}_k^+\overline{\mathbf{R}}_k\big]^{-1}\mathbf{T}_{k+1} . \tag{1-65}
$$

The composite coefficient matrices for incidence from below have similar structures to the related ones for incidence from above. It is the presence of the phase delay factor, $\mathbf{\Lambda}_k^+$, in these expressions that makes them frequency dependent. Thus though the Zoeppritz equations are independent of frequency, the composite reflection and transmission coefficients are not.

Most details about scattering coefficients both of the single interface and the layer stackshave already been discussed by Kennett (1983, ch.5-6). As stated previously, the objective of this study is to understand the basic similarities and differences between major modeling methods and the phase shift cascade. One major difference between the

propagator matrix method and phase shift cascade lies here in the use of the inverse matrix or a *reverberation operator*, appearing in every coefficient formula.

The reverberation operator (Kennett, 1983, p.131), $\left[\mathbf{I} - \mathbf{\Lambda}_k^+ \overline{\mathbf{R}}_k \mathbf{\Lambda}_k^+ \mathbf{R}_{k+1}\right]^{-1}$ generates all internal reflections and mode conversions in a layer bounded between kth and $(k+1)$th interfaces. The operator can be expanded in a power series as

$$\left[\mathbf{I} - \mathbf{\Lambda}_k^+ \overline{\mathbf{R}}_k \mathbf{\Lambda}_k^+ \mathbf{R}_{k+1}\right]^{-1} = \mathbf{I} + \mathbf{\Lambda}_k^+ \overline{\mathbf{R}}_k \mathbf{\Lambda}_k^+ \mathbf{R}_{k+1} + \mathbf{\Lambda}_k^+ \overline{\mathbf{R}}_k \mathbf{\Lambda}_k^+ \mathbf{R}_{k+1} \mathbf{\Lambda}_k^+ \overline{\mathbf{R}}_k \mathbf{\Lambda}_k^+ \mathbf{R}_{k+1} + \dots.$$

(1-66)

Each successive term, other than the leading term, introduces a further internal reaction between z_k and z_{k+1} by including two more layer effects (phase delays) and one of each interface effect from the upper and lower bounds. The development of the composite transmission coefficient from interfaces k and $(k+1)$ is shown in Figure 1-3 as an example. The total response to an incident field can be considered as the sum of contributions from each term in the series. If the series is truncated after a finite number of terms then such approximation only includes a finite number of internal reverberations. The phase shift cascade method is equivalent to a finite truncation of this series.

The construction of overall coefficient matrices for the whole stack of homogeneous layers can be done in either recursive or propagator schemes (Kennett, 1983, ch.6). They both produce all peg-leg events possible from every layer.
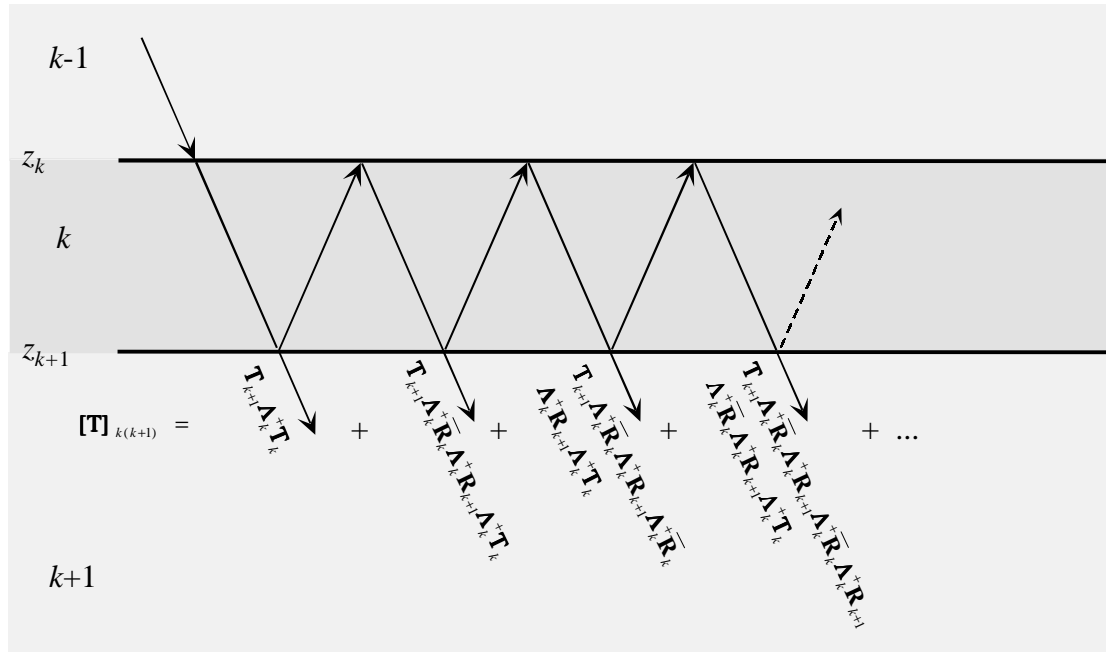
Figure 1-3. Composite transmission coefficient of a homogeneous layer embedded in between the uniform half spaces shown multiple scattering effects from the reverberation operator.

1.4.6. Example of propagator matrix application

The overall wavefields in layer m-1 at z_m and can be related to those in layer n at z_n, where $z_n > z_m$ as

$$\mathbf{f}(z_m^-) = \prod_{k=n}^{m} \mathbf{P}(z_{k-1}, z_k)\mathbf{f}(z_n) \qquad (1\text{-}67)$$

If every propagator $\mathbf{P}(z_k, z_{k+1})$ transfers the whole wavefield from the bottom of layer k up through the interface k to the bottom of layer k-1, by the application of the propagator chain rule, it is merely a product of the kth interface upward propagator and the kth inverse layer propagator

$$\mathbf{f}(z_m^-) = \mathbf{D}(z_m^-)\left[\prod_{k=n}^{m}\left[\mathbf{Q}_u(z_k)\mathbf{\Lambda}_k^{-1}\right]\mathbf{Q}_u(z_n)\right]\mathbf{D}^{-1}(z_n)\mathbf{f}(z_n). \qquad (1\text{-}68)$$

In the opposite direction, the propagator equation is written as

$$\mathbf{f}(z_n) = \mathbf{D}(z_n)\left[\mathbf{Q}_\mathrm{d}(z_n)\prod_{k=m}^{n-1}\left[\mathbf{\Lambda}_k\mathbf{Q}_\mathrm{d}(z_k)\right]\right]\mathbf{D}^{-1}(z_m^-)\mathbf{f}(z_m^-).$$ (1-69)

An application of propagator technique is to compute the overall responses from composite homogeneous stacked layers embedded between uniform half spaces or a free surface. In the lower uniform region, a radiation condition is imposed that the wavefield should only be downward traveling waves or evanescent waves decaying with depth, depending on the horizontal slowness (Kennett, 1983, p.158). The reflection and transmission coefficients are defined by relating the up and downgoing wave amplitudes in the upper and lower half spaces starting with the radiation conditions. The coefficient matrices are constructed under the basis of efficient recursive schemes, which can be derived from the chain rule for the wave-propagator.

A simple procedure for calculating the response of a stratified elastic half space to the stimulation of a P source in the upper half space can be conducted as follows. Let the initial condition which represents a unit amplitude downgoing P waves at the top of the stacked layers be

$$\mathbf{w}_{z_m^- t_0} = \begin{pmatrix} 1 & 0 & 0 & 0 \end{pmatrix}.$$ (1-70)

The arriving P and S responses at the surface are then separated into total R_pp and R_ps. At the stratification bottom, the radiation condition is also set up to exclude the upcoming waves. Therefore the boundary conditions for the harmonic plane waves at z_m in the (m-1)th layer and at z_n in layer n are reduced to

$$\mathbf{w}_m^- = \begin{pmatrix} 1 \\ 0 \\ [R_\mathrm{pp}] \\ [R_\mathrm{ps}] \end{pmatrix}, \qquad \mathbf{w}_n = \begin{pmatrix} [T_\mathrm{pp}] \\ [T_\mathrm{ps}] \\ 0 \\ 0 \end{pmatrix}.$$ (1-71)

The surface displacement now is expressed in terms of the downgoing wavefields at z_0 as

$$\mathbf{f}(z_m^-) = \mathbf{P}(z_m^-, z_n)\mathbf{f}(z_n)$$ (1-72)

$$\mathbf{w}_m^- \mathbf{F}_m = \mathbf{P}(z_m^-, z_n)\mathbf{F}_n \mathbf{w}_n$$ (1-73)

$$\begin{pmatrix} 1 \\ 0 \\ [R_{\text{pp}}] \\ [R_{\text{ps}}] \end{pmatrix} = \mathbf{F}_m^{-1} \mathbf{P}(z_m^-, z_n) \, \mathbf{F}_n \begin{pmatrix} [T_{\text{pp}}] \\ [T_{\text{ps}}] \\ 0 \\ 0 \end{pmatrix} \qquad (1\text{-}74)$$

There are four equations with four unknowns. A particular coefficient can be directly obtained. The explicit formulae for every element of the inverse $\mathbf{E}^{-1}$ matrix is given by Aki and Richards (1980, p.167) for P-SV problem as in equations 1-17 and 1-18.

CHAPTER **2**

Theory of 2-D elastic seismogram construction by the phase shift cascade method

2.1. Basic Wave Equations

The elastic wave equation for a homogeneous and isotropic medium is a vector equation of motion written as

$$r\ddot{u} = (l + m)\overline{\nabla}(\overline{\nabla} \cdot u) + m\overline{\nabla}^2 u \tag{2-1}$$

where u is a particle displacement vector, l and m are the Lame elastic parameters and r is the density of material the wave is traveling through. By Helmholtz's theorem we represent the displacement field (Lay and Wallace, 1995, p.54) as

$$u = \overline{\nabla}\phi + \overline{\nabla} \times y = u_{\mathrm{p}} + u_{\mathrm{s}} \tag{2-2}$$

where f is a curl-free scalar potential field $(\overline{\nabla} \times f = 0)$ and y is a divergenceless vector potential field $(\overline{\nabla} \cdot y = 0)$. P-wave displacement ($u_p$) is obtained from $\overline{\nabla} f$ and S-wave displacement (u_s) from $\overline{\nabla} \times y$. Substituting equation (2-2) into equation (2-1), using the vector identity (Bath and Berkout, 1984, p.9)

$$\nabla^2 \boldsymbol{u} = \overline{\nabla}(\overline{\nabla} \cdot \boldsymbol{u}) - (\overline{\nabla} \times \overline{\nabla} \times \boldsymbol{u}) \tag{2-3}$$

and assuming λ, μ, ρ constant separates the elastic wave equation into two wave equations for P-wave and S-wave potentials

$$\ddot{\boldsymbol{f}} = \boldsymbol{a}^2 \nabla^2 \boldsymbol{f} \tag{2-4}$$

where
$$\boldsymbol{a} = \sqrt{\frac{\boldsymbol{l} + 2\boldsymbol{m}}{\boldsymbol{r}}} \tag{2-5}$$

and
$$\ddot{\boldsymbol{y}} = \boldsymbol{b}^2 \nabla^2 \boldsymbol{y} \tag{2-6}$$

where
$$\boldsymbol{b} = \sqrt{\frac{\boldsymbol{m}}{\boldsymbol{r}}} . \tag{2-7}$$

Equation (2-4) is a scalar wave equation for $\boldsymbol{f}$ and uses the P-wave velocity, $\boldsymbol{a}$. The vector wave equation in (2-5) has a vector solution $\boldsymbol{y}$ and uses $\boldsymbol{b}$, the shear wave velocity. Thus, the potentials in the wave equation are separated into P and S components, each of which involve one wave velocity at a time. Therefore, it is simpler to solve the elastic wave equation using potentials for the elastic displacement than directly. Once the potentials are determined, displacements can be computed from equation (2-2).

2.2. Solutions for Potentials

In two dimensions with Cartesian coordinates (see Aki and Richards, 1980, p.128-129, for complete discussions), the vector potential for an SV-wave has only one component, $\boldsymbol{y} = (0, \boldsymbol{y}(x,z,t), 0)$, with displacement

$$\boldsymbol{u}_s = \overline{\nabla} \times \boldsymbol{y} = (-\frac{\partial \boldsymbol{y}}{\partial z}, 0, \frac{\partial \boldsymbol{y}}{\partial x}) . \tag{2-8}$$

When equation (2-8) is substituted into (2-6), the vector wave equation in (2-6) is reduced to a scalar form as

$$\ddot{\boldsymbol{y}}(x,z,t) = \boldsymbol{b}^2 \nabla^2 \boldsymbol{y}(x,z,t) . \tag{2-9}$$

For a P-wave, $\boldsymbol{f} = \boldsymbol{f}(x,z,t)$ and the displacement is

$$\boldsymbol{u}_p = \overline{\nabla}\boldsymbol{f} = (\frac{\partial \boldsymbol{f}}{\partial x},0,\frac{\partial \boldsymbol{f}}{\partial z}) . \qquad (2\text{-}10)$$

Now the solution to equation (2-4) will be developed using a Fourier method. The P-wave potential is represented as a Fourier plane wave superposition by

$$\phi(x,z,t) = \left(\tfrac{1}{2\pi}\right)^2 \int \int_{-\infty}^{\infty} \Phi(k_x,z,\omega)e^{i(k_x x-\omega t)} dk_x d\omega \qquad (2\text{-}11)$$

where $\boldsymbol{w}$ is an angular frequency and k_x is an angular horizontal wavenumber. In this expression, Φ is the Fourier spectrum of $\boldsymbol{f}$ and represents the contribution of each Fourier plane wave, $e^{i(k_x x-\boldsymbol{w} t)}$, to the construction of $\boldsymbol{f}$. A wave equation for a plane wave Φ can be derived by substituting equation (2-11) into equation (2-4). After some manipulation and assuming $\boldsymbol{a}$ is constant, we obtain

$$\int \int_{-\infty}^{\infty} [-k_x^2 \Phi + \frac{\partial^2 \Phi}{\partial z^2} + \frac{\boldsymbol{w}^2}{\boldsymbol{a}^2} \Phi]e^{i(k_x x-\boldsymbol{w} t)} dk_x d\boldsymbol{w} = 0 . \qquad (2\text{-}12)$$

This can only be satisfied for all k_x and $\boldsymbol{w}$, by requiring the term in brackets to vanish. Thus

$$\frac{\partial^2 \Phi}{\partial z^2} = -k_z^2 \Phi \qquad (2\text{-}13)$$

where k_z is an angular vertical wavenumber given by

$$k_z^2 = \frac{\boldsymbol{w}^2}{\boldsymbol{a}^2} - k_x^2 . \qquad (2\text{-}14)$$

Equation (2-13) is an ordinary differential equation for the spectrum Φ. Its general solution can be verified by substitution to be

$$\Phi(k_x,z,\omega) = A(k_x,\omega)e^{ik_z z} + B(k_x,\omega)e^{-ik_z z} \qquad (2\text{-}15)$$

where k_z is the positive square root of (2-14). Here, A and B represent the strengths of waves traveling in the $+z$ direction (downward) and $-z$ direction (upward) respectively. Since equation (2-13) is a second order differential equation, two such undetermined quantities are expected to be calculated from the boundary conditions for a particular

problem. Finally, a general solution for the P-wave potential of equation (2-4) is obtained by substituting equation (2-15) into (2-11) to get

$$\phi(x,z,t) = \left(\tfrac{1}{2\pi}\right)^2 \int \int_{-\infty}^{\infty} (A(k_x,\omega)e^{ik_z z} + B(k_x,\omega)e^{-ik_z z})e^{i(k_x x - \omega t)}\,dk_x\,d\omega \qquad (2\text{-}16)$$

Note that the sign convention for Fourier transforms follows that used in solving wave-propagation problems relevant to seismology by Aki and Richards (1980, p.129-130). In equation (2-16), the exponential term, for positive real k_x and k_z, is a plane wave propagating in the direction of increasing x and z. When k_z is imaginary, the exponential in (2-16) changes from a complex sinusoid to a growing or decaying real exponential. Therefore, the sign of the imaginary k_z is chosen to be positive so that these waves are not physically increasing with vertical distance. Plane waves associated with this imaginary k_z are called evanescent waves. Thus, in summary, k_z is given by

$$k_z = \begin{cases} \sqrt{\dfrac{w^2}{a^2} - k_x^2}\ , & \dfrac{w^2}{a^2} \geq k_x^2 \\[3mm] i\sqrt{k_x^2 - \dfrac{w^2}{a^2}}\ , & \dfrac{w^2}{a^2} < k_x^2 \end{cases} \qquad (2\text{-}17)$$

In a similar process, equation (2-6) can be solved for the S-wave potential, $y(x,z,t)$, and expressed in the Fourier domain as:

$$\Psi(k_x,z,\omega) = C(k_x,\omega)e^{ik_z z} + D(k_x,\omega)e^{-ik_z z} \qquad (2\text{-}18)$$

and in the space-time domain as

$$\psi(x,z,t) = \left(\tfrac{1}{2\pi}\right)^2 \int \int_{-\infty}^{\infty} (C(k_x,\omega)e^{ik_z z} + D(k_x,\omega)e^{-ik_z z})e^{i(k_x x - \omega t)}\,dk_x\,d\omega \qquad (2\text{-}19)$$

where k_z has essentially the same interpretation as for the P-wave in equation (2-17) except that the velocity changes from a to b:

$$k_z = \begin{cases} \sqrt{\dfrac{\omega^2}{\beta^2} - k_x^2} \quad , & \dfrac{\omega^2}{\beta^2} \geq k_x^2 \\[4mm] i\sqrt{k_x^2 - \dfrac{\omega^2}{\beta^2}} \quad , & \dfrac{\omega^2}{\beta^2} < k_x^2 \end{cases} \cdot \tag{2-20}$$

Considering a monochromatic plane P wave at a depth z in a homogeneous medium, $\Phi(k_x, z, \omega)$, equation (2-15) suggests it contains two wavefields, downgoing and upgoing:

$$\Phi(k_x, z, \omega) = \Phi_d(k_x, z, \omega) + \Phi_u(k_x, z, \omega) \tag{2-21}$$

where $_d$ $+ k_z$ Φ_u the second

term with $-k_z$ $z = z + \Delta$ Δz

each wave component of Φ k $, z, \omega$ can be traced upward or downward in depth (and

$$\Delta z$$

histories of both wave components, Φ k $, z, \omega$ has to be arranged in terms of

$\Phi_{dc}(z - \Delta z)$, and upcoming waves from below,

$\Phi_{uc}(z + \Delta z)$. After some basic manipulations of equations (2-15) and (2-21), the history of a plane P wave at a depth z is restored to predict $\Phi(k_x, z, \omega)$ as

$$\Phi(k_x, z, \omega) = \Phi_{dc}(z - \Delta z)e^{ik_z\Delta z} + \Phi_{uc}(z + \Delta z)e^{ik_z\Delta z} . \tag{2-22}$$

On the other hand, a backward derivation is obtained to bring back $\Phi(k_x, z, \omega)$ in terms of a downgoing wave at $z + \Delta z$ and an upgoing wave at $z - \Delta z$ as

$$\Phi(k_x, z, \omega) = \Phi_{dg}(z + \Delta z)e^{-ik_z\Delta z} + \Phi_{ug}(z - \Delta z)e^{-ik_z\Delta z} , \tag{2-23}$$

which has been used in phase shift migration (Gazdag, 1978).

The term $e^{ik_z\Delta z}$ in equation (2-22), which is called the phase shift extrapolator, delays the phase of $\Phi_{dg}(z)$ for $\Phi_{dg}(z + \Delta z)$ and of $\Phi_{ug}(z)$ for $\Phi_{ug}(z - \Delta z)$, according to a depth interval Δz. Equation (2-22) is then used to extrapolate a downgoing

component from $z + \Delta z$ and an upgoing component from $z - \Delta z$ for a forward modeling of $\Phi(k_x, z, \omega)$. The forward phase-shift equation for an S wave is achieved by the same consideration from equation (2-18) and written as

$$\Psi(k_x, z, \omega) = \Psi_{dc}(z - \Delta z)e^{ik_z\Delta z} + \Psi_{uc}(z + \Delta z)e^{ik_z\Delta z}$$

(2-24)

where $$\Psi(k_x, z, \boldsymbol{w}) = \Psi_d(k_x, z, \boldsymbol{w}) + \Psi_u(k_x, z, \boldsymbol{w})$$ (2-25)

and k_z for S wave is given by equation (2-20).

2.3. Scattering Considerations

In the phase-shift cascade method, equation (2-22) is used for a P-wave and (2-24) for an S wave to recursively extrapolate each Fourier plane wave from a surface source downward to reflectors and from reflectors upward to the surface. Four possible wave fields in equation (2-15) and (2-18), corresponding to up and downgoing P and S potentials, are maintained along the calculation path. At every interface, the complex amplitudes $A, B, C,$ and D must be redetermined by four boundary conditions for four unknowns. Fortunately, this work has been formulated into a set of amplitude ratios of resulting waves to their incident waves. These ratios are called reflection and transmission coefficients. In terms of displacements, the Zoeppritz equations are derived for these 16 coefficients in a P-SV plane wave system at a plane interface (Aki and Richard, p.144). The system consists of four possible incident waves and their four resulting scattered waves as shown in Figure 2-1.
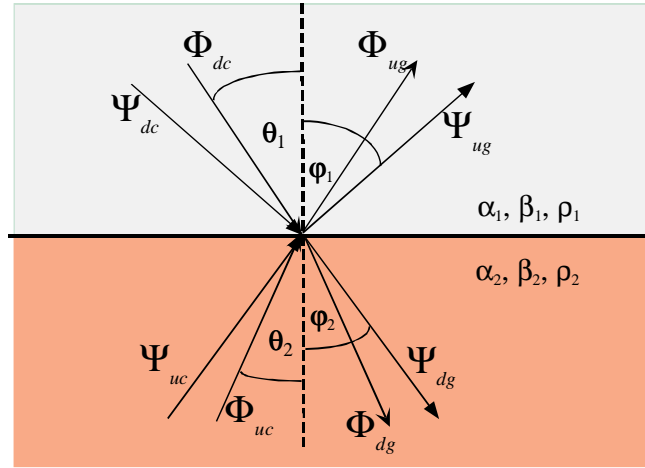
Figure 2-1. Incoming and outgoing P and S potentials at a
computation node

In Figure(2-1), denotation "*d*" is for down and "*u*" for up in the directions of propagation, "*c*" for coming or incident waves and "*g*" for going or resultant waves as their current status. In order to solve this P-SV problem, these four boundary conditions are applied for each incident wave:

continuity of vertical displacement : $\displaystyle\sum_{medium1} U_z = \sum_{medium2} U_z$ (2-26)

continuity of horizontal displacement $\displaystyle\sum_{medium1} U_x = \sum_{medium2} U_x$ (2-27)

continuity of normal stress : $\displaystyle\sum_{medium1} t_{zz} = \sum_{medium2} t_{zz}$ (2-28)

continuity of tangential stress : $\displaystyle\sum_{medium1} t_{zx} = \sum_{medium2} t_{zx}$ (2-29)

where *U* symbolizes a displacement magnitude for a monochromatic component of the Fourier transform of *u*. The complete results for all incident waves and full discussion are given in Aki and Richards, p.144-151. The reflection coefficients are modified and summarized in a scattering matrix in the following text. The Zoeppritz equations determine the displacement amplitudes of the reflected and refracted plane waves. In order to apply them to the wave potentials which are preferred to work with, an amplitude relation between displacement and potential, given by Aki and Richards (p.139), is required

$$A_U = \frac{w}{a} A_\Phi = \frac{w}{b} A_\Psi \tag{2-30}$$

where A_U, A_Φ and A_Ψ are the amplitudes of total displacement, P-wave potential and S-wave potential, respectively, for a plane wave. Equation (2-30) can be obtained by taking spatial derivatives of the wave potential for the displacement as written in equations (2-8) and (2-10) of P and S waves. For Fourier plane waves, these spatial derivatives are merely vertical and/or horizontal wavenumbers with 90 degree phase shifts. Then the vector magnitude of displacement is computed and using equation (2-14) gives the relationship in (2-30). Since the reflection coefficients are amplitude ratios of scattered waves to incident waves, the coefficients obtained from Zoeppritz equations can be modified for potential by multiplying by a ratio of a scattering velocity to an incident velocity. Let subscripts i and s indicate a type (P or S) of an incident and a scattered waves, respectively and v is a velocity $(a_1, a_2, b_1, and, b_2)$ of the subscripted wave for the medium 1 or 2 in which it is traveling. Then a general relation between reflection or transmission coefficients for potential and displacement can be written as

$$R_{is}(\Phi) = \frac{v_s}{v_i} R_{is}(U) . \tag{2-31}$$

Thus, the algorithm is expressed completely in terms of elastic potentials with displacements computed at the end, if desired.

Now the relation between four outgoing potential wavefields (on the left-hand side of the equation) and four incoming potential wavefields at an interface can be expressed by a matrix equation as

$$\begin{bmatrix} \Phi_{dg} \\ \Psi_{dg} \\ \Phi_{ug} \\ \Psi_{ug} \end{bmatrix} = \begin{bmatrix} T_{pp} & T_{sp} & \overline{R}_{pp} & \overline{R}_{sp} \\ T_{ps} & T_{ss} & \overline{R}_{ps} & \overline{R}_{ss} \\ R_{pp} & R_{sp} & \overline{T}_{pp} & \overline{T}_{sp} \\ R_{ps} & R_{ss} & \overline{T}_{ps} & \overline{T}_{ss} \end{bmatrix} \begin{bmatrix} \Phi_{dc} \\ \Psi_{dc} \\ \Phi_{uc} \\ \Psi_{uc} \end{bmatrix} . \tag{2-32}$$

In this expression, T_{sp} is, for example, the transmission coefficient for an S wave converting to a P wave where the S wave is an incident from above and $\overline{T}_{sp}$ is similar

except that the S wave is incident from below. The scattering matrix summarizes all possible reflection and transmission coefficients in a (4×4) matrix where each row represents four contributions from the four incident waves to a particular type of resultant wave. This explicit formulation allows us to acquire various desired physical results with selective contributions. This is a major advantage of the phase shift cascade over other wave equation based methods. For example, if it is required to have merely P and converted primaries and to suppress all multiples, those reflection coefficients of the upcoming waves in scattering matrix shall be set to zero. Then equation (2-32) becomes

$$
\begin{bmatrix} \Phi_{dg} \\ \Psi_{dg} \\ \Phi_{ug} \\ \Psi_{ug} \end{bmatrix} = \begin{bmatrix} T_{pp} & T_{sp} & 0 & 0 \\ T_{ps} & T_{ss} & 0 & 0 \\ R_{pp} & R_{sp} & \overline{T}_{pp} & \overline{T}_{sp} \\ R_{ps} & R_{ss} & \overline{T}_{ps} & \overline{T}_{ss} \end{bmatrix} \begin{bmatrix} \Phi_{dc} \\ \Psi_{dc} \\ \Phi_{uc} \\ \Psi_{uc} \end{bmatrix}.
\tag{2-33}
$$

If mode conversions are not desired:

$$
\begin{bmatrix} \Phi_{dg} \\ \Psi_{dg} \\ \Phi_{ug} \\ \Psi_{ug} \end{bmatrix} = \begin{bmatrix} T_{pp} & 0 & \overline{R}_{pp} & 0 \\ 0 & T_{ss} & 0 & \overline{R}_{ss} \\ R_{pp} & 0 & \overline{T}_{pp} & 0 \\ 0 & R_{ss} & 0 & \overline{T}_{ss} \end{bmatrix} \begin{bmatrix} \Phi_{dc} \\ \Psi_{dc} \\ \Phi_{uc} \\ \Psi_{uc} \end{bmatrix}.
\tag{2-34}
$$

If, at some nodes, primaries are preferable without mode conversion, equation (2-33) is combined with (2-34) to give

$$
\begin{bmatrix} \Phi_{dg} \\ \Psi_{dg} \\ \Phi_{ug} \\ \Psi_{ug} \end{bmatrix} = \begin{bmatrix} T_{pp} & 0 & 0 & 0 \\ 0 & T_{ss} & 0 & 0 \\ R_{pp} & 0 & \overline{T}_{pp} & 0 \\ 0 & R_{ss} & 0 & \overline{T}_{ss} \end{bmatrix} \begin{bmatrix} \Phi_{dc} \\ \Psi_{dc} \\ \Phi_{uc} \\ \Psi_{uc} \end{bmatrix}.
\tag{2-35}
$$

In case that only P-S converted primaries should be designed for, the scattering matrix expression becomes:

$$
\begin{bmatrix} \Phi_{dg} \\ \Psi_{dg} \\ \Phi_{ug} \\ \Psi_{ug} \end{bmatrix} = \begin{bmatrix} T_{pp} & 0 & 0 & 0 \\ 0 & 0 & 0 & 0 \\ 0 & 0 & 0 & 0 \\ R_{ps} & 0 & 0 & T_{ss}^{-} \end{bmatrix} \begin{bmatrix} \Phi_{dc} \\ \Psi_{dc} \\ \Phi_{uc} \\ \Psi_{uc} \end{bmatrix}.
\tag{2-36}
$$

There are many possibilities that similar manipulations of the scattering matrix can isolate or exclude some other physical effects. Some examples of this application are shown in section 3.3.

2.4. Source Representation

In the real world, it is impractical to generate plane waves but, mathematically, it is difficult to deal directly with spherical waves. Fortunately, for a horizontally homogeneous medium, we can use Fourier analysis to decompose the spherical wave of the real world into a sum of harmonic plane waves in our numerical world. However, the boundless span with constant amplitude of a harmonic plane wave could give us an enormous energy, which is not physical. For a realistic source, to have finite energy, we implement the Weyl integral (Brekhovskikh, 1980, p.228-231). It describes a point source in a three-dimensional spectral domain by defining a radial-dependent amplitude attenuation for each plane wave for a harmonic spherical wave expansion. The potential for a spherical wave emanating from a point source in a homogeneous material is given by the Weyl integral:

$$\frac{e^{i(kR-\mathbf{w}t)}}{R} = \frac{i}{2\mathbf{p}} \int\int_{-\infty}^{\infty} e^{i(k_x x + k_y y \pm k_z z - \mathbf{w}t)} \frac{dk_x dk_y}{k_z} \qquad (2\text{-}37)$$

where $R = \sqrt{x^2 + y^2 + z^2}$ and $k = \sqrt{k_x^2 + k_y^2 + k_z^2}$. The plus or minus sign of k_z corresponds to direction of wave propagation in positive or negative depth, respectively, as discussed earlier.

A pulsed spherical wave is realized by multiplying a harmonic spherical wave in this expression with a complex wavelet spectrum and summing harmonic spherical waves in equation (2-37) over frequency (Tygel and Hubral, 1987, p.40). It is equivalent to convolving an impulsive spherical wave with a wavelet in the time domain. In two dimensions, we can summarize an expression for a wave potential for a pulsed point source in a form parallel to the wave solution in (2-16) by setting $k_y = 0$

$$w(t) * \int_{-\infty}^{\infty} \frac{e^{i(kr-\textbf{w}t)}}{\text{r}} d\textbf{w} = \left(\frac{1}{2\textbf{p}}\right)^2 \int_{-\infty}^{\infty} W(\textbf{w}) \int_{-\infty}^{\infty} (\frac{i}{k_z} e^{i(k_x x + k_z z - \textbf{w}t)} + \frac{i}{k_z} e^{i(k_x x - k_z z - \textbf{w}t)}) dk_x d\textbf{w},$$

(2-38)

where an inverse Fourier transform over ω is performed explicitly. Substitute $k = \dfrac{\textbf{w}}{v}$ in the exponential argument on the left-hand side of this equation and the integration becomes an impulsive cylindrical wave function:

$$w(t) * \frac{\textbf{d}(r/v - t)}{r} = \left(\frac{1}{2\textbf{p}}\right)^2 \int_{-\infty}^{\infty} W(\textbf{w}) \int_{-\infty}^{\infty} (\frac{i}{k_z} e^{i(k_x x + k_z z - \textbf{w}t)} + \frac{i}{k_z} e^{i(k_x x - k_z z - \textbf{w}t)}) dk_x d\textbf{w} \quad \text{(2-39)}$$

where $w(t)$ is a wavelet function, $W(\textbf{w})$ is a wavelet spectrum, $r = \sqrt{x^2 + z^2}$, and $k = \sqrt{k_x^2 + k_z^2}$. Compare equation (2-38) to the wave solutions in (2-16) for P wave and (2-19) for S wave. If a pulsed point source for a cylindrical P-wave is evaluated at the surface $(z = 0)$ and no attention is paid to the upgoing waves above surface, then a point source of P-wave becomes:

$$\textbf{f}(x,0,t) = w(t) * \frac{\textbf{d}(x/v - t)}{x}, \tag{2-40}$$

$$\textbf{y}(x,0,t) = 0, \tag{2-41}$$

$$\Psi(k_x,0,\textbf{w}) = 0, \qquad (C = 0, \ D = 0), \tag{2-42}$$

and
$$\Phi(k_x,0,\omega) = A(k_x,\omega)e^{i(k_x x - \omega t)}, \qquad (B = 0), \tag{2-43}$$

where
$$A(k_x,\omega) = W(\omega)S(k_x,\omega) = \frac{i}{k_{z1}} W(\omega) \tag{2-44}$$

and a source term
$$S(k_x,\omega) = \frac{i}{k_{z1}} = \frac{i}{\sqrt{\dfrac{\omega^2}{\alpha_1^2} - k_x^2}}. \tag{2-45}$$

Therefore, the boundary condition on Φ for a point source in 2-D is:

$$\Phi(k_x, 0, \omega) = \frac{i}{k_{z1}} W(\omega) e^{i(k_x x - \omega t)}$$

(2-46)

The source term is evaluated at the surface for this boundary condition. Therefore the P-wave velocity in (2-45) is a_1 for the layer where the source is located. It is, then, independent of depth while the initial plane wave propagates up and down through the media. The wavelet term $W(w)$ depends only on frequency. So these two functions can simply multiply to the output (k_x, w) spectrum at the end of the extrapolation process. An S-wave point source can be emanated, which with a similar consideration, a statement for such source term is

$$\Psi(k_x, 0, \omega) = \frac{i}{k_{z1}} W(\omega) e^{i(k_x x - \omega t)}$$

(2-47)

where the velocity in equation (2-45) for k_{z1} is β_1. In the case both P and S sources are required, the source term is a combination of equation (2-46) and (2-47).

The derivation of equation (2-37) suggests there must be inhomogeneous plane waves propagating in the horizontal plane with a vertical wavenumber which converges to zero at the critical angle, and most rapidly attenuates in the vertical direction. Such waves correspond to a complex angle of incidence (Bath and Berkout, 1984, p.191). They have to be included for this expansion of cylindrical wave emanating from a point source into plane waves. This type of wave was referred to earlier as an evanescent wave, in the discussion of imaginary vertical wavenumbers, equation (2-17). The effects of this type of wave can be studied or turned on and off using phase shift cascade. There are also head waves, or conical waves or, sometimes, merely refractions which, in this method, associate to the same incident plane waves as the evanescent waves. They appear in a shot record after a critical distance where the waves are refracted at 90 degrees. Phase shift cascade produces these waves as shown in the experimental section 3.2 and might as well be turned off if ever required.

2.5. Implementation of the algorithm

A package to implement the phase shift cascade method for 2-D seismogram generation, Elmo, was written in the Matlab environment. The source codes of relevant programs in the package are available through the CREWES Project. At this stage, Elmo assumes that the source and receivers are at the same level, $z=0$. However an extension for a different level of source and receivers can be done easily. The plane-wave cascade in Figure 2-2 illustrates how Elmo tracks the travel path of a plane wave to reflectors and determine their physical interactions along every possible way within the grid that waves can propagate back to the receiver. Waters (1981, p.131) originally used this diagram to describe a 1-D normal incidence seismogram method. Comparison with Figure 1-3 shows graphically how the cascade is equivalent to a finite expansion of the reverberation operator.
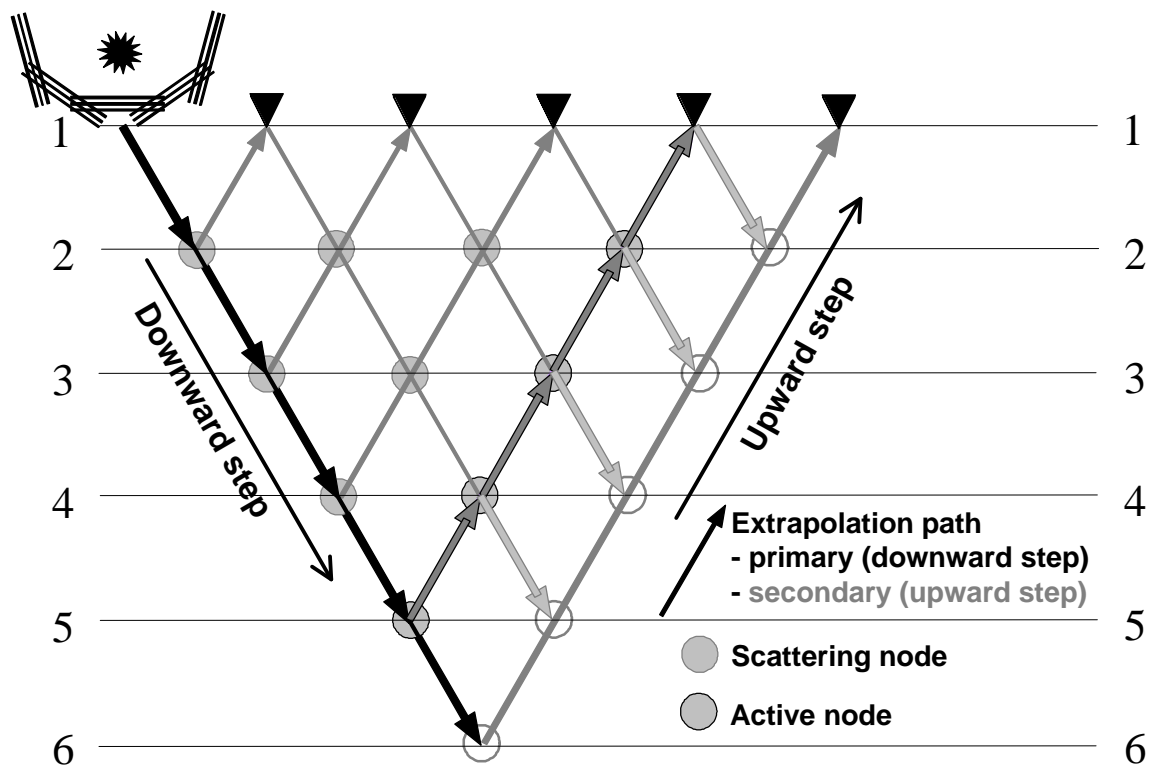
Figure 2-2. Plane-wave cascade

The proposed algorithm for Elmo can be summarized in pseudo-code as:

- initialize the model
- initialize output arrays
- for each k_x
    - initialize the source wavefields as vectors of ω
    - for each Δz downward step
        - for each active upward node
            - propagate (phase shift) the four ω vectors up and down to the next nodes
            - compute the four scattered ω vectors with the scattering matrix
        - end
        - sum any waves arriving at a surface node into the output arrays for P and S
    - end
- end
- add appropriate free surface corrections
- resolve accumulated P and S wavefields at z=0 into horizontal and vertical displacement components
- inverse Fourier transforms over ω and k_x

Reduction to 1D is quite simple and conceptually amounts to running the k_x loop only once for $k_x = 0$. Additional simplifications are that only two wavefields must be computed at each node and the Zoeppritz reflection and transmission coefficients become the simple normal incidence expressions.

In the first step of the calculation, a compressional point source is initiated at $z = 0$ in $(k_x, \boldsymbol{w})$ domain, and yields $\Phi(k_x, z = 0, \boldsymbol{w})$ in equation (2-46). On the computational grid in Figure 2-2, it is set up at (interface or downward step1, upward step1) which we shall call node(1,1). The output $\Phi'_{uc}(z = 0)$ and $\Psi'_{uc}(z = 0)$ in $(k_x, \boldsymbol{w})$ coordinates are zeros at this beginning node(1,1). The extrapolator in equation (2-22) is employed to downward continue each $(k_x, \boldsymbol{w})$ component of Φ to the second interface, node(2,2), by Δz_1. Note: there is no wavefield to upward continue. In order to propagate

a wavefield across a solid-solid interface, four boundary conditions in equation (2-26)-(2-29) are required. So equation (2-32) is applied to the potentials at node(2,2) setting

$$\Phi_{dc} = \Phi(k_x, \Delta z_1, \boldsymbol{w}) \tag{2-48}$$

and
$$\Phi_{uc} = \Psi_{dc} = \Psi_{uc} = 0. \tag{2-49}$$

Thus the four outgoing wavefields are established and ready to be propagated up and down separately to be the incoming wavefields of the next two nodes, (3,3) and (2,1), as shown in Figure 2-3.
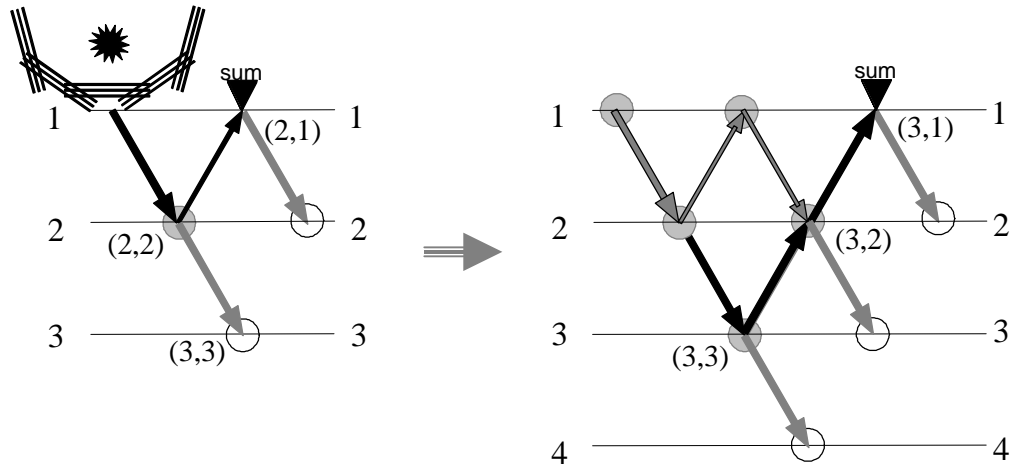

Figure 2-3. Computation step in plane wave cascade

Figure 2-3 illustrates the procedure in the triangular computation grid where Elmo traces down one node along the downward step and then up, to cover every node on the upgoing path to the surface while keeping all downgoing scattered waves from every upward step for the next step-down iteration. Each event arrives at the surface (interface1) and is summed into the output f-k spectra (Φ' and Ψ'). Then the calculation continues at the next downward step and repeats the procedure along the upward step through the surface again.

When every element of P- and S-potential spectra, $\Phi'_{ucf}(k_x, 0, \boldsymbol{w})$ and $\Psi'_{uc}(k_x, 0, \boldsymbol{w})$, are computed at the surface, surface reflections can be separately added for

free-surface effects (Dankbaar, 1985). Then the displacement conversion may be applied using

$$U = i(k_x\Phi' - k_z\Psi')\hat{l} + i(k_z\Phi' + k_x\Psi')\hat{n}$$

(2-50)

which is developed from equation (2-2) using equations (2-8) and (2-10) with equations (2-16) and (2-19). In this expression $\hat{l}$ is a unit vector in the x direction and $\hat{n}$ in the z direction.

2.6. Summary of phase shift cascade algorithm for Elmo

In summary, after evaluating the wavefield for a P-wave point source at the surface, Elmo extrapolates every plane wave component downward across arbitrarily thick homogeneous layers to reflectors via the computation diagram in Figure 2-2 which produces every possible multiple and converted mode within the grid. Elmo computes the reflections, transmissions, and conversions at interfaces using modified-for-potential Zoeppritz equations. All four incident waves are used to generate the four resultant waves for a full solution. At this stage, Elmo can include or exclude some physical effects with a properly reformed scattering matrix as illustrated in equations (2-33) to (2-36). This partitioned modeling can be depth dependent. The upgoing P and S waves from reflectors are propagated upward to the surface by applying the extrapolators and boundary conditions. Then the output component in the *f-k* domain is determined as a sum of the multiple arrivals of an individual potential wavefield at the surface. If freesurface effects are required, P- and S- potential reflections are added to the output plane before displacement conversions (again, if desired) and inverse Fourier transform to achieve a final result in the space-time domain

2.7. Feature discussion of the propagator matrix method in comparison to phase shift cascade

There are different orders of approximations and several possible manipulations of the propagator matrix method in performing forward modeling. The best-known application probably is the reflectivity method which computes synthetic seismograms for a portion of a plane layered earth, using displacement potentials. Due to its high accuracy, the reflectivity method is commonly used in global seismology, although in the exploration field, it has fairly limited application because of its long computing time requirement.

The key strength of the propagator matrix application is the ability to include all internal scatterings in one closed-form matrix operation. Refracted waves also can be included in the synthetics using complex angle of incidence (Waters,1992). Hence the accuracy of the amplitudes and phases of arrivals is very high. However, it cannot easily be extended to the lateral heterogeneous case because the reverberation operator implies lateral homogeneity. Moreover a long calculation time and wraparound problems are typical.

The calculation diagram (Figure 2-2), in phase shift cascade, of each layer is equivalent to a finite expansion of the reverberation operator (Figure 1-3). High accuracy is still gained and also flexibility of independent computation at each scattering node is granted. Though the run time comparison for both methods is unavailable at the present, Elmo can be improved in several ways, due to its intuitive nature. The wraparound is also found in phase shift cascade and handled, rather easily for the spatial case and very possibly in temporal case, as will be discussed later in this thesis.

The computation of the propagator matrix method is totally done in frequency domain. Though this leads to its best advantage as mentioned and is able to accommodate all frequency dependent effects, it is difficult to gain physical insight. In comparison, phase shift cascade is a straightforward procedure with explicit formulae which allow its most attractive feature of selective synthesizing of different scattered wavefields.

Propagator matrix methods are mostly formulated and applied in the (p,ω) domain and an inverse Hankel transform is required to obtain the time domain seismogram. The plane wave sampling is systematic over the ray parameter, whereas over the k_x axis it is irregular and courser at high frequency. Thus in time domain, it is lacking accuracy in delineation for a spherical or cylindrical composition, especially at far offset of deep reflections. Phase shift cascade works in the (k_x,ω) domain and obtains the seismogram through an inverse 2-D Fourier transform. The plane wave integration is regular over k_x and irregular over the ray parameter. Therefore the cylindrical wave in time domain is better formed by the inverse Fourier transform, according to the more complete plane wave distribution at any radius.

CHAPTER **3**

Experimental Results and discussions

3.1. Normal incidence synthetic seismograms (1-D)

To test those concepts proposed in chapter 2, phase shift cascade is implemented in the 1-D acoustic case and compared to the method commonly used in the exploration industry (Berryman et al., 1958, Waters, 1992, Easley and Foltinek, 1993, Hubral et al., 1980). Here the phase shift cascade for 1-D will be referred to as the depth domain method and the industry technique as the time domain method (it is also often called the Goupillaud seismogram). The phrase "time domain" refers to the fact that the standard method requires the input model to have layer thicknesses chosen such that the two-way traveltime across each layer is constant. Usually the constant traveltime is taken to be the desired time sample rate of the output seismogram and the input model is taken from well logs which will be resampled to have constant layer traveltimes. Originally, this resampling was done to reduce computational times but theoretical justification for it is lacking. Phase shift cascade does not involve such a resampling, though like the time domain method, it can still compute all possible multiples. A major effect of the equal traveltime resampling is a strong smoothing of the well log reflectivity. This can be comprehended by considering that logs are usually sampled at about 1/3 meter intervals and supposing a typical velocity of 3000 m/s, obviously around ten depth samples are

averaged to obtain .002 second layers. This averaging can be expected to alter the character of the seismogram.

Primaries-plus-multiples synthetic seismograms created by the time domain method often are difficult to match to seismic data while primaries-only synthetics usually tie well. This may be due in part to the fact that seismic processing is designed to attenuate multiples but it may also indicate a problem with multiple generation in synthetic seismograms. Therefore the multiple generation is examined by phase shift cascade compared to the time domain algorithm. There are two simple acoustic-impedance situations considered, whose effects have been described by O'Doherty and Anstey(1971) and Waters(1992). These are monotonic changes in impedance and alternating impedance changes (Figure 3-1). They are the two end members of a possible continuum of models which cause interbed multiples (O'Doherty and Anstey, 1971). They shall be called the step impedance model and the random impedance model respectively.

Two versions of each model are used where the impedance is the same in each version. However, in one case, the density is held constant at 2500 kg/m^3 and in the other case velocity is kept constant at 2500 m/s. The step model shows the impedance increasing at each depth interval (according to a linear function Imp=2500*(1800+0.6*z)) while the random model has impedance fluctuations about the same trend.

For the step model, the generated first-order multiples are opposite in sign to the primary pulses. Though each multiple would be small, the total effect can become very large through the superposition of events from many layers. Since the primaries are steadily decreasing through transmission losses, the multiples will eventually dominate and could cause an apparent flip of polarity (Waters, 1992).

The random model produces large reflection coefficients of alternating signs. Most of the first-order multiples generated by this model are relatively large and of the same polarity as the primaries. With enough layers, the amplitude of the composite multiples can surpass that of the primaries (Waters, 1992).
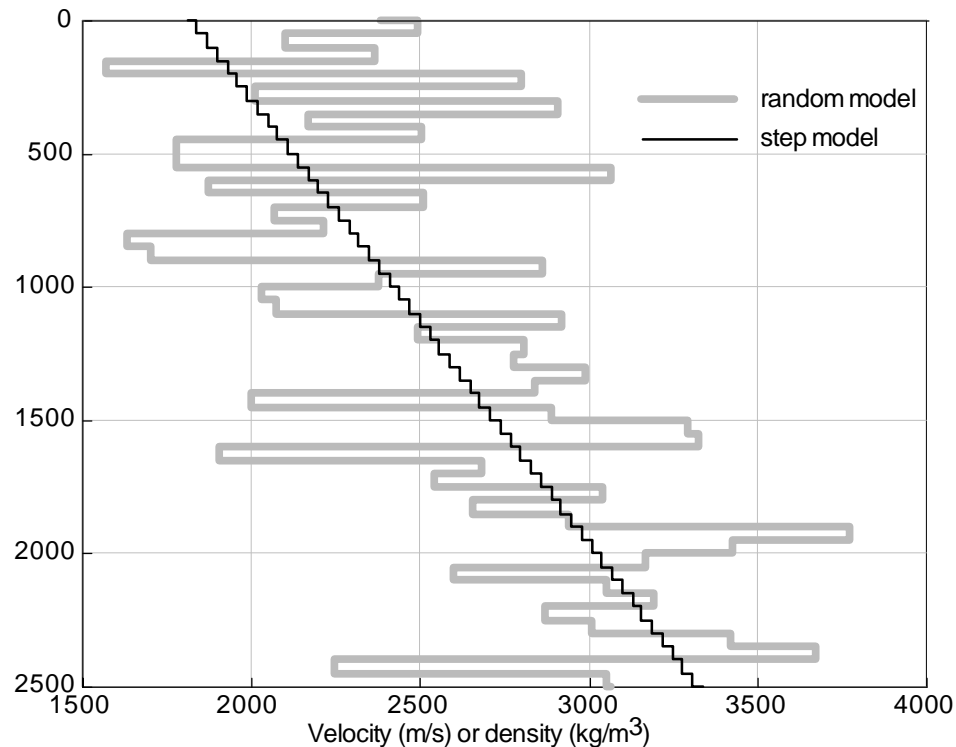
Figure 3-1. Synthetic acoustic impedance models They give either density for
the constant velocity model or velocity for the constant density model.
The constant velocity or density is 2500 (in MKS units)

The purpose in assuming constant velocity in the two impedance cases is to force all of the reflection coefficients to be exactly at output sample times. The depth interval for each layer is 50 meters and with constant velocity of 2500m/s the time thickness of every layer will be 40ms which will fall precisely on output sample times for the sample rate used (2ms). Therefore the time domain algorithm does not need to resample the model and the results from both methods should be identical. The constant density models were chosen as a contrast to the constant velocity case. There is an expectation that the differences between the two methods will be very obvious in this case. Since the layer traveltime now fluctuates, the time domain algorithm must alter the depth layering considerably.

Thus four synthetic acoustic impedance models are examined: (1) step model with constant density, (2) random model with constant density, (3) step model with constant velocity and (4) random model with constant velocity. In addition, real data results from

the Blackfoot 08-08 well log are also represented. The density and velocity logs from Blackfoot 08-08 are shown in Figure 3-2. The Mannville coals, which are a known source of multiple problems are located between 1500-1750m.
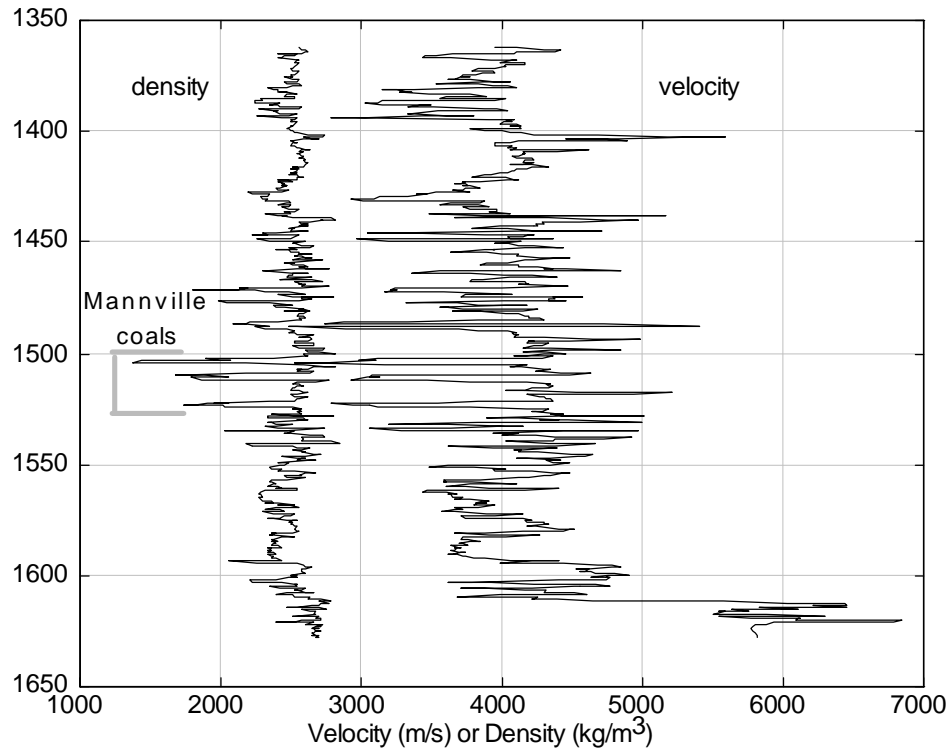
Figure 3-2 Interval velocity and density of Blackfoot 08-08 well logs

Figures 3-3, 3-5, 3-7 and 3-9 display responses of both algorithms to each artificial model. They are all band limited with a 50Hz Ricker wavelet to make the physical effects more apparent. At first glance, the differences between the two methods are difficult to distinguish. The 50m layer thickness of these models are much larger than real well logs. The smaller layers is expected to give more obvious differences as shown with the real data example. To aid in the comparison, Figures 3-4, 3-6, 3-8 and 3-10 are difference plots of primaries and multiples for each case.

(a) Depth domain method

(b) Time domain method
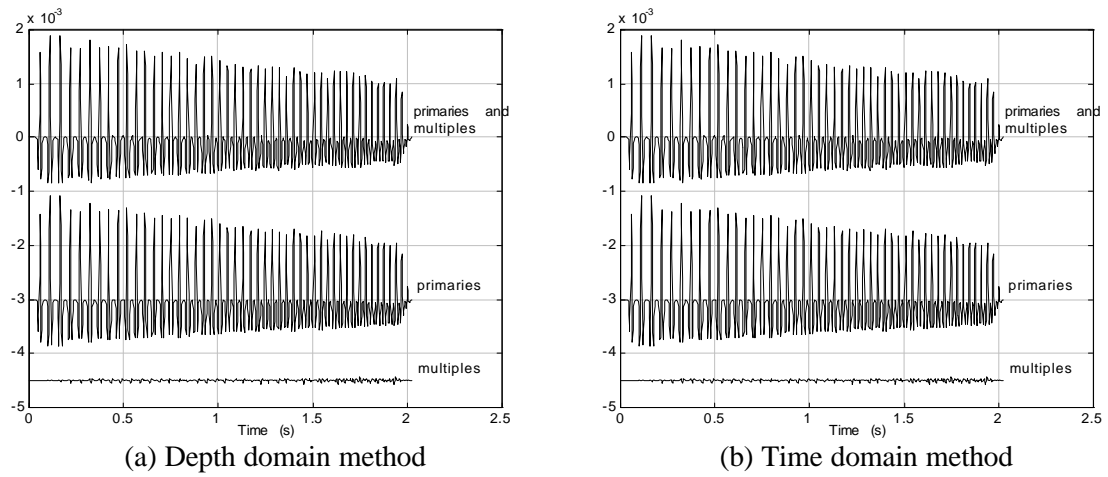
Figure 3-3. Responses of the two methods for the constant density step model

(a) Primaries

(b) Multiples
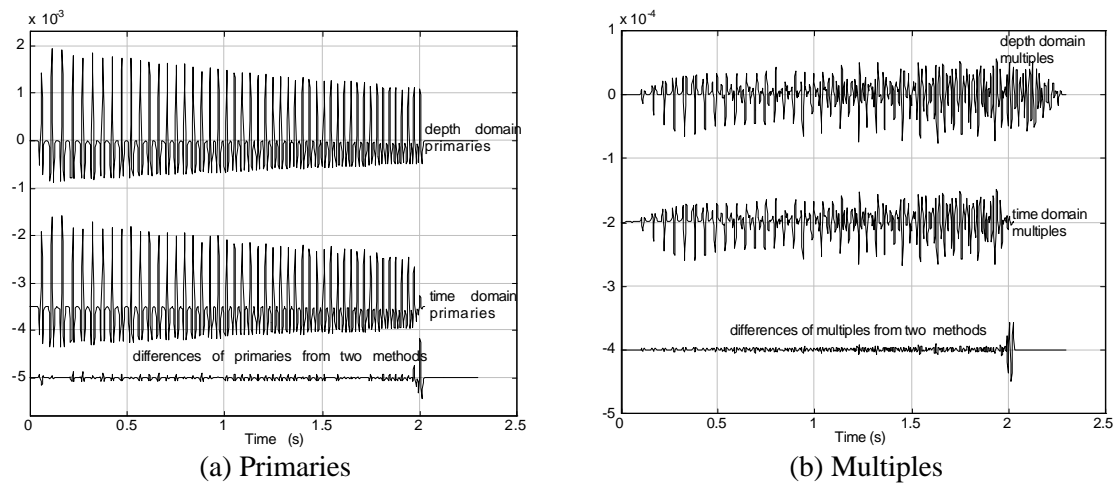
Figure 3-4. Comparisons with difference plots for constant density step model.

(a) Depth domain method

(b) Time domain method
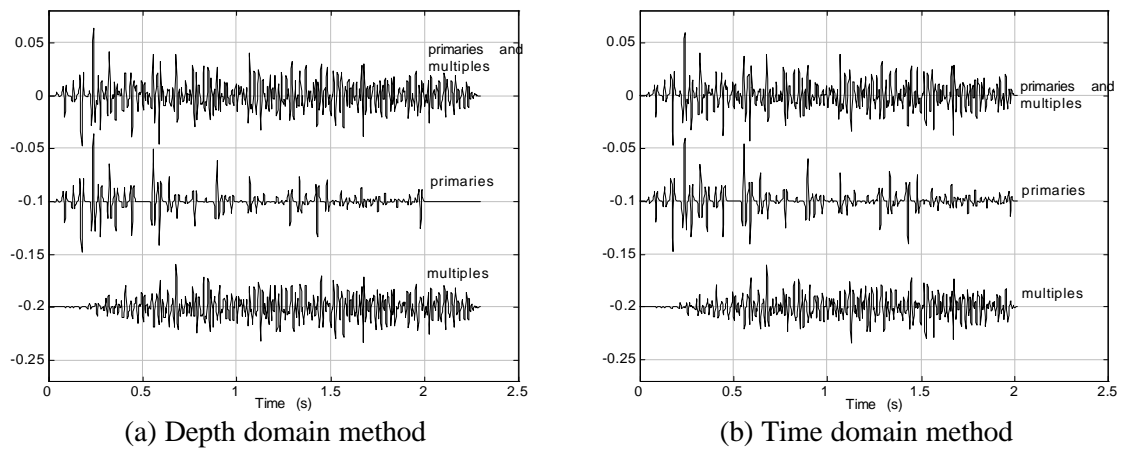
Figure 3-5. Responses of the two methods for the constant density random model

51

(a) Primaries (b) Multiples
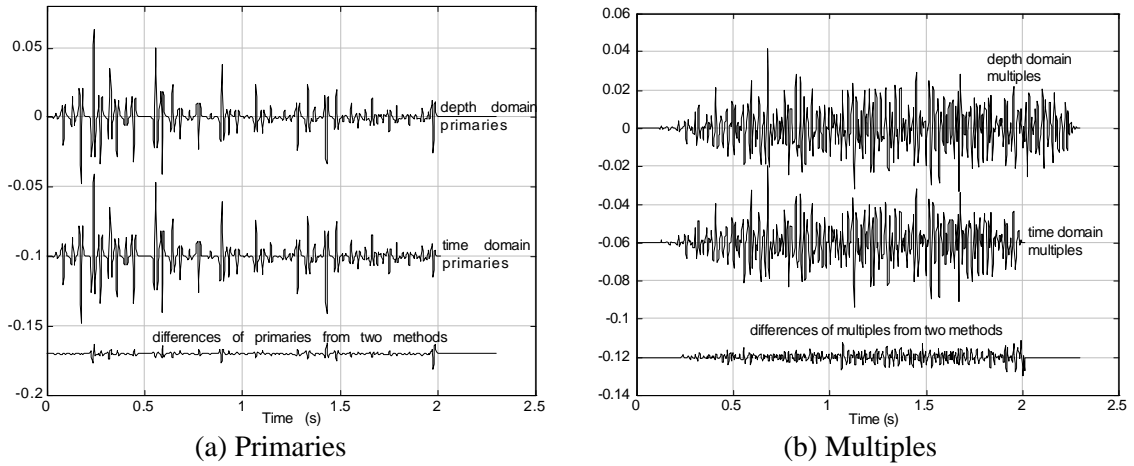
Figure 3-6. Comparisons with difference plots for the constant density random model.

(a) Depth domain method (b) Time domain method
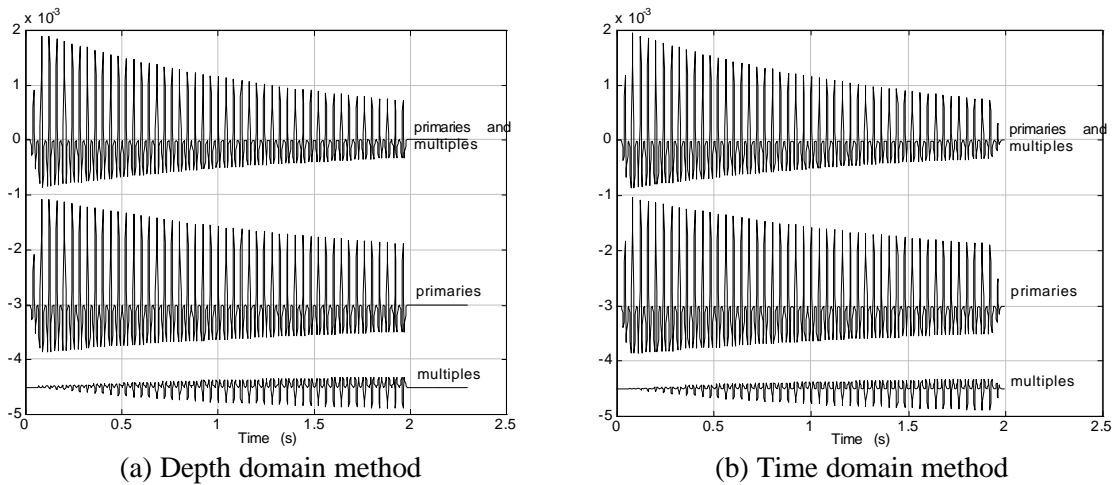
Figure 3-7. Responses of the two methods for the constant velocity step model

(a) Primaries (b) Multiples
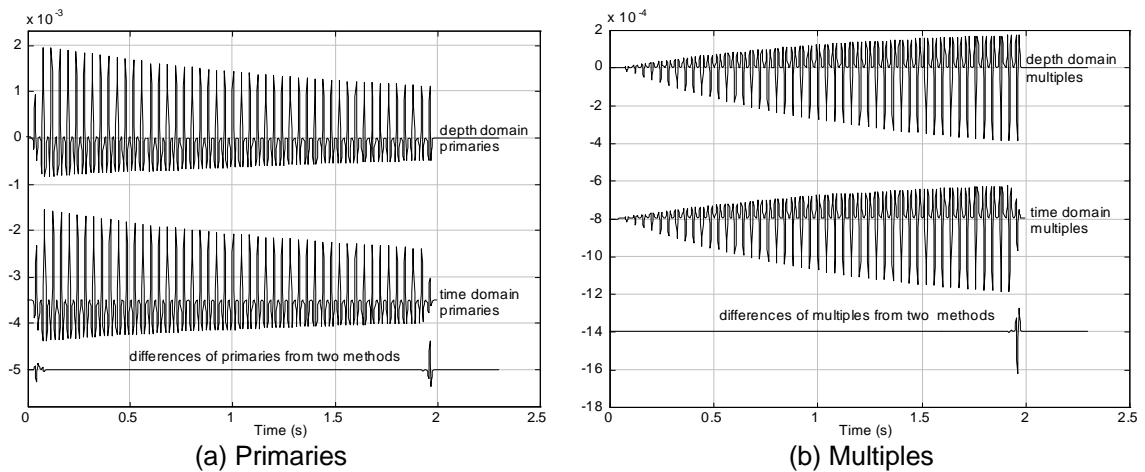
Figure 3-8. Comparisons with difference plots for the constant velocity step model.

(a) Depth domain method   (b) Time domain method
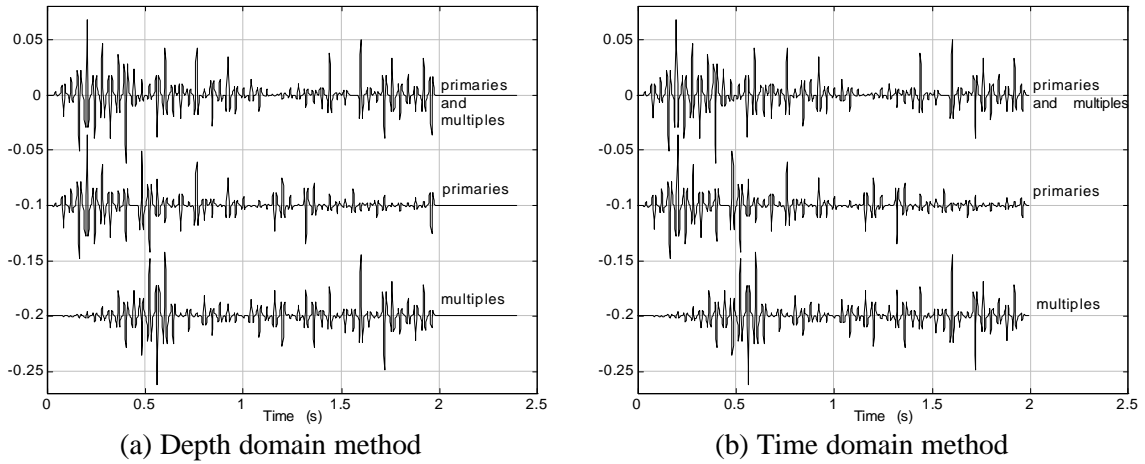
Figure 3-9. Responses of the two methods for the constant density random model

(a) Primaries   (b) Multiples
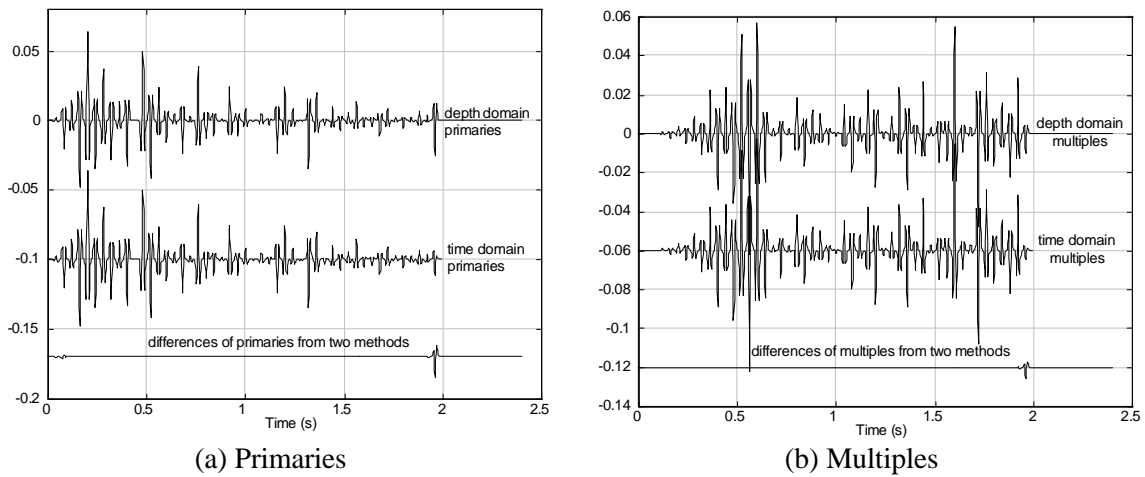
Figure 3-10. Comparisons with difference plots for the constant velocity
random model.

(a) Depth domain method   (b) Time domain method
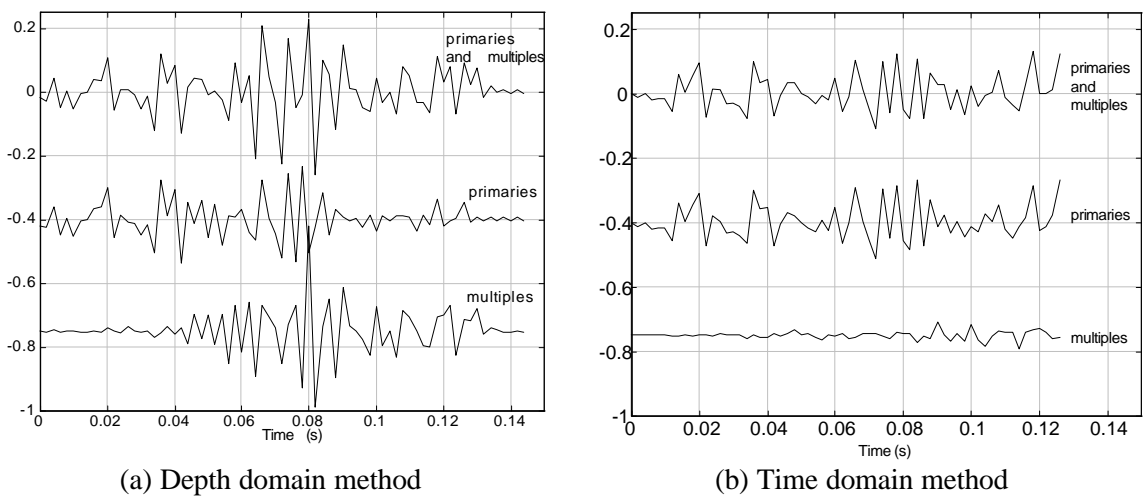
Figure 3-11. Responses of the two methods for the Blackfoot 08-08 well log data

(a) Primaries
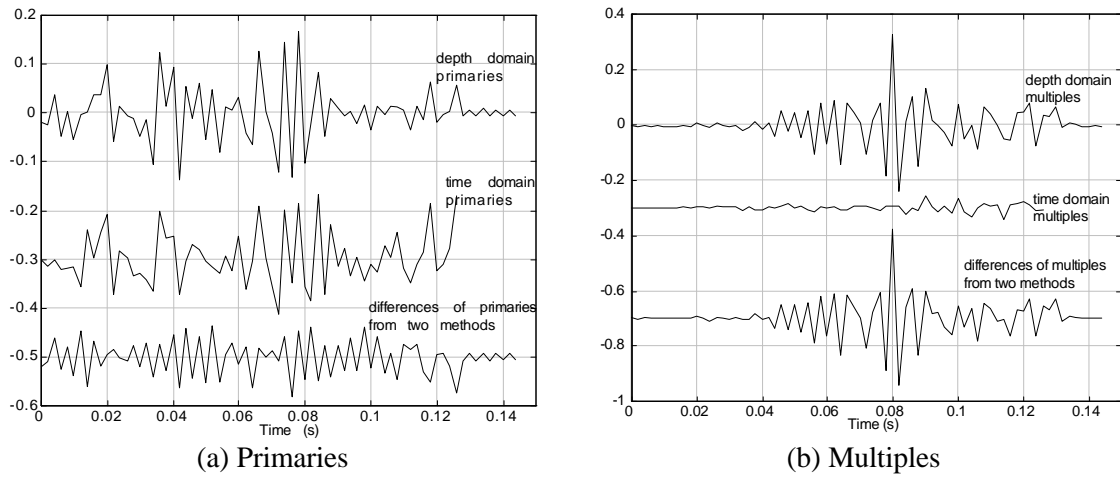
(b) Multiples

Figure 3-12. Comparisons with difference plots for Blackfoot 08-08.

(a) Primaries with multiples
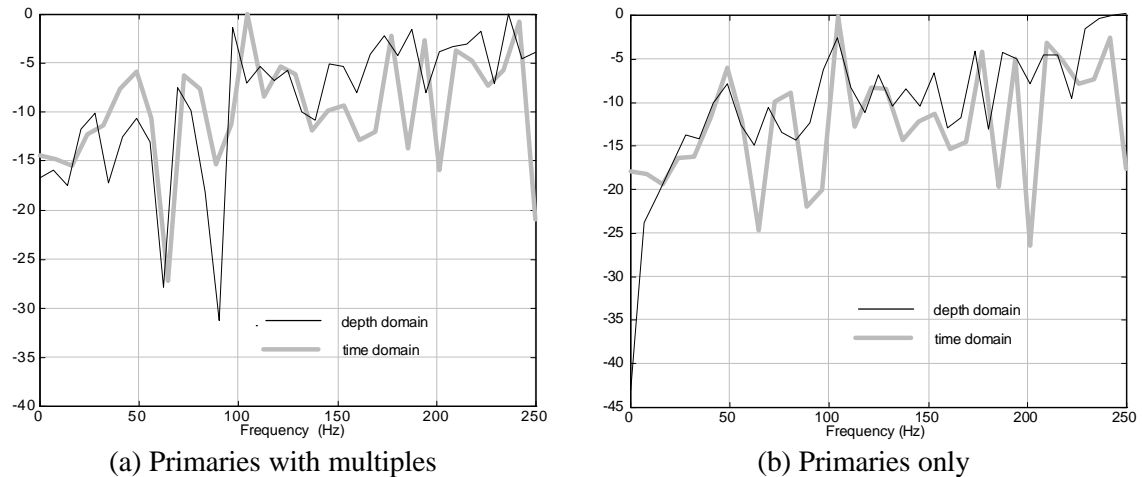
(b) Primaries only

Figure 3-13. Amplitude spectra of primaries with multiples and primaries only
from Blackfoot 08-08.

Considering the step model, as expected, the primaries are all positive, multiples
are negative and both are relatively small (Figures 3-3 and 3-7). From the comparison in
Figure 3-4, there are slight differences of primaries and multiples between the time
domain and depth domain solutions. On the other hand, for the constant velocity results
in Figure 3-7 primaries and multiples produced by time domain and depth domain
calculations are exactly alike, Figure 3-8, and more mathematically regular than in the
constant density case. Notice that primaries and multiples in Figure 3-7 appear evenly
along time axis while in Figure 3-4 only the primaries show systematic spacing. The
multiples in Figure 3-4 are initially regular but then become chaotic.

From Figures 3-5 and 3-6 of the random model, the relatively more chaotic nature of the multiples from the constant density model is again apparent. Comparisons of primaries and multiples between the two methods are given in Figure 3-6 for constant density and in Figure 3-10 for constant velocity. All of the responses have large positive and negative amplitudes. In the constant density case, the differences of primaries between the two algorithms tend to come from the large reflection coefficient interfaces (Figure 3-6(a)).The two algorithms are more divergent for the random model than for the step model (compare Figures 3-6 and 3-4). As expected, the overall power of the multiples is much larger for the random model than for the step model. The multiples often exceed primaries in amplitude so that they reinforce, cancel out or even dominate.

The greatest interest is with the real Blackfoot 08-08 logs, for which the responses of the time domain and depth domain techniques are given in Figure 3-11. Unlike the synthetic examples, these are shown without a wavelet because the logs are very short and a normal wavelet removes most of the detail. The results of the two methods are surprisingly different, even for the primaries (Figures 3-11 and 3-12). The time domain method creates primaries with less amplitude range and much smoother multiples than the depth domain method does. These are due to the small depth interval for these logs (0.3m) and the rapid fluctuations of acoustic impedance (Figure 3-2). The time domain algorithm, whose time thickness (2ms) is now much larger than the true depth thickness, strongly averages the log properties. Thus the very important detail of the logs is altered. Theoretically, if the logs are sampled finely enough in time, the time domain method should give the same result as the depth domain. It seems also likely that the differences between the two algorithms will be increasingly important for high resolution data. This can be a subject for future investigation. The results from the depth domain algorithm show higher amplitude primaries and severe multiples. The multiples are small in the early part but accumulate rapidly from .04s reaching the highest peak at .08s due to interbed multiples from the coals

The other very interesting result from these synthetics are the spectral notches, in primaries plus multiples traces from both methods (Figure 3-13). Coulombe and Bird

(1996) recently showed that interbed multiples created by the Mannville coals cause a notch at 50-70Hz in the spectra of real data. Also, by a formula given by O'Doherty and Anstey (1971), the calculated amplitude spectrum shows significant notches between 55-110Hz. There is good qualitative agreement between these and the results. The coals occur in Blackfoot 08-08 at about 1500-1750m (Figure 3-2) and there are two notches at 60Hz and 90Hz in the amplitude spectra of primaries plus multiples (Figure 3-13). Though the time domain algorithm shows similar effects they are again different detail.

3.2. 2-D Elastic seismograms from simple synthetic geological models

The three synthetic layered models in Figure 3-14 were used to test and show results from Elmo. All experiments in 3.2 and 3.3 assume a cylindrical P-wave source and receivers located in a uniform layer immediately below a freesurface at z=0 and the free surface effect is excluded. Above z=0 every model has a half space of very low acoustic impedance and has the lower half space as the deepest layer of the model. In this section, there are two single-interface models with the same two layers but switching places. The third model has more layers and produces more complicated results. The density for every layer in all models is constant (1.00g/cm^3).

Figure 3-14. Configuration of the three simple models

The time sample rate for modeling was 4ms and the trace interval was 25m. Maximum offset for model #1 and #2 was 3200m and for model #3 2000m. An

appropriate range of ray parameter is evaluated for every depth in these three models. A compressional wavelet with a Gaussian frequency spectrum was used as a source.

The results for PS waves in term of potential and horizontal displacement have polarity reversal at the negative offset in every model, Figure 3-15(b), 3-15(d), 3-18(b) and 3-18(d).

The synthetic potentials and displacements from model #1, which has a lower velocity layer on top (vp1<vs2<vp2), show PPP and PPS headwaves in both P and S arrivals as marked in Figure 3-15. The results from model #2 which has a higher velocity layer on top, do not show headwaves, Figure 3-18. There are phase changes in supercritical reflections of the results from model#1, Figure 3-15. These imply phase shift cascade produces headwaves which correspond to ray parameters within the model range. The Zoeppritz equations thus give the correct amplitude and phases for the reflection coefficients and plane wave superposition then correctly constructs such waves here.

Taking advantage of scattering matrix manipulation, cylindrical reflection coefficients can be obtained by dividing actual reflections by reference reflections, Figure 3-16. A reference PP reflection was computed by the same procedure and parameters as the actual wave but only with Rpp=1 (or Rps=1 for a reference PS) at a particular reflector, for every plane wave. Then traveltimes for the reflection have been raytraced for amplitude interpolation of the actual wave and the reference waves. Two methods of amplitude determination were conducted at this stage: Sinc-function interpolation of Hilbert envelope and instantaneous phase or Sinc-function interpolations of the real and imaginary parts of the analytic trace. The Hilbert envelope gives data magnitude at the specific traveltime. The Sinc function interpolation is required to compute a result at the present ray-traced traveltime. The cylindrical reflection coefficient is then estimated by dividing the actual amplitude by the reference amplitude. Due to two different amplitude extractions, we can get both amplitude and instantaneous phase information or both real and imaginary parts of the constructed reflection coefficients. They are plotted together with the analytic results from Zoeppritz equations at different offsets in Figure 3-17 (a) and (b) for model#1. The phase information are plotted in the multiplication of π radian

and shifted down 0.4π in order to be shown in the same chart as the amplitude information. For model#2, only the real part of the reflection coefficient from Zoeppritz equations is shown in Figure 3-19, because the imaginary part is zero. There are correlation trends in every case but the maximum coefficient from model#1 is shifted to farther offset and smoothed compared to plane wave coefficients. Amplitude maxima associated with critical angles also appear shifted to farther offsets than predicted from the Zoeppritz equations. This has been observed and discussed previously by Rendleman and Levin (1988) and Krail and Brysk (1983). Further references can also be found in Cerveny and Ravindra (1971) and Cerveny et al (1977).

The potential responses from the third model, PP primaries plus multiples, PP primaries, PS primaries plus multiples and PS primaries, are displayed in Figure 3-20. With this type of plotting, some very fine events can be seen and thus it aids the study of wavefield separation better than the common wiggle trace plot at some points. However all Figures in 3-20, especially the full responses of P and S waves in (a) and (c), still show spatial wraparounds as a result of using Fourier transform for the integration of plane waves with boundless span. To reduce this unwelcome effect, some attenuation was applied to a few plane waves surpassing a maximum horizontal slowness. Some small amounts are already applied to plane waves within a necessary range of horizontal slowness for results in Figure 3-20. The attenuation is increased and applied to a wider range for the full response of displacement fields, vertical and radial components, in Figure 3-21. An extreme plane-wave reduction with an exaggerated extent is visible in Figure 3-22. The method for attenuation is to turn the elastic problem into a strongly visco-elastic for the range of plane waves to be attenuated. This is accomplished by adding an imaginary component to the elastic constants and is described more fully in section 4.1.

As for this model, #3, the code calculated for 275 wavenumbers and 348 frequencies through 4 interfaces and 4 algorithm steps within 160seconds.

There are numerous events comprised in those records responded to only four interfaces. The number of only PP and PS primaries in Figures 3-20(b) and 3-20(d) can

be counted together to 170 events, as illustrated by a diagram in Figure 3-24. However some events arrive in the same time and some have too low amplitude compared to other events in the same record.
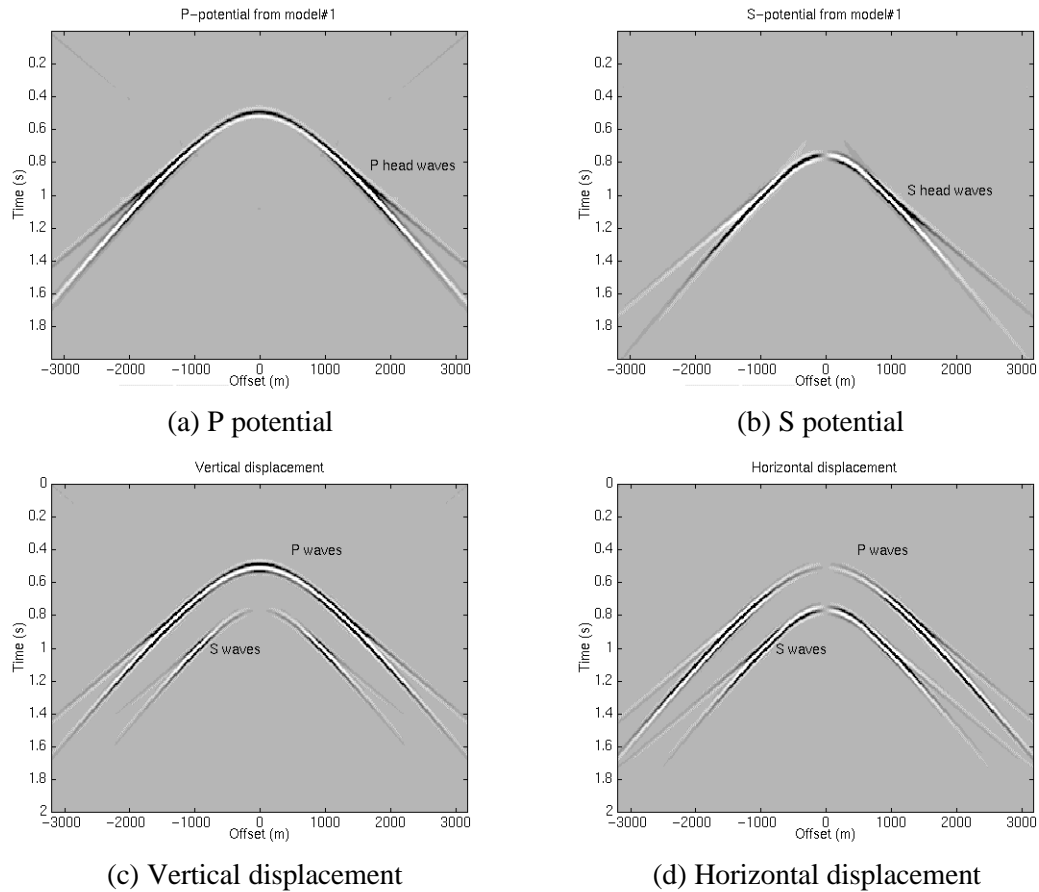

(a) P potential   (b) S potential

(c) Vertical displacement   (d) Horizontal displacement

Figure 3-15. Potential and displacement responses from model #1
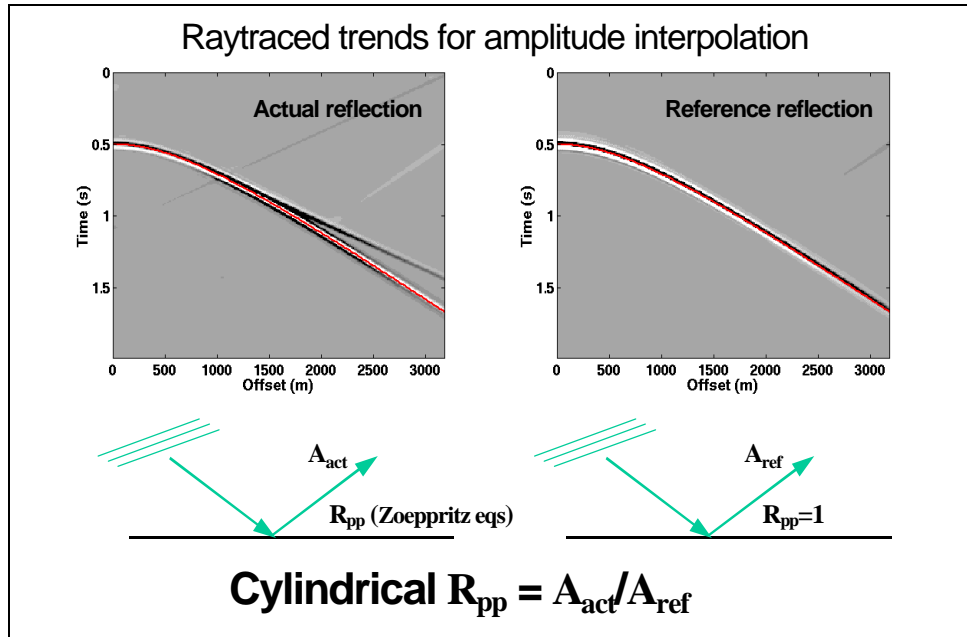
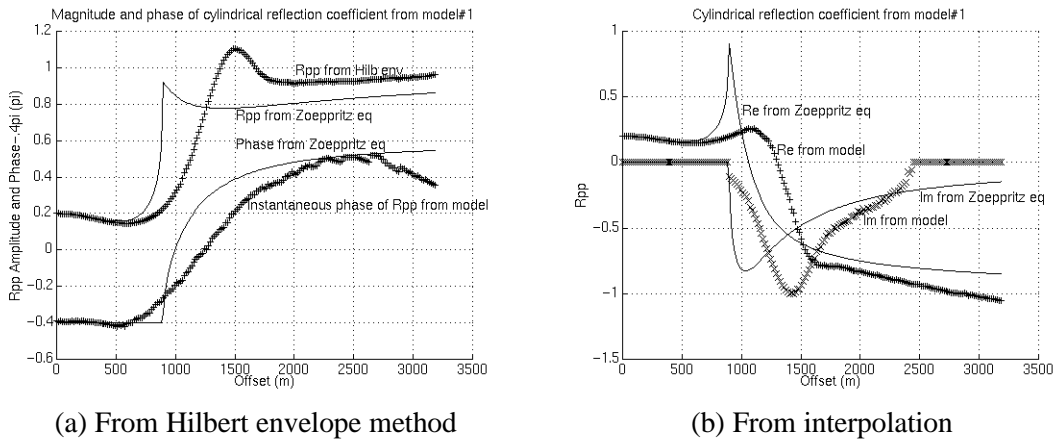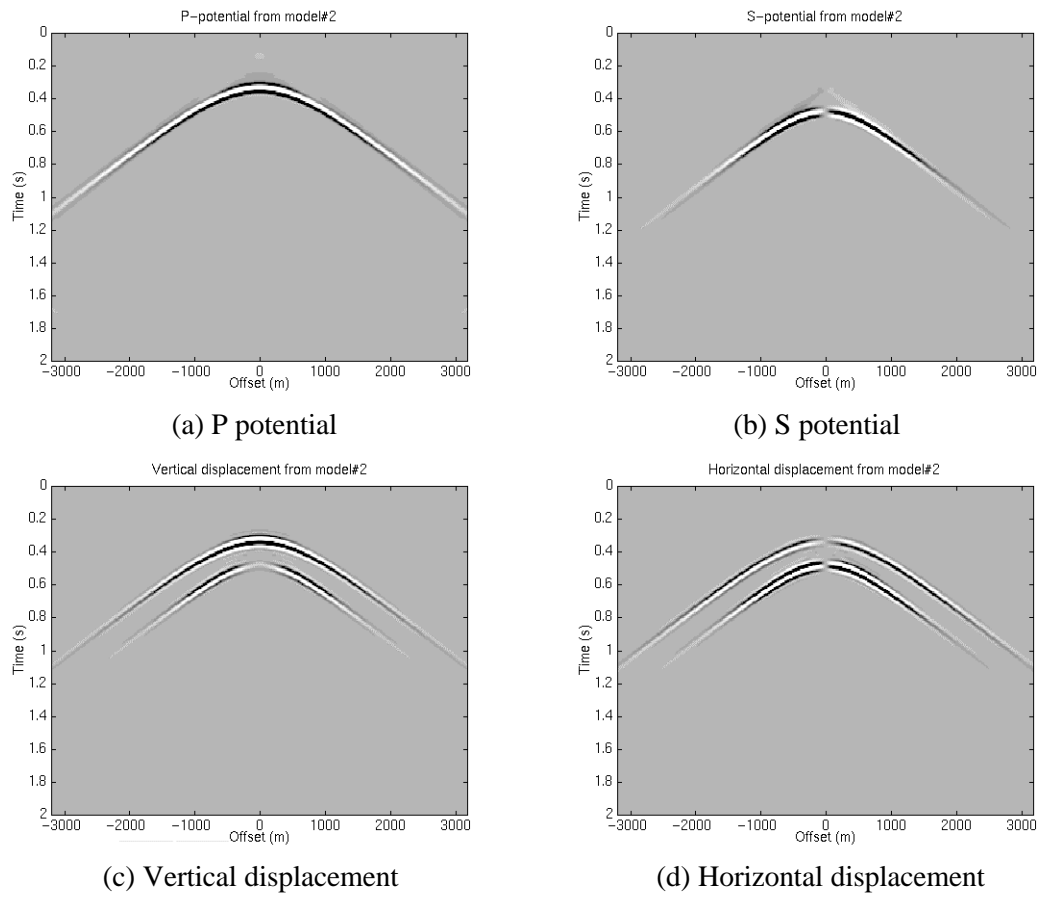Figure 3-16. Construction of cylindrical PP reflection coefficients directly
from synthetic data

(a) From Hilbert envelope method   (b) From interpolation

Figure 3-17. Extracted reflection coefficients from synthetic data of model #1

(a) P potential

(b) S potential

(c) Vertical displacement

(d) Horizontal displacement

Figure 3-18. Potential and displacement responses from model #2
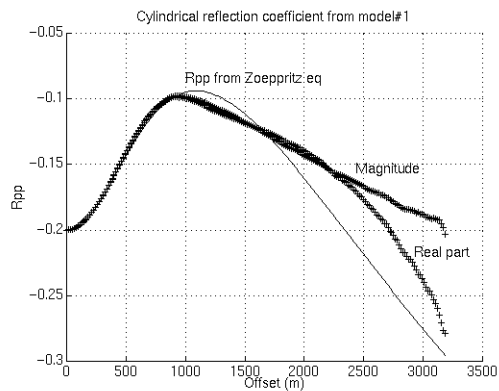
Figure 3-19. Extracted reflection coefficients from synthetic data of model #2
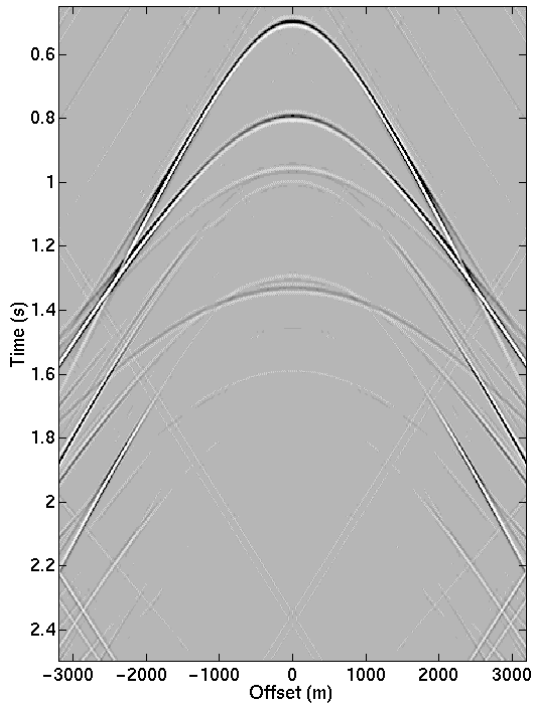
(a). P-potential primaries plus multiples
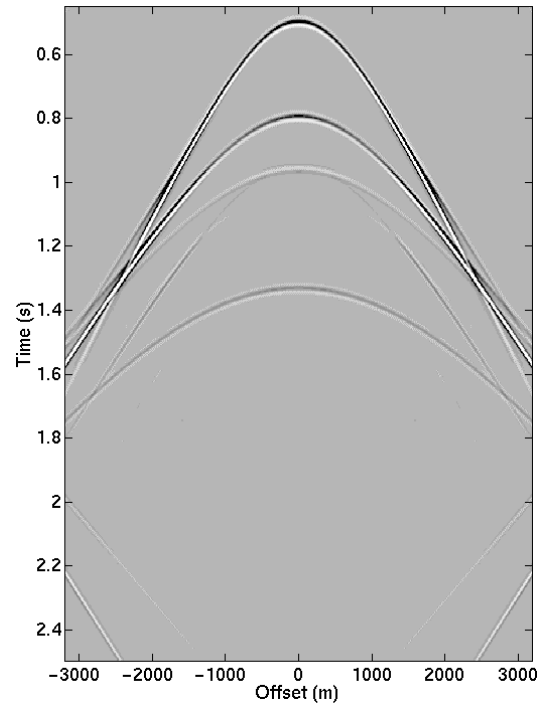
(b). P-potential Primaries.
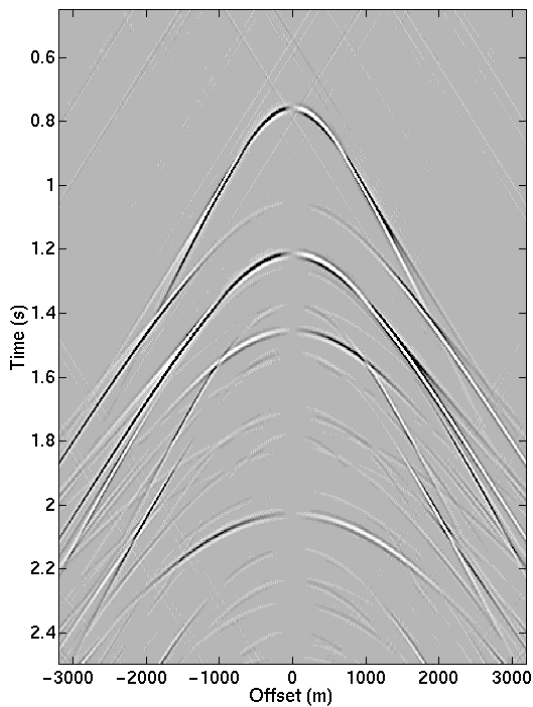
(c) S-potential primaries plus multiples.
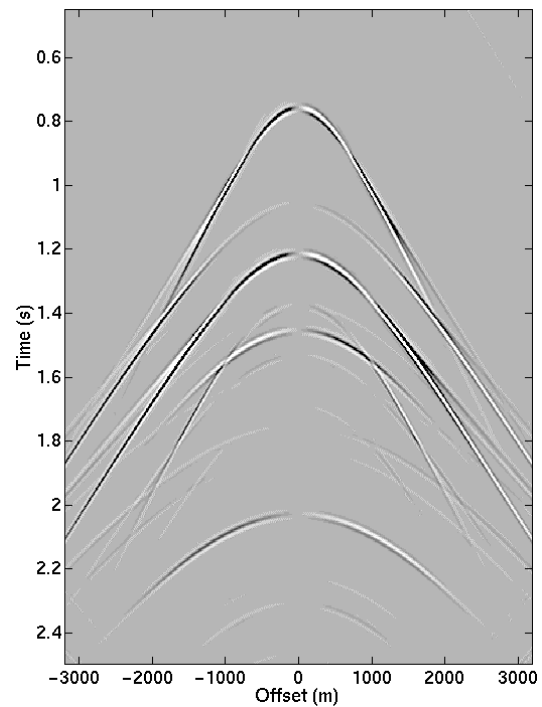
(d). S-potential Primaries.

Figure 3-20. P and S potentials from model #3 with a narrow transition range and very low attenuation.
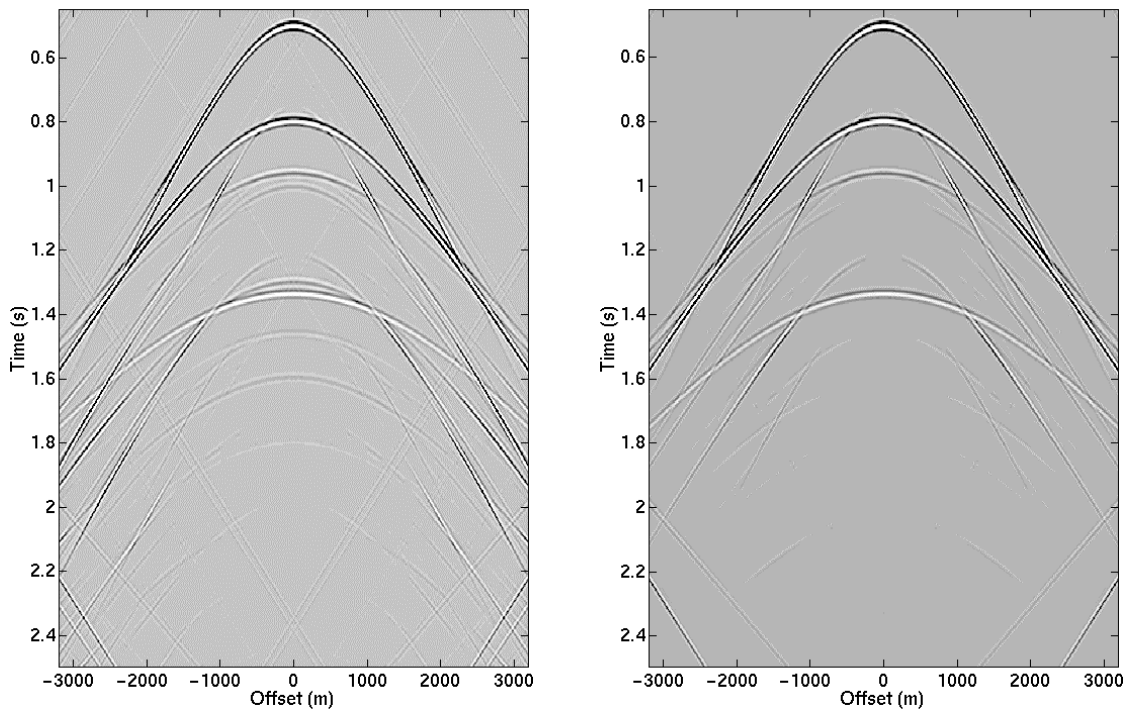
(a). Vertical displacement of full response.

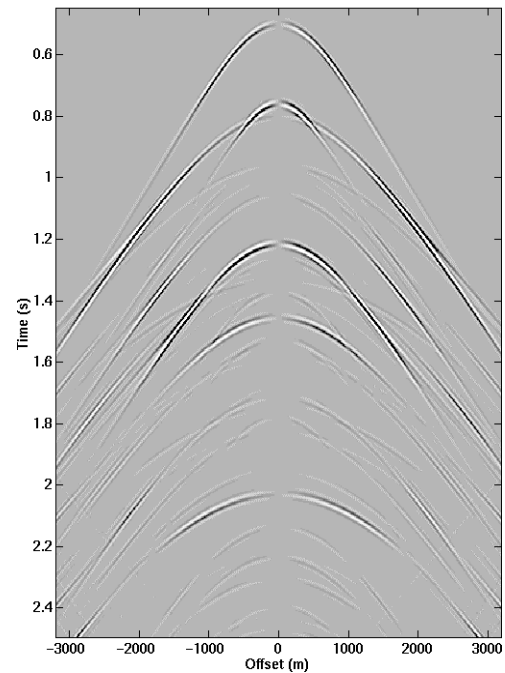(b). Vertical displacement of primaries.
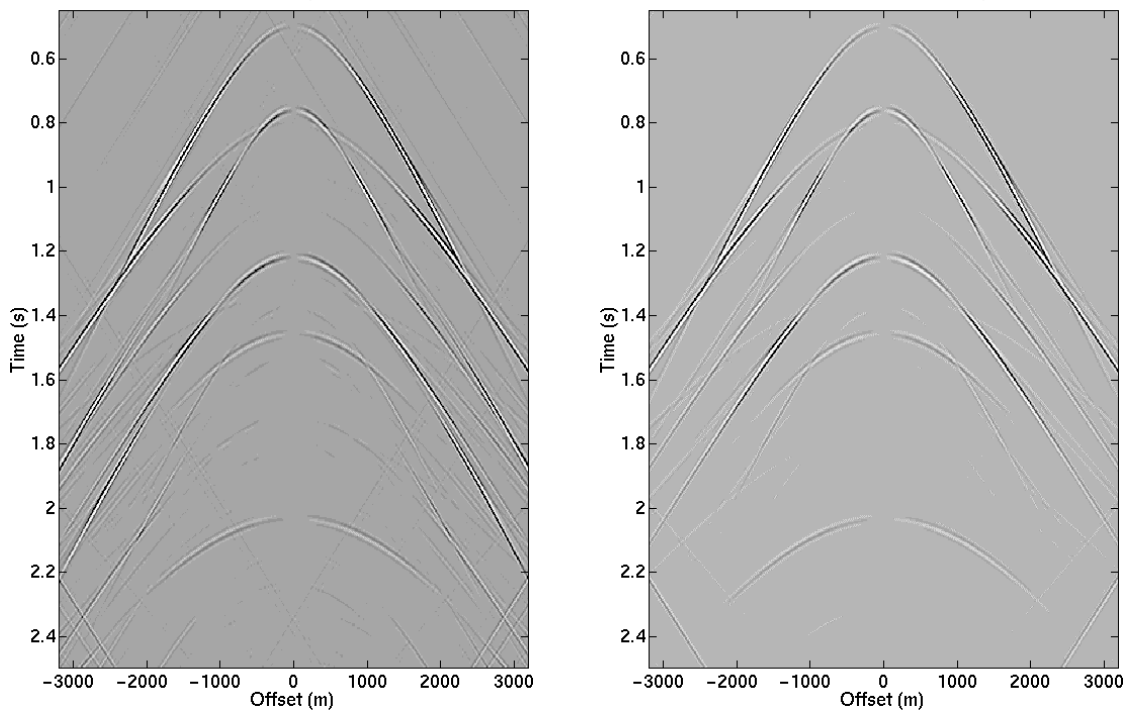
(c). Horizontal displacement of full response.

(d). Horizontal displacement of primaries.

Figure 3-21. Vertical and horizontal displacements from model #3 with a narrow transition range and very low attenuation
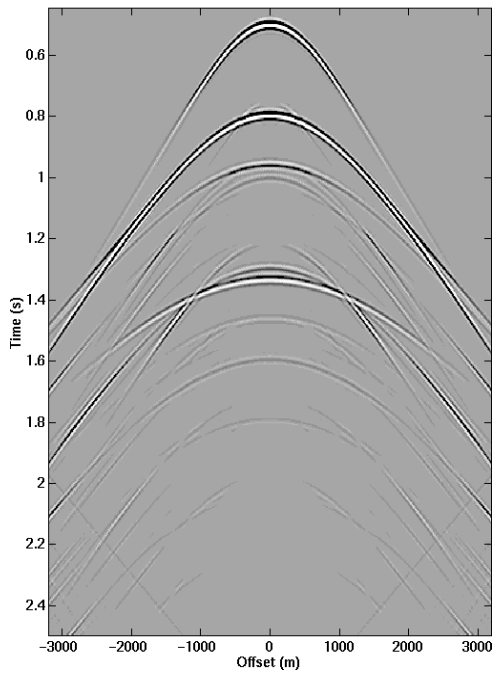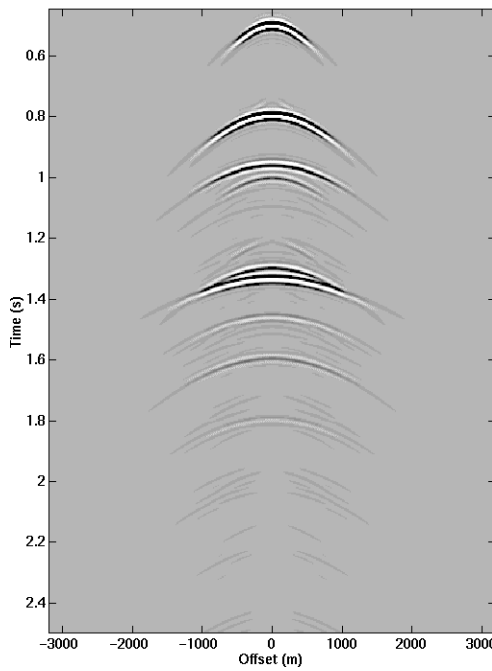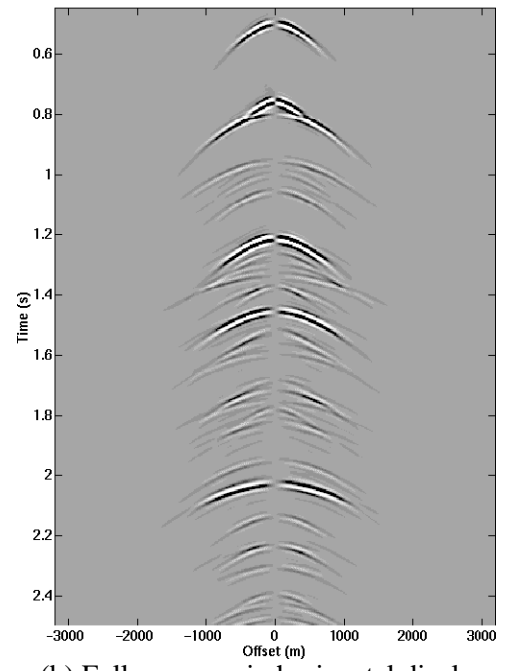
(a) Full response in vertical displacement

(b) Full response in horizontal displacement

Figure 3-22. Vertical and Horizontal displacements from model #3 with
moderate range of Butterworth filter and rather high attenuation.

(a) Full response in vertical displacement.

(b) Full response in horizontal displacement

Figure 3-23. Vertical and Horizontal displacements from model #3 with wide
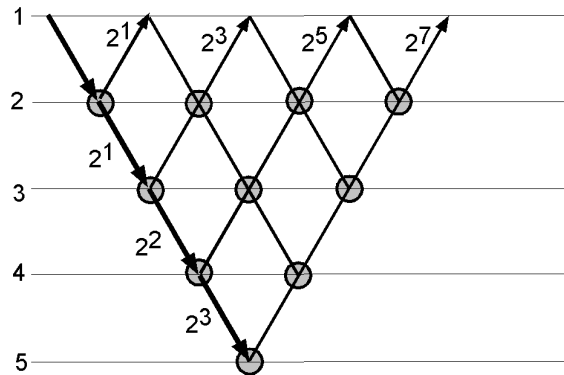range of Butterworth filter and high attenuation.

Figure 3-24. Computation diagram showing number of primary events along each path arriving at the surface, which are the power of two of the number of scattering nodes within the traveling path

3.3. Examples of selective modeling with depth partitioning

As is commonly accepted, the wave equation methods produce all (or almost all) seismic effects in forward modeling. An intuitive understanding of each individual effect is often lacking. From the perspective of phase shift cascade, all events that share the same arrival path (upcoming) to receivers (Figure 2-2) have the same number of scatterings. There are numerous events using such paths added up together, though most of them have different traveltimes. The total count for events on a single route from source to receiver, without any incidence waves other than the source-direct downcomings, is a power of two of the number of nodes within that path. If there are other incident waves, all the total scattering numbers from those paths must be summed to deduce the number of overall events. As an illustration, the total number of primaries, with mode conversion in both transmission and reflection, from a five-layer model as counted in Figure 3-24 is 2+8+32+128=170.

Phase shift cascade offers the possibility to study any given event separately by manipulating the scattering matrix. By varying the scattering matrix within the grid, the manipulation can be depth dependent. There is a model partitioning facility in Elmo that divides the entire model into three depth zones and then different modified scattering matrices are used in each division. Thus, different effects of wavefields are generated from those zones. This tool is very useful to study the variety of events within a particular

zone of interest. The complication of an entire geological model, in that case, is simplified. Secondary scattered wavefields such as multiples can be isolated by subtracting two models, one with the desired secondary wavefield and one without.

A few examples of the wavefield separations from a particular depth range were constructed based on the real well log data. The Blackfoot 08-08 well log was used again, for comparison with 1D case of section 3.1. The logs, density, P- and S-velocity, were blocked into 17 layers and, conceptually, three zones are recognized in Figure 3-25. Coal beds dominate zone B which generates multiples and converted waves tending to obscure the lower target, the Glauconitic channel sands in zone C. All wavefield simulations were generated assuming a P-wave source so all S-wave recordings represent mode conversions. A 2ms sample rate and ~5 m receiver interval were also used.
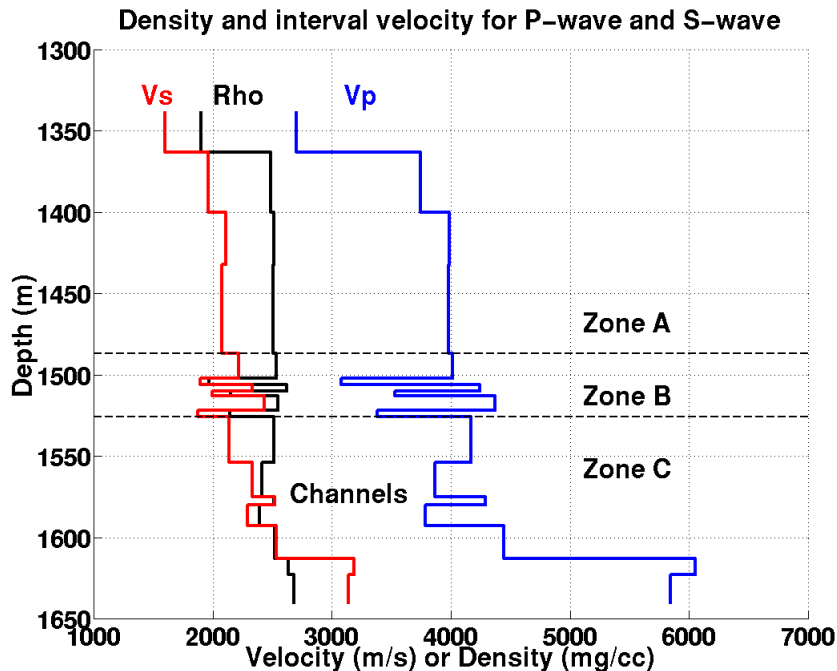

Figure 3-25. A 17-layer model blocked from density and dipole sonic logs of Blackfoot 08-08 well.

The full responses from the entire model of P and S potentials are presented in Figure 3-26. The vertical and radial components of displacement are in Figure 3-27. The primary response from the zone of interest can be seen between 1 and 1.2 seconds (zero offset time) on the P-wave potential and 1.4 to 1.6 seconds on the S-wave potential. A

package of surface multiples is also obvious on the P wave potential. The displacements show significant S-wave energy on the vertical channel and P wave energy on the radial channel. This is probably more event mixing than on the real data because a low-velocity near-surface layer was not part of the model. A wavefield separation into primaries and multiples of potentials and displacements is shown in Figures 3-28, 3-29, 3-30 and 3-31. Note that the interbed multiples on the P and S potentials are rather small except for several events which probably are related to the coals of zone B.

It is fairly difficult to analyze all events in those records. Hence some interesting areas were separately investigated. The region of Mannville coal beds, zone B in Figure 3-25, was chosen to produce various wave effects. The effects from a limited zone are also based upon their incident waves. That means there are still influences from conditions, or scattering matrices, set outside the zone of interest. Among many possibilities included, here are tests of some partitioned modelings from zone B with two zoned external biases.

In the first example, the full response of zone B is generated from primaries-with-conversions in zones A and C. The result is represented separately in Figures 3-32 and 3-33 which show double plots of primaries from all three zones and only multiples from zone B, in P and S potentials respectively. An illustrative explanation for multiple isolation is drawn in Figure 3-36. Thus the multiple field here can be considered as a composite produced from primary transmissions through zone A and primary reflections from zone C, as incident waves, both with mode conversion.

In another case from zone B, there only is an incident wave of non-converted PP transmissions through the upper region and also no conversions on the receiver-arrival paths. The consequences of zone C are excluded. The full response is compared with primaries-without-conversions and the isolated multiples are shown in Figures 3-34 and 3-35, for P and S arrivals. Figure 3-37 shows a descriptive picture of this construction. Compared to the results of the previous case, the multiples are apparently dissimilar, though they both correspond to the same region. There are a few factors for the difference between them. Zoned internal and external mode conversions, incoming waves from both

above and below the region, and scattering orders within zone B are the main ones. Especially complex are several types of mode conversions: P-to-S, S-to-P, reflecting, transmitting, in-primaries, in-multiples, downgoing and upcoming conversions. We can see from equation 2-32 that they comprise half of the scattering matrix. The significance of each type of conversion depends on offsets and elastic contrasts at interfaces. Considering the numbers of primaries-only from zone B in these both examples, there are 14 primaries, the number of interfaces within zone B multiplied by 2, for both P and S arrivals in the second one. Whereas there are $2^7+2^9+2^{11}+2^{13}+2^{15}+2^{17}+2^{19}$ P and S primaries from zone B comprised in Figure 3-32 and 3-33 of the first example. Some of them appear at the same times, and many are very close, on the records. There are also many that certainly have very weak amplitudes.

Figure 3-32 shows that the strongest P-wave internal-multiples from zone B appear in the record at the same time as the primaries from the Channel, between 1.4 to 1.6 seconds. The results shown in Figure 3-33 suggest those strong multiples may be induced not only from zone B but also the external factors that more likely from below and/or the higher-order multiples. S-wave internal multiples of zone B, Figure 3-32, have less amplitude effects to the S primaries from the Channel.
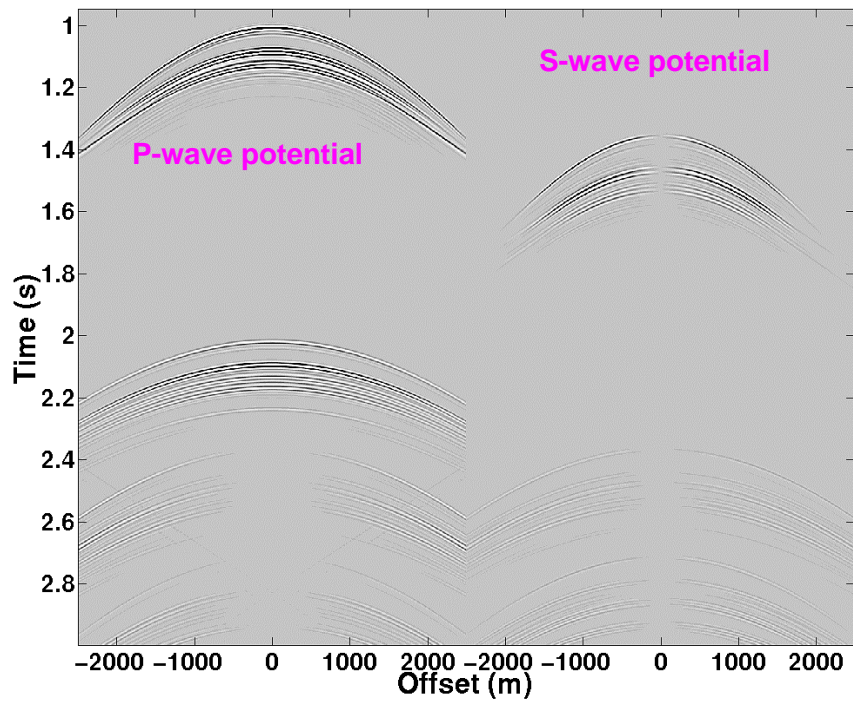
Figure 3-26. Full responses of P and S potentials from 17-layer model of
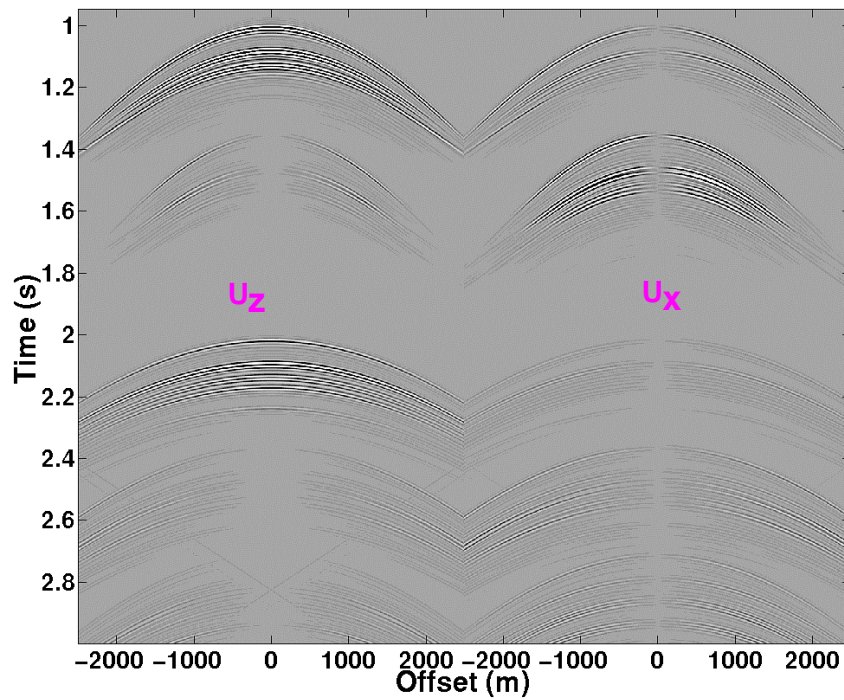Blackfoot 08-08.

Figure 3-27. Full responses from 17-layer model of Blackfoot 08-08 in
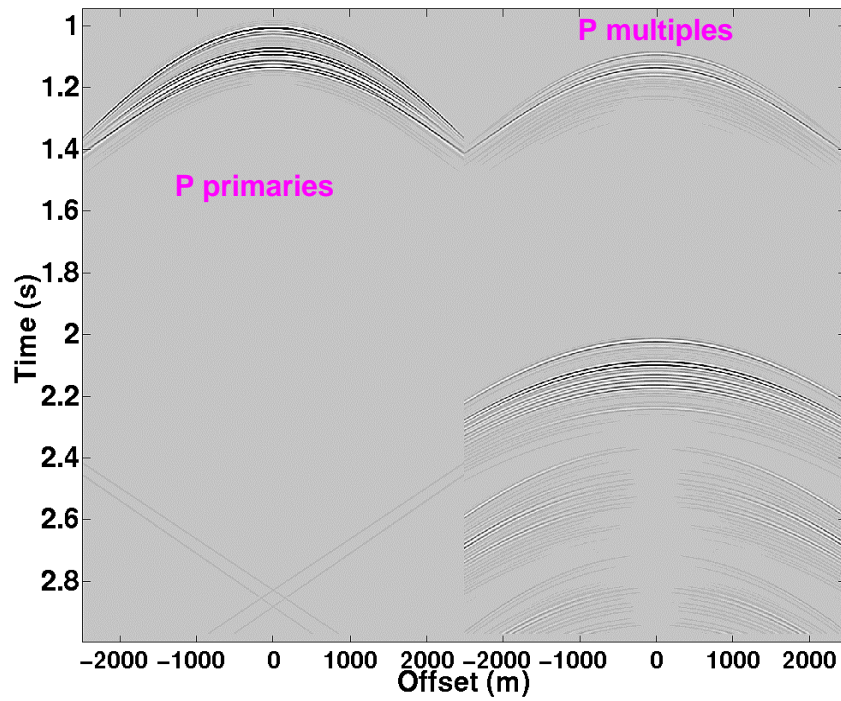vertical and horizontal displacements.[i]

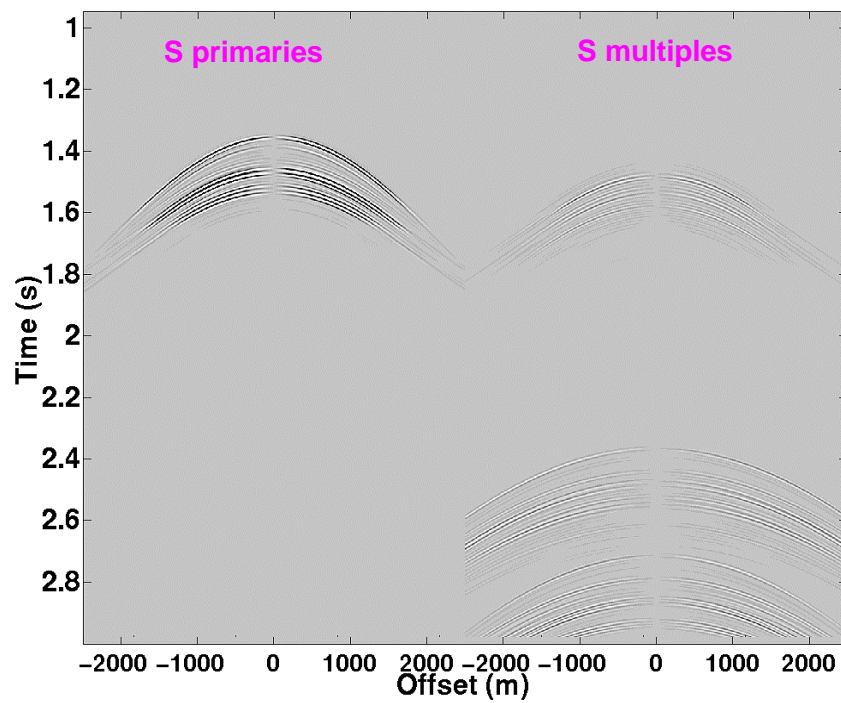Figure 3-28. Primaries and multiples of P potentials from entire 17-layer model of Blackfoot 08-08.

Figure 3-29. Primaries and multiples of S potentials from entire 17-layer model of Blackfoot 08-08.
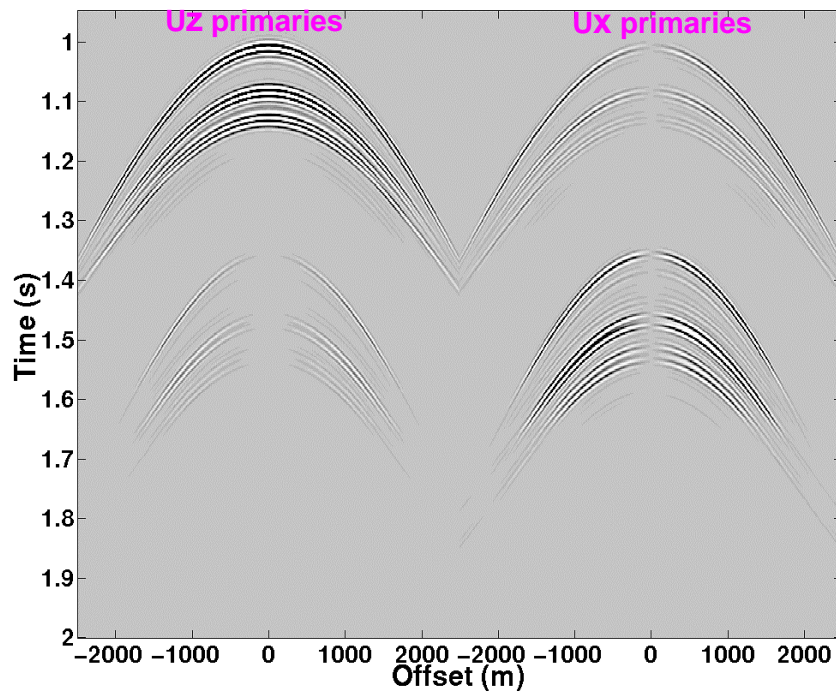
Figure 3-30. Primary reflections from entire 17-layer model of Blackfoot 08-08 logs in vertical and horizontal displacements.
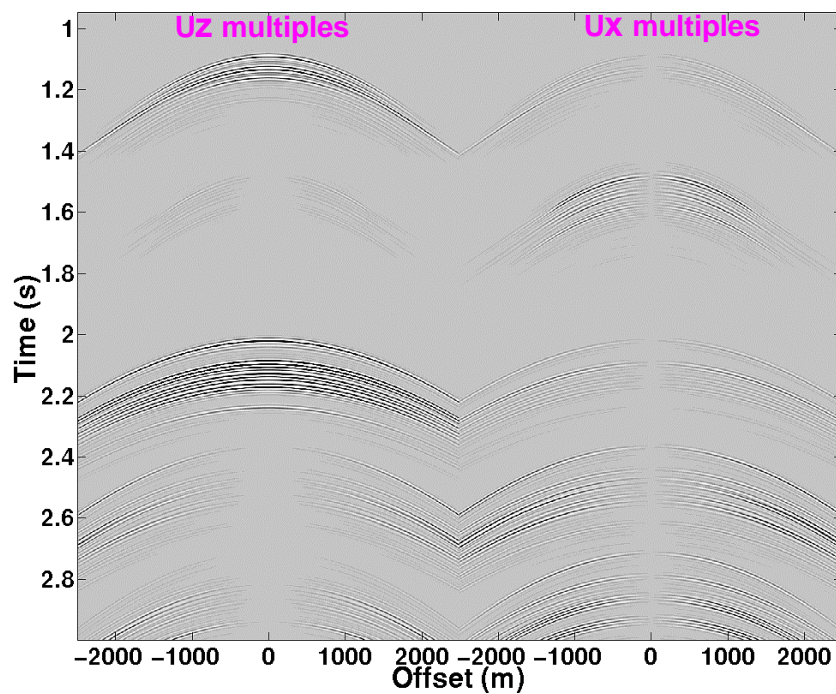

Figure 3-31. Multiples only from entire 17-layer model of Blackfoot 08-08 in vertical and horizontal displacements.
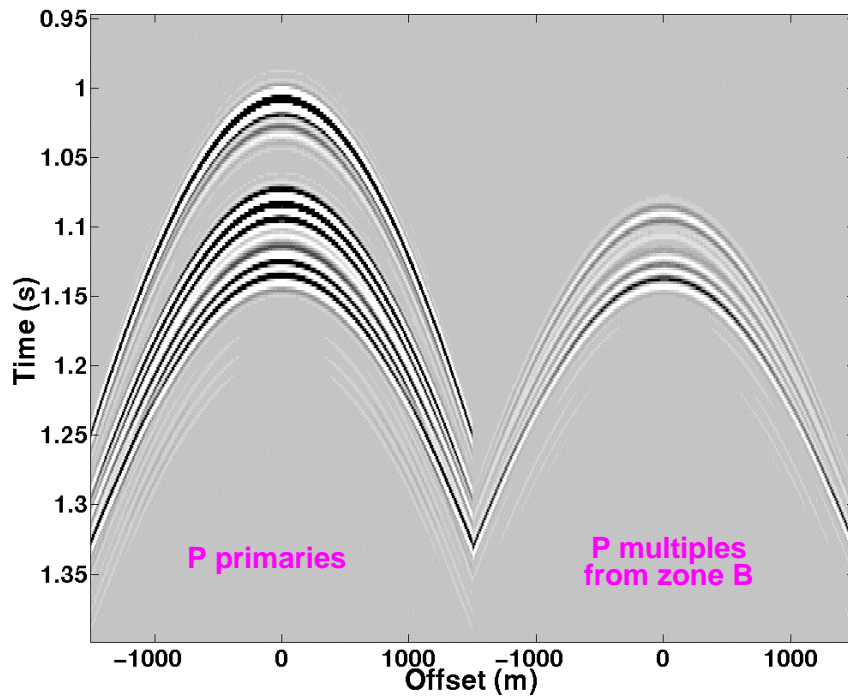
Figure 3-32. P primaries from the whole model and P multiples generated from zone B
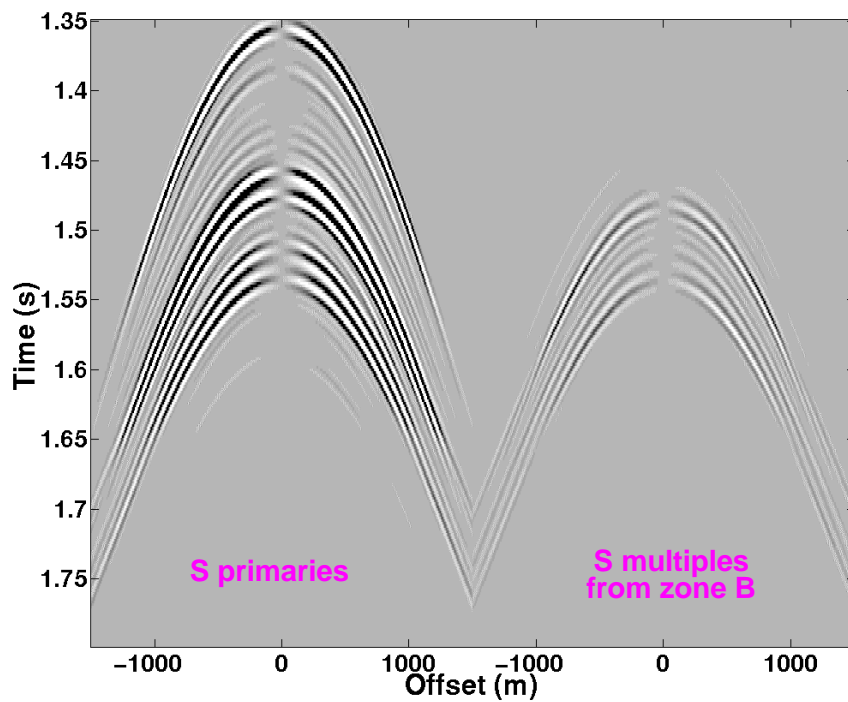

Figure 3-33. S primaries from the whole model and S multiples generated from zone B.
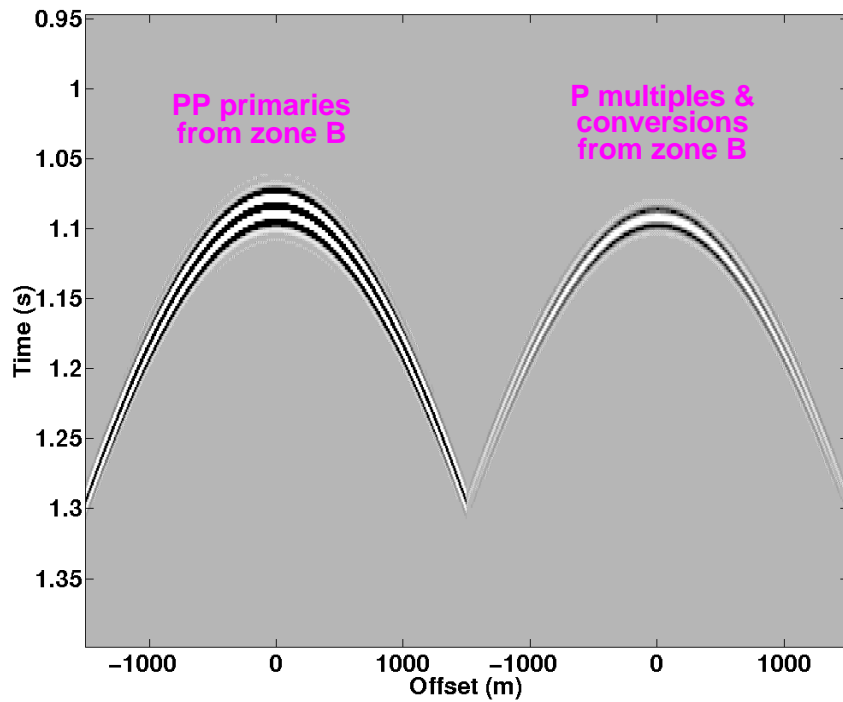
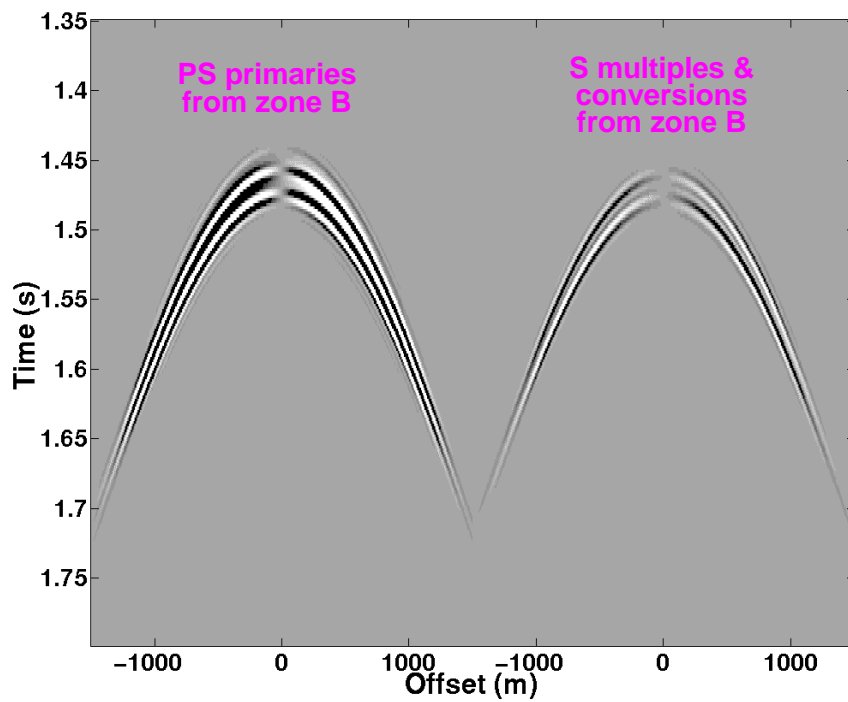Figure 3-34. Genuine PP primaries and multiples generated from zone B with a scheme in Figure 3-36.

Figure 3-35. Genuine PS primaries and SS multiples generated from zone B with a scheme in Figure 3-37.

Subtraction scheme to isolate multiples

First Model

$$\begin{bmatrix} T_{pp} & T_{sp} & 0 & 0 \\ T_{ps} & T_{ss} & 0 & 0 \\ R_{pp} & R_{sp} & T_{pp}^- & T_{sp}^- \\ R_{ps} & R_{ss} & T_{ps}^- & T_{ss}^- \end{bmatrix}$$ **Zone 1 Primaries only**

$$\begin{bmatrix} T_{pp} & T_{sp} & R_{pp}^- & R_{sp}^- \\ T_{ps} & T_{ss} & R_{ps}^- & R_{ss}^- \\ R_{pp} & R_{sp} & T_{pp}^- & T_{sp}^- \\ R_{ps} & R_{ss} & T_{ps}^- & T_{ss}^- \end{bmatrix}$$ **Zone 2 Full response**

$$\begin{bmatrix} T_{pp} & T_{sp} & 0 & 0 \\ T_{ps} & T_{ss} & 0 & 0 \\ R_{pp} & R_{sp} & T_{pp}^- & T_{sp}^- \\ R_{ps} & R_{ss} & T_{ps}^- & T_{ss}^- \end{bmatrix}$$ **Zone 3 Primaries only**

Minus

Second Model

$$\begin{bmatrix} T_{pp} & T_{sp} & 0 & 0 \\ T_{ps} & T_{ss} & 0 & 0 \\ R_{pp} & R_{sp} & T_{pp}^- & T_{sp}^- \\ R_{ps} & R_{ss} & T_{ps}^- & T_{ss}^- \end{bmatrix}$$ **Zone 1 Primaries only**

$$\begin{bmatrix} T_{pp} & T_{sp} & 0 & 0 \\ T_{ps} & T_{ss} & 0 & 0 \\ R_{pp} & R_{sp} & T_{pp}^- & T_{sp}^- \\ R_{ps} & R_{ss} & T_{ps}^- & T_{ss}^- \end{bmatrix}$$ **Zone 2 Primaries only**

$$\begin{bmatrix} T_{pp} & T_{sp} & 0 & 0 \\ T_{ps} & T_{ss} & 0 & 0 \\ R_{pp} & R_{sp} & T_{pp}^- & T_{sp}^- \\ R_{ps} & R_{ss} & T_{ps}^- & T_{ss}^- \end{bmatrix}$$ **Zone 3 Primaries only**

Figure 3-36. Modeling scheme for the selective results in Figure 3-33.

Subtraction scheme to isolate multiples and mode conversions.

First Model

$$\begin{bmatrix} T_{pp} & 0 & 0 & 0 \\ 0 & T_{ss} & 0 & 0 \\ 0 & 0 & T_{pp}^- & 0 \\ 0 & 0 & 0 & T_{ss}^- \end{bmatrix}$$ **Zone 1 Transmissions only**

$$\begin{bmatrix} T_{pp} & T_{sp} & R_{pp}^- & R_{sp}^- \\ T_{ps} & T_{ss} & R_{ps}^- & R_{ss}^- \\ R_{pp} & R_{sp} & T_{pp}^- & T_{sp}^- \\ R_{ps} & R_{ss} & T_{ps}^- & T_{ss}^- \end{bmatrix}$$ **Zone 2 Full response**

$$\begin{bmatrix} 0 & 0 & 0 & 0 \\ 0 & 0 & 0 & 0 \\ 0 & 0 & 0 & 0 \\ 0 & 0 & 0 & 0 \end{bmatrix}$$ **Zone 3 Turned off**

Minus

Second Model

$$\begin{bmatrix} T_{pp} & 0 & 0 & 0 \\ 0 & T_{ss} & 0 & 0 \\ 0 & 0 & T_{pp}^- & 0 \\ 0 & 0 & 0 & T_{ss}^- \end{bmatrix}$$ **Zone 1 Transmissions only**

$$\begin{bmatrix} T_{pp} & 0 & 0 & 0 \\ 0 & T_{ss} & 0 & 0 \\ R_{pp} & 0 & T_{pp}^- & 0 \\ 0 & R_{ss} & 0 & T_{ss}^- \end{bmatrix}$$ **Zone 2 Primaries only**

$$\begin{bmatrix} 0 & 0 & 0 & 0 \\ 0 & 0 & 0 & 0 \\ 0 & 0 & 0 & 0 \\ 0 & 0 & 0 & 0 \end{bmatrix}$$ **Zone 3 Turned off**

Figure 3-37. Modeling scheme for the selective results in Figure 3-34.

CHAPTER **4**

Facilities and extendibility of Elmo and Conclusions

4.1. Elmo facilities and possible extensions

This section provides information for Elmo users and for further development of this method. Various techniques, employed in Elmo or suggested for future work, are thoroughly explored.

4.1.1. Wraparound in space

It is well known that the attempt to solve many problems using Fourier analysis in the frequency-wavenumber domain can lead to significant alaising problems. This is also one of the major problems for phase shift cascade, i.e. wraparound of seismic data in both time and space axes. The Fourier transform proposes plane wave decomposition for the forward operation and plane wave integration for the inverse. When there are some certain plane-waves that can not penetrate through a layer, due to a critical angle, the range of integration is reduced. However such plane waves, though isolated spikes in ω-k_x coordinates, are widespread over the time-space domain. These infinite span plane waves will give a perfect integration, here to form the plane into a sphere or cylinder, if they all have compatible "neighbors" along at both sides (i.e. there is a complete set of

them). The neighbors mean the adjacent horizontal-slowness plane waves in the summation. If not, the reconstruction and cancellations are incomplete. Therefore the limited reconstruction of plane waves, for hyperbolic reflections of a cylindrical or a spherical waveform, mostly affects the *x-t* results in the form of the spatial wraparound of infinite span plane waves.

One of the techniques used in Elmo to deal with this spatial wraparound is to attenuate the reflections at far offsets. By this technique the plane waves which directly develop the far offsets of reflections are fractionally weighted. The amount of such attenuation for each plane wave is determined by a Butterworth filter. The filter commences at a given horizontal slowness, corresponding to a user-prescribed proportion of the maximum offset. In this manner, the main parts of reflections are least disturbed. The attenuation is implemented by making the elastic parameters complex which means that beyond the prescribed horizontal slowness, a visco-elastic model is actually computed.

4.1.2. Estimation of plane wave integration of reflections

Elmo uses raytracing for PP-waves to estimate a suitable ray parameter range for every reflection in a model. The calculation zone in the *f-k* plane for each layer is thus minimized. This assumes the evanescent waves are all filtered on transmission at boundaries. This is not always true. However, only a few plane waves at high incident angles, for the far offset construction of the deeper reflections, are usually sacrificed. The higher the impedance contrast and the finer the layer, the more plane waves are missed during modeling. If the information is wanted, the full calculation can always be conducted.

4.1.3. Depth-dependent masking matrix for scattering manipulation

The facility for scattering matrix control with model partitioning of Elmo was introduced and some figurative examples were also provided in section 3.3. Practically, two depth levels are specified to divide the entire model into three consecutive zones. Then three 4x4 masking matrices for those zones are assigned in which elements are 1

and 0. They correspond to the "on" and "off" coefficients structured in the scattering matrix in equation 2-32. This simplifies the code because Elmo always computes all scattered modes and then applies the appropriate mask to isolate selected wavefields.

4.1.4. Wraparound in time

The common problem, caused by the inverse Fourier transform from frequency to time, is that some long travel-time multiples, with significantly high amplitude, wrap back into earlier time, especially where the freesurface is concerned. It is difficult to know when or if there is a wraparound with amplitudes high enough to distort the output. A common way to control this time domain wraparound is to choose a sufficient record length. However this leads to another problem of very long computation time and insufficient memory. Another possible way is to switch off the downward reflections and upward transmissions at the free surface, $z_{k=1}$, or some particular set of top boundaries, $z_{k=1,\dots,m}$, which is the assumed trouble maker. The full response $[\mathbf{R}]_{1n}$ can be obtained from a multiplication of the total reflection $[\mathbf{R}]_{mn}$, from the entire region beneath such a multiple-free zone, by finite expansion of reverberation operator between these zones and of the upward composite transmission $[\overline{\mathbf{T}}]_{1m}$. The expansion of the reverberation operator $\left[\mathbf{I} - \mathbf{\Lambda}_{m-1}^{+} \mathbf{R}_m \mathbf{\Lambda}_{m-1}^{+} [\overline{\mathbf{R}}]_{1m}\right]^{-1}$ and an expression for $[\overline{\mathbf{T}}]_{1m}$ were given in section 1.4.5 by equation (1-66) and (1-64), respectively. A similar mathematical description for this procedure was also given previously for a composite reflection coefficient,

$$[\mathbf{R}]_{1n} = [\overline{\mathbf{T}}]_{1m}\left[\mathbf{I} - \mathbf{\Lambda}_{m-1}^{+} \mathbf{R}_m \mathbf{\Lambda}_{m-1}^{+} [\overline{\mathbf{R}}]_{1m}\right]^{-1}[\mathbf{R}]_{mn}$$

$$[\mathbf{R}]_{1n} = [\overline{\mathbf{T}}]_{1m}[\mathbf{R}]_{mn} + [\overline{\mathbf{T}}]_{1m}\mathbf{\Lambda}_{m-1}^{+} \mathbf{R}_m \mathbf{\Lambda}_{m-1}^{+} [\overline{\mathbf{R}}]_{1m}[\mathbf{R}]_{mn} +$$
$$[\overline{\mathbf{T}}]_{1m}\mathbf{\Lambda}_{m-1}^{+} \mathbf{R}_m \mathbf{\Lambda}_{m-1}^{+} [\overline{\mathbf{R}}]_{1m}\mathbf{\Lambda}_{m-1}^{+} \mathbf{R}_m \mathbf{\Lambda}_{m-1}^{+} [\overline{\mathbf{R}}]_{1m}[\mathbf{R}]_{mn} + \dots$$

Each term may be computed separately in the frequency domain and then they can be accumulated into the total results later in time domain. Therefore some part of the temporal wraparound can be excluded from the summation. For the surface reverberation, setting $m=2$ so $[\overline{\mathbf{R}}]_{12}$ is the surface downward reflection $\overline{\mathbf{R}}_1$, $[\overline{\mathbf{T}}]_{12}$ is a product of one-

way phase advance in the 1st layer and the upward freesurface transmission $\mathbf{\Lambda}_1^+\overline{\mathbf{T}}_1$, and a matrix of the full response from below is $[\mathbf{R}]_{2n}$.

4.1.5. Order-of-multiple control

With the ordinary plane-wave cascade diagram, Figure 2-2, phase shift cascade computes a certain number of scatterings at an interface, dependent on the total number of interfaces in the layered model. The scattering number grows by one, from one count at the deepest reflector, up to the topmost. This means the intrabed multiples have the highest order in the top layer, equal to the number of layers in the model. There are only primary reflections from the bottommost interface. The strategy of this original grid, in brief, calculates and includes every event which has the number of scatterings less than a certain integer, dependent on the geological model. If a certain order of multiple reflections from every boundary are required, a variation of the plane wave cascade diagram is suggested in Figure 4-1.

The computation should be traced downward through the bottom of model while parameters of upgoing waves for all of the adjacent nodes are maintained. This process then repeats with the number of the maximum multiple order and the upward continuation through the surface or detectors from every unfinished node can be done after that. A diagram for this calculation is shown, Figure 4-1, as though the ordinary grids are appended together.
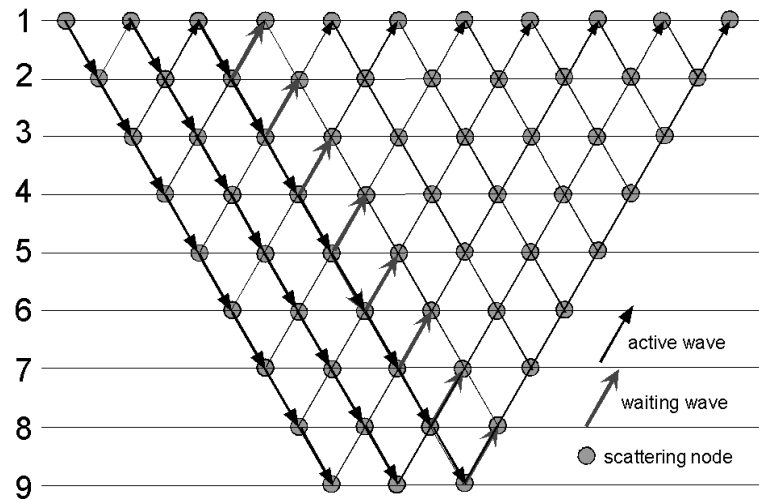
Figure 4-1. plane wave cascade for order-of-multiple control

4.1.6. Miscellaneous

As a feasible extension, frequency-dependent effects can be easily simulated, such as absorption. Phase shift cascade can properly take into account the diversity of absorption with both frequency and depth, assuming the absorption coefficient varies linearly with frequency. Anisotropic and anelastic cases are also possible in the *f-k* domain by this method. It can also be extended to 3-D simulation.

Another problem with phase shift cascade is the need to block the logs to a small number of layers due to run time and memory limitations. This causes a loss of detail similar to the time domain 1-D seismogram of section 3.1. This can be addressed by several methods including the brute force computation of more layers or the replacement of blocked log segments by composite reflection and transmission coefficients.

4.2. Conclusions

The seismic problem is to determine the structure and properties of the interior of the earth based upon seismic data obtained at the surface. To study the features on recorded seismograms as they relate to the properties of the subsurface, mathematical modeling is a major tool. There are several methods of elastic modeling already available to obtain synthetic data. However they are all different in terms of limitations, accuracy,

computing time, analytical ease and other factors. An appropriate method must be chosen with acceptable cost still giving the information required. A new numerical approach called phase shift cascade is presented here which offers new flexibility for synthetic seismograms in layered 2-D media.

The 1-D acoustic modeling of phase shift cascade (or the depth domain algorithm), works well and gives qualitatively correct results for synthetic models and also for the real data from Blackfoot 08-08. The time domain algorithm, commonly used in industry, produces results similar though not identical to the depth domain method. For a constant velocity model, the two methods are exactly equivalent. However, in the more realistic variable velocity setting they can give quite different results. For real log data, the time domain method requires an extra small time interval to maintain all of the original log information. From the results, at a normal sample rate (2ms), the time domain method created notably different primaries compared to the depth domain method. This is a direct consequence of the time averaging. However the methods have an acceptable correlation for many purposes. On the other hand, the solutions of multiples created from the same logs by the two methods are very different.

Both results support the conclusion of Coulombe and Bird (1996) that a series of coal beds causes notches in the amplitude spectrum of the seismograms. It seems quite likely that interbed multiples cause (or at least accentuate) these notches.

In the 2-D elastic case, phase shift cascade generates realistic synthetic amplitudes and traveltimes with head waves for potential and displacement seismograms. It is fast and stable. Cylindrical reflection coefficients are obtainable and show distinct departure from plane wave coefficients for post critical reflections. Multiples and mode conversions are controlled via the scattering matrix. The scattering matrix manipulations can vary with depth.

The separation of a complex seismic wavefield into primaries and multiples for both P and S waves can be a valuable exploration tool. In this case it was found that PP interbed multiples from a coal bed fall on top of the Glautonite channel and this increases exploration risk.

Spatial and temporal wraparound is a serious problem for phase-shift cascade modeling, and is caused by the utilization of the Fourier transform. Nonetheless, the attenuation for plane waves at high angle of incidence using numerical viscosity suppresses wraparound in space. Evanescent waves can be alternatively included in the output model. A partial time-domain convolution, of a reverberation operator of the high impedance contrast zone to the composite reflection of region below such zone, is suggested to avoid the wraparound in time.

The algorithm is intuitive, stable, very extendible and gives realistic results. It has advantages from both main modeling categories, raytracing and wave equation simulations. This method is a good tool to conveniently study various complicated cases that need insightful and realistic modeling, such as thin layers with high impedance contrasts.

References

Aki, K., and Richards, P.G., 1980, Quantitative Seismology, Theory and Methods, W.H. Freeman and Company.

Bath, M. and Berkout, A.J., 1984, Mathematical aspect of seismology, Seismic exploration, **17**, Geophysical Press.

Berryman, L.H., Goupillaud, P.L. and Waters, K.H., 1958, Reflections from multiple transition layers, part I-theoretical results : Geophysics, 23, 244-252.

Bording, R.P. and Lines, L.R., 1997, Seismic modeling and imaging with the complete wave equation, SEG.

Brekhovskikh, L.M., 1980, Waves in layered media, Academic Press.

Cerveny, V., Molotkov, I.A. and Psencik, I., 1977, Ray method in seismology, Univerzita Karlova, Praha.

Cerveny, V. and Ravindra, R., 1971, Theory of seismic head waves, University of Toronto Press.

Chapman, C. H., 1978, A new method for computing seismograms: G. J. R. A. S., **54**, 481-518.

Clayton, R., and Enquist, B., 1977, Absorbing boundary conditions for acoustic and elastic wave equations: Bull., Seis. Soc. Am., **67**, 1529-1540.

Coulombe, C.A., and Bird, N.D., 1996, Transition filtering by high-amplitude reflection coefficients: Theory, practice and processing considerations: The Leading Edge, 15, 1037-1042.

Dankbaar, J.W.M., 1985, Separation of P and S waves: Geophysical Prospecting, 33, 970-986.

Dohr, G, 1985, Seismic shear waves; Part A: Theory, Geophysical press.

Easley, D.T., and Foltinek, D.S., 1993, Synthetic seismogram for P and S waves using the Goupillaud model, 1993 Annual Research Report of The CREWES Project.

Fornberg, B., 1987, The pseudospectral method: comparisons with finite differences for the elastic wave equation, Geophysics, **52**, 483-501.

Frasier, C.W., 1980, A new time domain reflection seismogram, presented at 12th Offshore Technology Conference in Houston, Tex., May5-8.

Fuchs, K., and Muller, G., 1971, Computation of synthetic seismograms with the reflectivity method and comparison with observations: G. J. R. A. S., **23**, 417-433.

Gazdag, J., 1978, Wave-equation migration by phase shift: Geophysics, 43, 1342-1351.

Gilbert, F and Backus, G.E., 1966, Propagator matrices in elastic wave and vibration problems, Geophysics, **31**, 326-332.

Haskell, N.A., 1953, The dispersion of surface waves on multilayer media, *Bull. Seism. Soc. Am*., **43**, 17-34

Hearn, D.J., and Krebes, E.S., 1990, On computing ray-synthetic seismograms for anelastic media using complex rays, Geophysics, **55**, 422-432.

Kelly, K. R., Ward, R. W., and Treitel, S., 1976, Synthetic seismograms: A finite-difference approach: Geophysics, **41,** 2-27.

Kennett, B.L.N., Kerry, N.J. and Woodhouse, J.H., 1978, Symmetries in the reflection and transmission of elastic waves, G.J.R.A.S., **52**, 215-229.

Kennett, B.L.N. and Kerry, N.J., 1979, Seismic waves in a stratified half space-I. G.J.R.A.S., **57**, 557-583.

Kennett, B.L.N., 1980, Seismic waves in a stratified half space-II. Theoretical seismograms: G.J.R.A.S., **61**, 1-10.

Kennett, B.L.N., 1983, Seismic wave propagation in stratified media, Cambridge University Press.

Krail, P.M., and Brysk, H., 1983, Reflection of spherical seismic waves in elastic layered media: Geophysics, **48**, 655-664.

Krebes, E.S. and Le, L.H.T., 1994, Inhomogeneous plane waves and cylindrical waves in anisotropic anelastic media, J. Geophysical research, **99**, 23899-23919.

Krebes, E.S. and Slawinski, M.A. , 1991, On raytacing in an elastic-anelastic medium, Bull. Seismol. Soc. Am., **8**1, 667-686.

Lawton, D.C., and Howell, T.C., 1992, P-P and P-SV synthetic stacks, Expanded Abstract, 62nd SEG Annual International Meeting, October 25-29, New Orleans, USA, 1344-1347.

Lay, T., and Wallace, T. C., 1995, Modern global seismology, Acadamic Press.

Margrave, G.F., and Foltinek, D.S., 1995, Synthetic P-P and P-SV cross sections, 1995 Annual Research Report of The CREWES Project.

Rendleman, C.A., and Levin, F.K., 1988, Reflection maxima for reflection from single interfaces: Geophysics, **53**, 271-275.

Robinson, E.A., 1967, Predictive decomposition of time series with application to seismic exploration, Geophysics, **32**, 418-484.

Sheriff, R.E. and Geldart, L.P., 1995, Exploration seismology, Cambridge University Press.

Thomson, W.T., 1950, Transmission of elastic waved through a stratified solid medium, *J. Appl. Phys.*, **21**, 89-93.

Tygel, M., and Hubral, P., 1987, Transient waves in layered media, Elsevier.

Waters, K.H., 1992, Reflection Seismology: A tool for energy resource exploration, 3rd edition, Krieger Publishing Co.